Plasma gasification of water hyacinth

D Claasens

orcid.org/ 0000-0002-4806-53524

Dissertation accepted in fulfilment of the requirements for the degree *Master of Engineering in Chemical Engineering* at the North-West University

Supervisor:	Prof HWJ Neomagus
Co-supervisor:	Prof JR Bunt
Co-supervisor:	Dr IJ van der Walt

Dedication and Acknowledgements

I thank YHWH, Yeshua and Ruach Hakodesh for the opportunity afforded me to do this research, for inspiring me and for providing the means to do so.

I want to thank my supervisors, Prof. Hein WJ Neomagus, Prof. John R Bunt and Dr. I Jaco van der Walt, for their continued support and guidance throughout the duration of this study. I have great respect for you all, thank you for supporting my growth as a professional. I also want to acknowledge with thanks, Clement Mgano and Romanus Uwaoma for their assistances in laboratory work. My sincere appreciation to NECSA for the use of their PlasWEn system and laboratories. Thanks to Vasagan Reddy and Melvin Alihusain from Club of Engineers for their input with the techno economic evaluation, and Michael Gallenetti for providing relevant financial factors.

In order to express my appreciation to my family and friends, for the love, prayers, support and space you hold for me, the number of pages of this study would not be enough. I want to thank, with appreciation and love, especially my father Willem and mother Bertha, for your continued love and encouragement throughout my academic years. To Barry for your deep understanding and wholesome influence. To Daleen for your graciousness. To Thamari and Alastair for your example and relentlessly rooting for my success. To Engela for your unwavering celebration of every step and milestone. To Stephan for countless authentic conversations and keeping me on my toes. To Magdie for reminding me to keep pursuing my dreams. To Lizaan, Colleen, Cameron, Aimee, Danitza, Ruben and Ernst for authentic friendship, encouragement, challenging me to be better and reminding me that life is good, and as good as we make it. I appreciate you all. May God double every ounce of energy, resource and prayer you have invested in me. I count myself truely blessed.

It is my hope that we can provide for the present without stealing from the future, while empowering people to empower themselves. This, along with being a good steward is my life's vocation. The completion of this study marks another step toward that goal.

Declaration

I, Deoné Claasens, declare that this report is a presentation of my own original work for the sole purpose to motivate my M.Eng (Master degree) and may not be replicated without my written consent.

Whenever contributions of others are involved, every effort was made to indicate this clearly, with due reference to the literature.

Signed on this day the 27th Nov 2023, in Port Elizabeth

Deoné Claasens

Contents

List of Figures

List of Tables

List of Abbreviations

AC	Alternating current
Amp	Ampere
APC	Air pollutant control
CPI	Consumer Price Index
CV	Calorific value
DC	Direct current
DPP	Discount payback period
DTG	Differential thermographic graph
dtha	Dry ton per hectare per annum
ER	Efficiency ratio
FC	Fixed carbon
GC	Gas chromatography
GHG	Greenhouse gas
HCV	Higher calorific value
HCV_i	Higher calorific value (i denotes specific the material, waste or syngas)
IGCC	Integrated gasification combined cycle
IRR	Internal rate of return
LEL	Lower explosive limit
LCV	Lower calorific value
LHA	Low ash algae
MR	Million Rands
MRP	Equity market risk premium
MSW	Municipal solid waste
NECSA	Nuclear Energy Corporation of South Africa
NPV	Net present value
PGE	Plasma gasification efficiency
PL	Project lifetime
PPI	Producer Price Index
PPP	Public private partnership
PSA	Pressure swing adsorption
PSR	Plasma power to syngas ratio
R	Rands
RF	Radio frequency
RDF	Refuse derived fuel
RFR	Raw forest residue
RGM	Raw grape marc
RIRR	Real internal rate of return
RMA	Raw micro algae
PPP	Public private partnership
RRS	Raw rice straw
RPW	Raw pine woodchips
RTC coal	River-Tracding-Company coal
Scn i (i=1,2)	Scenario 1 or scenario 2
S/C	Steam carbon ratio

SPP	Simple payback period (years)
syn	Syngas
TEE	Techno economic evaluation
TGA	Thermogravametric analysis
tpa	Ton per annum
tpd	Ton per day
TW	Treated wood
VC	Variable cost
VM	Volatile matter
Volt	Voltage
WACC	Weighted average cost of capital
WC	Working capital
WHL	Water hyacinth leaf/(leaves)
WHR	Water hyacinth root(s)
WHR(1,2,3)	Water hyacinth root(s) from literature
WHS	Water hyacinth stem(s)
WHSh(1,2,3)	Water hyacinth stem(s) and leaves from literature
WHW	Water hyacinth whole
wt %	Weight percentage
XRF	X-Ray Fluoresence Spectrometer

List of Symbols

α	Small stock premium (%)
β	Systematic risk (-)
a	Cost factor (-)
C_e	Equipment cost (R)
C_i	Total cost (R)
C_f	Fixed costs (R)
C_n	Net cashflow (R)
C_o	Operational cost (R)
C_{syn}	The amount of carbon in the syngas (kg) or (mol)
C_v	Variabe costs (R)
C_w	Working costs (R)
C_{waste}	The total amount of carbon input from the waste (kg) or (mol)
CGE	Cold gas efficiency (%)
CO_{syn}	The amount of carbon monoxide in the syngas (kg) or (mol)
CPI	Consumer Price Index (%)
CV	Calorific value (kJ/kg)
CV_{WHL}	Calorific value of WHL (kJ/kg)
CV_{WHS}	Calorific value of WHS (kJ/kg)
CV_{WHR}	Calorific value of WHR (kJ/kg)
CV_{waste}	Calorific value of waste (kJ/kg)
CV_{WHW}	Calorific value of WHW (kJ/kg)
CV_{syn}	Calorific value os syngas(kJ/kg)
d	Debt financing (%)
D_j	Depreciation (R)
DPP	Discount payback period (years)
e	Equity financing (%)
H_{syn}	The amount of hydrogen in the syngas (kg) or (mol)
H_{input}	The total amount of hydrogen input (kg) or (mol)
H:C	Molar H per molar C ratio (-)
HCV	Higher calorific value (MJ/kg)
IRR	Internal rate of return (%)
K_d	Cost of debt (%)
K_e	Cost of equity (%)
K_t	Cost of debt (pre tax) (%)
LCV_{syn}	Lower calorific value of syngas (MJ/kg)
$LCV_{syn,exp}$	Lower calorific value of syngas based on experimental values(MJ/kg)
$LCV_{syn,\ theo}$	Lower calorific value based on theoretical values(MJ/kg)
LCV_{waste}	Lower calorific value of waste (MJ/kg)
LCV_{WHW}	Lower calorific value of WHW (MJ/kg)
$\dot{m}_{syn,}$	Mass flow of syngas (kg/hr)
$\dot{m}_{syn,exp}$	Mass flow of syngas based on experimental values (kg/h)
$\dot{m}_{syn,\ theo}$	Mass flow of syngas based on theoretical values (kg/h)
$\dot{m}_{waste}$	Mass flow of waste feed (kg/h)

$\dot{m}_{WHW}$	Mass flow of WHW(kg/hr)
MGE	Mechanical gas efficiency (%)
MRP	Equity market risk premium (%)
n_i	Plant size (i = 5, 10, 20, 30, 50, 100 tpd)
NPV	Net present value (R)
O:C	Molar O per molar C (-)
P_g	Gross profit (R)
P_{ga}	Gross profit after depreciation (R)
P_{gb}	Gross profit before depreciation (R)
PGE	Plasma gasification efficiency (%)
P_{sys}	Pressure of the system (bar)
P_n	Net profit (R)
$P_{reactor}$	Pressure inside the reactor (bar)
$P_{gas,in}$	Pressure of the input gas (bar)
PPI	Producer Price Index (%)
R_f	Risk free rate (%)
RIRR	Real internal rate of return (%)
S_f	Scaling factor
S_i	Sales income (R)
SPP	Simple payback period (years)
T_i	Tax due (R)
T_i	Input gas stream temperature (°C)
$T_{injected\ gas}$	Input waste or WHW temperature (°C)
T_r	Tax rate (%)
$T_{reactor}$	Reactor temperature (°C)
T_{syn}	Syngas temperature (°C)
VC	Variable cost (R)
w	Moisture (%)
WACC	Weighted average cost of capital (%)
$WACC_{nominal}$	Nominal weighted average cost of capital (%)
$WACC_{real}$	Real weighted average cost of capital (%)
WC	Working capital (R)

Abstract

This study evaluates the feasibility of water hyacinth as a carbon fuel source for energy production, as a waste valorization method. The H-PlasWEn system at NECSA was evaluated as a possible plasma waste-to-energy (PlasWEn) process for hyacinth (H). Hyacinths collected from the Hartbeespoort dam were prepared and characterized through chemical and elemental analysis, calorific value (CV) tests and devolatilization. The WHW sample can be chemically described as 45.8% C, 5.9% H, 2.7% N, 45.4% O and 0.2% S on moisture and ash free basis, with a HCV of 14.3 MJ/kg. Various plasma gasification experiments were performed where the O:C molar ratio, specific power input (kWh/kg) and reactor temperature (°C) were varied. The produced gas is referred to syngas in this study. The averaged results for the syngas, from Run A with 0.9 O:C, is 12.6% H_2, 12.5% CO, 0.3% CO_2, 0.05% CH_4, 0.09% C_2H_2, 0.02% O_2 and remaining a 74.4% N_2, and for Run B is with 1.2 O:C, 10.3% H_2, 6.4% CO, 0.02% CO_2, 0.03% CH_4, 0.03% C_2H_2, 0.06% O_2 and 80.7% N_2. The carbon conversion efficiency (CCE) for Run A and Run B were determined to be 95.6% and 63.2% respectively. The experimental results, simulated using FactSage, and the plasma generated gas composition approached chemical equilibrium, specifically at high temperatures. The results deviated more from equilibrium as the O:C ratio increased, and also as the specific power input was decreased. Finally, a techno-economic evaluation (TEE) was conducted on the H-PlasWEn system based on the syngas composition of Run A, where a syngas LCV value, of 14.7 MJ/kg was derived using the experimental gas composition of H_2, CO, CO_2, CH_4, C_2H_2 and O_2 on kg/kg feed basis. The PlasWEn techno-economic analysis considered two scenarios: one involving the conversion of both syngas and heat energy into electricity, sold as a single product (Scn1), and another where only the syngas was converted into electricity and sold independently from the heat energy, resulting in two distinct products (Scn2). A PlasWEn plant size of 20 tpd was chosen as it is sized according to the largest plasma gasification reactor built in South Africa. The total capital investment of MR 66 is required of which the total fixed capital investment is MR 54.9 and operational costs are MR 3.4/year (75% attributed to labour). The plant requires 5 551.3 kWh/d and is self sufficient once operational, and generates 23 371 kWh/d electricity for sale. A 20 tpd system show an 20.8% IRR,12.7% RIRR, 43.6 MR NPV, 5.7 years SPP and 9.3 years DPP and determined economically viable and a promising waste-to-energy project.

Keywords: Plasma gasification, hyacinth, waste-to-energy, techno economic evaluation

Chapter 1 Introduction

1.1 Background and Motivation

1.1.1 Background

The Hartbeespoort Dam, located in the North West Province, like many other dams in South Africa, is eutrophic, therefore, rich in nutrients and biological activity (Murray et al., 2002). The dam's main inflow is the Crocodile River, which contains high levels of nitrates and phosphates (Harding, et al., 2004). The main sources of pollution are domestic, agricultural and industrial effluent, from mining, power generation and urbanization (Harding, et al., 2004; Musingafi & Tom, 2014). Due to its eutrophic state, the Hartbeespoort Dam experiences high proliferation rates of algae, cyanobacteria and water hyacinth (*Eichhornia crassipes*) (van Ginkel & Michael, 2007). Water hyacinth is considered the worst aquatic weed in the world (Gaurav et al., 2020) and is a free-floating, aquatic plant that is of interest in the renewable energy sector and wastewater management (Li, et al., 2021). Due to its high proliferation rate (doubling in volume every 1 - 2 weeks), reproductive means (sexual and asexual), tolerance to a wide variety of environmental factors (temperature, pH and varying nutrient levels) water hyacinth proves to be an effective invading plant species (Ruiz Téllez, et al., 2008). Water hyacinth has proven to be detrimental to water systems and ecological biodiversity, causing severe problems such as flooding, sedimentation, blocking water bodies, clogging irrigation systems, a decrease in fish population, and negatively affecting recreational activities and navigation (Gaurav et al., 2020; Ilo, et al., 2020)). Outbreaks of diseases like filariasis, dengue, malaria and encephalitis (for humans) occur due to the breeding ground that water hyacinths mats provide for mosquitos and snails (Gaurav et al., 2020). Rainfall is South Africa's primary water input and varies on seasonal and spatial scales, where it increases from the coastal regions and decreases toward the country's interior (Nel, et al., 2017). South Africa is classified as a semi-arid country, with a mean rainfall of 490 mm per year, which equals approximately half of the average rainfall worldwide (Nel, et al., 2017). Freshwater water sources constitute 8% of South Africa's total surface land area and provide up to 50% of the country's river water (Nel, et al., 2017). Due to infrastructural expansion, industrial development and population increase, South Africa's national water demand is projected to increase by 32% in 2030 (Nel, et al., 2017). There is an inherent need to clean and preserve the South African water systems and dams (Nel, et al., 2017).

On the positive side, water hyacinth absorbs dissolve N and P, controlling eutrophic conditions (Li, et al., 2021). Water hyacinth is also effective in the phytoremediation process by removing heavy metals such as Pb, Zn, Ni, Hg, Cr, As, Cd, and Cu from wastewater (Li, et al., 2021). Using water hyacinth for water bioremediation is favored over methods such as ion exchange, electro dialysis and reverse osmosis, which prove to be more energetically and economically intensive (Li, et al., 2021). Continuous removal of water hyacinth is therefore required to remove the pollutants before it is deposited back into the water (Li, et al., 2021). This occurs when the hyacinth detaches leaves or as part of the plant's metal tolerance mechanism to minimize metal toxicity, leaks previously absorbed metals through the roots (Newete, et al., 2016). Harvested, contaminant-enriched, hyacinth biomass requires timely conversion and management otherwise, as a waste, it can pose a health threat and environmental crisis (Li, et al., 2021). To date there are three methods of control: chemical, mechanical and biological (Ilo, et al., 2020): chemical control is cheap but cannot be seen as a long term solution and it pollutes the environment, mechanical control is effective but expensive; and biological control is considered as an optimistic solution, however suffers from the lack of experimental proof (Ilo, et al., 2020). In 2011, it was established that South Africa spends roughly R12.9 billion/annum ($700 million/annum) or approximately 0.3% of South Africa's GDP on invasive plant control, which can increase to up to 5% if not migrated (Ilo, et al., 2020). Financial and environmental returns can be realized, since water hyacinth has potential benefits as an alternative, lignocellulose, biomass fuel source and is abundantly available, at low cost and sustainable for waste management (Gaurav et al., 2020). As a waste, water hyacinth has potential in the energy production sector since it satisfies all the criteria for bio-energy production (Rezania et al., 2015). As a renewable energy source, hyacinth can be used as a substitute for conventional fossil fuels (Rezania et al., 2015). South Africa primarily relies on electricity generated from the coal industry; 82% of the power generated by Eskom is produced from coal (Chamber of Mines, 2018). In 2013 approximately 7.2 billion people used 104.7 PWh around the globe and consumption is projected to rise to 262.8 PWh by 250 (Sikarwar & Zhoa, 2017). Globally, the energy dependence on fossil fuels corresponds to 40% of the global energy consumption (Maraquesi, et al., 2015; Chamber of Mines, 2018). In 2017, Sikarwar & Zhoa, reported that 10% of the global energy demand is supplied by biomass. The production of biomass-based energy at local, national, and global levels helps mitigate social and politically unstable international energy dependence (Sikarwar & Zhoa, 2017). The technology and energy production related to the coal mining industry has been the most cost-effective

(Chamber of Mines, 2018). Globally, the importation of thermal coal is primarily driven by electricity generation (Chamber of Mines, 2020). However, its growth is already constrained due to a decrease in export demand, access to land, policy and legislation, capital availability, high water usage, and pollution related to mining activities and end-use processes (Chamber of Mines, 2018). The international coal trade is affected by the implementation of the IMO-2020 to limit the amount of S in shipping fuel and global situations such as the COVID pandemic (Chamber of Mines, 2020). The amount and reduction, of pollutants and greenhouse emissions associated with waste and energy production have become increasingly prevalent (Diaz et al., 2015). In response to the time-sensitive and environmentally significant climate issues, associated with industry greenhouse gas emissions, the South African Government passed new legislation in the form of the Carbon Tax Act (Republic of South Africa, 2019). This aims to ensure that both businesses and households consider the implications and cost of greenhouse emissions in production, consumption, and investment decisions. The first phase of the Carbon Tax Act was effective from the 1st of June 2019 and the second phase will run from 2023 – 2030 (Republic of South Africa, 2019). The establishment of a biomass conversion plants are not only more environmentally friendly, but labour intensive and can provide job opportunities for developing nations and improving the economy (Sikarwar & Zhoa, 2017).

1.1.2 Motivation

The Hartbeespoort Dam, among other water bodies in South Africa, is being overwhelmed by water hyacinth (Rezania et al., 2015) and a viable long-term solution is inevitably needed due to the millions of dormant seeds deposited (van Schalkwyk, et al., 2017). An unique situation presents itself, firstly due to the hyacinth's ability to remove and reduce heavy metals, pathogen and organic compound levels (Rezania et al.,2014), together with the urgent need to control this abundant and invasive aquatic plant species (The Department of Water and Sanitation, 2016). Secondly, due to the large amounts of biomass that will have to be removed regularly due to the high proliferation rate. It is feasible to achieve a circular bio-economy in phytoremediation, using hyacinth as bio-waste, through thermochemical conversion methods like torrefaction, carbonization, pyrolysis and gasification (Li, et al., 2021). NECSA has developed a waste-to-energy process, PlasWEn, which involves plasma gasification of different waste materials to produce syngas. Energy recovery and waste management (by elimination) as components of a circular economy, alleviate pressure on existing energy-producing processes, waste disposal systems and reduce dependence on traditional fuel sources

(Sariatli, 2017). Therefore, waste recovery and utilization is an essential part of a linear economy's transformation to a circular economy (Sariatli, 2017).

1.2 Aim and Objective

1.2.1 Problem Statement

This study aims to evaluate the feasibility of water hyacinth as a carbon fuel source in energy production. As a waste valorization method, the H-PlasWEn process was evaluated as a possible plasma waste-to-energy (PlasWEn) processing technology for hyacinth (H) as a biomass waste. This study serves as a means to: Aid in energy supply by utilizing the large amounts of hyacinth in the H-PlasWEn process to produce syngas, which can be converted to electricity. Alleviate the country's waste disposal system by implementing the thermal plasma gasification process. However, the sole focus of this project will be on the energy potential of water hyacinth as a feedstock for syngas production through the H-PlasWEn process.

1.2.2 Aim

The aim of this study is to evaluate the energy potential of water hyacinth collected from the Hartbeespoort Dam as a feedstock for plasma waste to energy.

1.2.3 Objectives

The objectives of this study are to:

- Procure, prepare and characterize the organic and inorganic fraction of hyacinth that was sourced from the Hartbeespoort Dam.
- Preform plasma gasification experiments using the H-PlasWEn system as a function of temperature, specific power input and the O:C ratio.
- Simulate the reactions taking place within the reactor using a chemical equilibrium model, FactSage
- Evaluate plasma gasification as a possible waste-to-energy means for hyacinth (H PlasWEn) by performing a techno economic evaluation.

1.3 Scope and Limitations

1.3.1 Scope

The scope of this study is to determine the feasibility of water hyacinth as a suitable fuel source. To accomplish this, a series of experiments were conducted. Thermogravimetric analyses (TGA) were conducted to evaluate the thermal behavior of sun-dried water hyacinth. Characterization by means of proximate analysis to determine the moisture content, volatile matter (VM), fixed carbon (FC) and the ash yield were performed. Ultimate analysis was done to determine the C, H, N, S and O content of the feedstock, which accounted for the produced syngas as well as the calorific value (CV) in order to measure the potential energy output. The sun-dried water hyacinth was then plasma gasified and reacted with different oxidant reagents in order to evaluate the quality of the syngas produced. The plasma reactor operating conditions was varied by adjusting the arc temperature and the current used, and the feedrate. To determine the composition of the inorganic fraction and give insight to the possible effects on the process and product quality, a XRF analysis was done. Thermodynamic modelling of the plasma gasification process, using FactSage, was also done in order to understand the chemical processes (speciation and portioning behavior) in the gasification reactor. Finally, a techno economic evaluation (TEE) was done and scaled from 5 – 100 tpd. The reaction conditions for the TEE was based on Run A, where the species in the product gas per kg hyacinth feed, were used to scale the system, where 10 % O_2 was added as oxidant and 10% N_2 as plasma gas. The final evaluation considered a financial feasibility for a 20 tpd system.

1.3.2 Limitation

The experimental plasma gasification runs were conducted at the NECSA premises in Pelindaba. Owing to the national lockdown implemented in response to the Covid-19 pandemic, the initial phase of the experiments had to be abruptly concluded, and access to the equipment for external visitors was unavailable for a duration of two years. A subsequent set of experiments was feasible; however, constrained timeframes were imposed by concurrent priority projects at NECSA. Consequently, heightened emphasis was directed towards the technical economic evaluation (TEE) in this research project.

1.4 Dissertation Layout

Chapter 1 Introduction

This chapter is divided into four sections, which provide the motivation and background for this study. This includes a discussion in Section 1.1 on South Africa's water, waste and energy resources. The problem statement, aim and objectives are presented in Section 1.2. The scope of the study is discussed in Section 1.3 and the dissertation layout per chapter is described in Section 1.4.

Chapter 2 Literature Study

This chapter is divided into two sections and gives an in-depth view on the various aspects of the study and insight into existing literature relevant to the study. In the first section, the review focusses on water hyacinth as a renewable energy source, how waste, namely water hyacinth, can be valorized by means of natural processes. Thermal methods of waste valorization and how the chemical characteristics of water hyacinth, determined by various analyses, provide insight to determine the energy potential and are all discussed in Section 2.1. The thermal plasma gasification process in general, performance, lab scale and industrial systems along with the waste materials valorized are discussed in Section 2.2.

Chapter 3 Hyacinth Preparation and Characterization

This chapter is divided into three sections, and gives the reader insight regarding the materials, methods, and procedures utilized, and to discuss the results pertaining to the characterization of water hyacinth. The materials used in this study, how the feed material was collected and prepared are discussed in Section 3.1. The sample origin, description and preparation are described in Section 3.2. The experimental method followed for the different types of characterization of water hyacinth is discussed in Section 3.3. The characterization results are given in Section 3.4.

Chapter 4 Experimental

Chapter 4 is divided into four sections and gives the reader insight to the different steps involved in the plasma gasification process and the specific reactor used in this study. The gases used are given in Section 4.1, the equipment and process description are discussed in Section 4.2, the experimental plan, procedure, process parameters and feed calculations are described in Section 4.3, followed by the thermodynamic modeling using FactSage and the inputs used for the simulation package are given in Section 4.4.

Chapter 5 Results and Discussion

This chapter consists of three sections. The results obtained from the H-PlasWEn lab setup are shown in Section 5.1. The results are analysed, compared with thermodynamic modelling, and discussed in Section 5.2. Finally, the H-PlasWEn performance analysis and mass balance are discussed in a summary shown in Section 5.3.

Chapter 6 Techno Economic Analysis

Chapter 6 is divided into 8 sections and evaluates the feasibility for a plasma gasification system as a waste-to-energy means for water hyacinth as a feedstock. An introduction and the project assumptions are given in Section 6.1. The site, hyacinth availability, harvesting and material preparation are discussed in Section 6.2, The H-PlasWEn system description and process flow diagram (PFD) is given in Section6.3, the capital flow and the fixed capital investment (material costing and operational costs) are described in Section 6.4. The production and sales revenue are discussed in Section 6.5, and the derived financial factors are given in Section 6.6. The Financial feasibility is discussed in Section 6.7, and the sensitivity and break even analysis is discussed in Section 6.8.

Chapter 7 Conclusion, Future Work and Recommendations

Chapter 7 summarize and concludes the work done in this study, discusses future work and recommendations.

Chapter 2 Literature Study

2.1 Valorization of Waste

2.1.1 Valorization by Natural Processes

Water hyacinth is effective in the phytoremediation process (Li, et al., 2021) incorporated to remove, reduce, and control nutrients, heavy metals, pathogens and organic compounds in different waste streams (Rezania et al., 2015). Water hyacinth roots absorb pollutants, *i.e.* alkaline oxides and sulfates and fix the absorbed elements to its physiological structure, primarily the roots (Salas-Rulz, et al., 2020). Hyacinth is applicable in the treatment of contaminated soils, wastewater and ground water, where a phytoremediation efficiency of 47% can be achieved (Gaurav, et al., 2020). Hyacinth can also be utilized for its phytotoxic effect (Gaurav, et al., 2020), converting toxins from a chemically active state to an inactive, non-toxic state (Rezania et al., 2015). Hyacinth also has potential in the biofuels industry; due to a low lignin, high cellulose and hemicellulose content, the conversion to fermentable sugars is readily obtained (Rezania et al.,2014). Hyacinth is suitable to produce ethanol and bioethanol by saccharification and enzymatic hydrolysis (Gaurav, et al., 2020) and bio-hydrogen (Pattra and Sittijunda 2015). Hyacinth is an alternative energy source material for the production of biogas, due to a high cellulose content and biodegradability (Gaurav, et al., 2020). Biogas can be produced through anaerobic digestion and primarily consists of CH_4, CO_2, H_2O and other trace constituents (EBA, 2019). The anaerobic digestion of hyacinth will require a large reactor volume and long retention time, due to the plants' high water content and the low biodegradability of cellulose (Bhattacharya et al., 2010; Rezania, et al., 2015). Biogas from water hyacinth contains 54% CH_4 and 45% CO_2 and can be used as a clean fuel (Gaurav, et al., 2020). Solid and effluent waste streams from biogas production can be used directly as fertilizer and compost (Rezania, et al., 2015). Hyacinth can also be utilized as an animal feed, due to its high protein, vitamin, and mineral content (Rezania et al., 2015). The preparation method is, however, dependent on the type of animal. Dried, milled hyacinth can be directly fed to poultry, fish, and swine (Rezania et al., 2015), where it needs to be ensiled, or fermented, prior to feeding rudiment and can only constitute up to 50% of their dietary intake (Hossain et al.,2015). Agriculturally, hyacinth can protect soil moisture and aid in nutrient recuperation by being used as mulch, organic fertilizer and compost; it is rich in nitrogen and has a C/N ratio of approximately 15 (Rezania et al.,

2015; Gaurav, et al., 2020). Hyacinth can also be incorporated in vermicomposting due to its vegetative nature (Gaurav, et al., 2020). The main disadvantages of hyacinth are its high moisture content (Rezania et al., 2015; Gaurav, et al., 2020) and the varying mineral and chemical composition which influences the energy output potential.

2.1.2 Valorization by Thermal Processes

The most commonly used thermal valorization processes of lignocellulosic biomass to biofuels are incineration, pyrolysis and gasification methods (Ansa, 2017); Sikarwar & Zhoa, 2017). The typical operational conditions and product output for combustion, pyrolysis and gasification processes are illustrated in Table 1.

Table 1: Conventional thermal processes, their operational conditions and reaction products

Parameter	Combustion	Pyrolysis	Gasification
Temperature (°C)	250 < T ≤ 1500	250 < T ≤ 1200	700 < T ≤ 1300
Pressure (bar)	1	1	1 - 45
Atmosphere (oxidant)	Air	Inert, N_2	Air, O_2, steam, CO_2 or mixtures thereof
Stoichiometric Ratio *	>1 (excess air)	0 (no air)	< 1 (partial air)
Products			
Gas	CO_2, H_2O, O_2 and N_2	H_2, CO, H_2O, N_2 and hydrocarbons`	H_2, CO, CO_2, H_2O, N_2, CH_4 and hydrocarbons
Liquid	-	Pyrolysis oil, carbon black, water	Tars, water
Solid	Ash, slag	Ash, char and coke	Ash, char and slag
* Inherent O excluded			
Reference	(Ansa,2017; Young, 2010; Neuwahl, 2019, 2006 and Couto et al., 2013)		

Thermochemical waste destruction offers a viable solution for both organic and synthetic waste management (Correa et al., 2019). With a growing demand for clean fuels and chemical feedstocks, these methods and technologies have received increasing attention (Materazzi et al., 2014), aligning with efforts to reduce fossil fuel dependency, lower greenhouse gas (GHG) emissions, and manage existing waste streams (Materazzi et al., 2014).Thermochemical decomposition occurs when a substance's decomposition temperature is reached, resulting in condensable and non-condensable volatiles and char (Correa, et al., 2019). The moisture content affects the combustion characteristics of a

material as it absorbs energy (heat) before decomposition and combustion can occur (Sukarni, et al., 2019); it is the most problematic parameter of hyacinth.

Incineration (combustion)

Incineration is an exothermal process, subjecting material to total oxidation in the presence of excess oxygen (air) and occurs in the temperature range of 250<T≤1500 ^{o}C (Young, 2010; (Ansa, 2017). The organic fuel material is converted into a hot flue gas, and the incombustible material into ash, a stable inorganic matter (Ansa, 2017): Gaurav, et al., 2020). Energy can be recovered from the process in the form of heat and electricity (Ansa, 2017). Electricity can be produced at an estimated 20% efficiency, and some mineral and chemical content can also be reclaimed (Ansa, 2017). Incineration is a common waste treatment method and alternative to landfilling waste (Ansa, 2017); Valmundsson & Janajreh, 2011). Incineration reduces waste by up to 75% in mass and 90% by volume (Ansa, 2017). Incineration is also feasible for biomass that has moisture contents <50%, however direct combustion can be ineffective and inefficient (Gaurav, et al., 2020). Pre-treatment of biomass can enhance the process efficiency but will increase overall operational costs (Gaurav, et al., 2020). However, incineration is the most frowned-upon method for the destruction of waste (Young, 2010), since it is associated with high economic and operating costs and air pollution (Ansa, 2017). According to Young, 2010, the total investment of incineration can be 25% higher than pyrolysis, 30.7% higher than conventional gasification and 12% higher than that of plasma gasification. The incineration process requires expensive flue gas clean-up in order to adhere to environmental standards and the produced toxic fly ash requires proper disposal (Valmundsson & Janajreh, 2011). Air pollution from the combustion process contains compounds that should be monitored and measured. These compounds include: particulates, CO, CO_2, HCl, HF, NOx, SOx, organic trace and heavy metals, *i.e*. Cd, Hg, Ni, Pb, Sb, Cr etc. (Ansa, 2017). From the organic compounds, several hydrocarbons produced include: halogenated aromatic hydrocarbons, benzene, toluene, polycyclic aromatic hydrocarbons (PAHs), xylene (BTX), dioxins and furans (Ansa, 2017). Dioxin and furan contain toxic chemical species that are considered both carcinogenic and weaken the immune system (Ansa, 2017)

Pyrolysis

Pyrolysis is the thermal decomposition of organic materials that takes place at a temperature range of 400<T≤1200 ^{o}C, in an oxygen deprived environment (Gaurav, et al.,

2020) and densifies both the mass and energy of a material. The different types of pyrolysis, hydrothermal carbonization and torrefaction, the primary product for each heat treatment and the operating parameters that correspond to the pyrolysis type and product are given in Table 2 (Ansa, 2017). The pyrolysis process is well adapted for the valorization of lignocellulosic materials (Hrabovsky, 2011). Pyrolysis can be split into two stages; 1) devolatilization (dehydration, decarboxylation and dehydrogenation) and 2) heavy compounds are converted into char and gaseous products (Gaurav, et al., 2020). Syngas and char are the main products, and the by-products include oil and tar (Mahlangu, 2009). The production of H_2 or syngas can be maximized with proper control of the process parameters (Hrabovsky, 2011). The char, oil and syngas can all be burnt to produce energy (Mahlangu, 2009).

Table 2: The types of heat treatment and the respective operating conditions for each method

Parameter	Hydrothermal Carbonization	Torrefaction	Slow Pyrolysis	Fast Pyrolysis	Flash Pyrolysis
Temperature Range (°C)	180 - 250	T < 280	400 – 800 400 - 550	400 – 1250 500 - 1250	800 - 1300
Heating Rate	Slow (< 10°C/min)	Slow (< 10°C/min)	0.1 – 1 °C/min (< 10°C/min)	10 – 200 °C/min (>100°C/min)	Very fast (>1000°C/min)
Residence Time	Minutes - hours	Minutes - hours	Minutes - days (for carbonization)	Seconds (0.5-10 s)	Seconds (< 0.5 s)
Particle Size	-	5 - 50 mm	6 - 50 mm	< 1 mm	< 0.2 mm
Primary Product	Stabilized viable feedstock, char	Stabilized viable feedstock, char	Char	(60 – 75%) liquid product (15 - 25%) Solid char (10 – 15%) Non-condensable	Bio-oil, tar products (acids, alcohols, ketones, aldehydes, esters)
Reference	a) (Correa et al., 2019)	b) (Ansa, 2017), c) (Gaurav, et al., 2020), d) (Sikarwar & Zhoa, 2017)			

Gasification

Gasification as a process was discovered by Dean Clayton in 1699 and only implemented in the 19th century for the production of town gas, with the first plant established in London in 1812 (Fabry et al., 2013). In the 1920's cars in Sweden were powered by wood

gasifiers due to the lack in petroleum, and during World War II numerous studies were done to optimize the wood based gasifiers (Sikarwar & Zhoa, 2017). However, after World War II, the gasification process and improving on the process were neglected due to readily available and cheap fossil fuels (Fabry et al., 2013). To generate heat and power, around 40 companies worldwide proposed to build biomass gasification plants in the 1970-1980's (Sikarwar & Zhoa, 2017). Gasification is the partial or total transformation of solid carbonaceous material through thermochemical conversion at high temperatures (Couto et al., 2013; Diaz et al., 2015) and considered an efficient and environmentally friendly method for electricity (Panwar, et al., 2012; Materazzi, et al., 2014; Mahlangu, 2009), or hydrogen-rich synthesis gas production (Materazzi, et al., 2014). Liquid or solid carbonaceous materials, containing mostly of chemically bound C, H and O (Hrabovsky, 2011) go through devolatilization and partial oxidation (Couto et al., 2013) to produce a gaseous fuel (Panwar, et al., 2012). The gasification of biomass is considered as the most efficient and economically viable method to convert lignocellulosic material (Sikarwar & Zhoa, 2017) into syngas. As a feedstock, biomass seems to be more promising than coal due to its low S content and higher reactivity (Panwar, et al., 2012). Gasification processes normally operate at a temperature range of $250 < T \leq 1300\ ^{o}C$ (Couto et al., 2013), where incomplete combustion of carbonaceous material occurs with the addition of a gasifying agent (air, oxygen, or hydrogen (steam)). Gasification can be considered to occur in four stages: drying, pyrolysis, reduction, and oxidation (Couto et al., 2013). Drying takes place at $T \leq 250\ °C$, where water is removed and converted to steam at $100 \geq T \leq 250\ °C$ (Couto et al., 2013). During the pyrolysis stage, volatile matter contained within biomass escapes as gas with increasing temperature, normally at $250 < T < 650°C$ (Sikarwar and Zhoa 2017). The reduction stage is the thermochemical decomposition of the lignocelluloses components of the biomass which leads to the production of char and volatiles (Couto et al., 2013). Finally, oxidation takes place when air is introduced to the reactor and generally takes place at $700 \geq T \leq 1000\ °C$ (Couto et al., 2013). Gasification involves chemical interactions between the different condensable and non-condensable gases, the biomass and the gasifying agent, whereby the resulting raw syngas is mainly comprised of H_2 and CO (Byun et al., 2012; Fabry et al., 2013). The product syngas' composition ratio, heating value, quality and quantity produced depend on the fuel source (type and state of biomass or other waste), mass flow rate, reactor type and operational conditions: temperature, heating rate, oxidizing agent, residence times and pressure (Couto et al., 2013; Sikarwar and Zhoa 2017; Diaz et al., 2015). Prior to going through the purification processes, the crude syngas may also contain low concentrations of CO_2,

H_2O, CH_4 and small amounts of other impurities such as N, S, alkali compounds and hydrocarbons (tars) (Hrabovsky, 2011; Panwar et. el, 2012; Fabry et al., 2013). Hydrocarbons and contaminants such as N_2, Ar, solid carbon particles and ash are present in low concentrations (Couto et al., 2013; Fabry et al., 2013).

Gasification Reactions

The reactions involved in the gasification process are depicted in Table 3. Heterogeneous reactions, R2 - R6, take place within the reactor in the gas-solid phase and homogeneous reactions, R7 – R14 take place in the gas-gas phase (Fabry et al., 2013). In contrast to the heterogeneous reactions, the homogeneous reactions are almost instantaneous at high temperatures (Fabry et al., 2013). The water-gas reaction, R5, Boudouard reaction, R4, and hydrogasification, R6, are independent gasification reactions (Fabry et al., 2013) and most important in gas-solid reactions that occur in gasification (Mazaheri, et al., 2019). These reactions can be reduced to two in the gas phase: the water-shift reaction, R12, which is the combination of R4 and R5, and methanation, R7, which is the combination of R4 and R6 (Fabry et al., 2013). The Water-gas shift reaction is the most important reaction to consider amongst the gaseous reactions (Mazaheri, et al., 2019). Reactions R2 – R6, R8 and R12 – R17 are considered the main reactions, and are all equilibrium reactions except R2 – R3, the oxidation reactions (Fabry et al., 2013 Mountouris et. Al., 2006) and R 13- R17 are added to take tar decomposition into account. Therefore reactions R4, R5, R6, R8 and R12 can be considered the equilibrium reactions, where R8 is favoured in steam gasification (high feed mositure content (Mountouris, et al., 2006; Diaz et al., 2015) and R4 is favoured in air gasification (Mazaheri, et al., 2019).. The reaction rates, the addition of a catalyst and the effect on the tar decomposition in the reactor will determine the final composition of the crude syngas, rather than thermodynamic equilibrium (Fabry et al., 2013). Considering temperature, equilibrium can not be achieved at temperatures significantly below $T \leq 800$ °C, therefore higher temperatures are required and can be readily reached in plasma gasification (Mountouris, et al., 2006). The formation of soot is promoted when either low temperatures or low steam content is present during operation, resulting in reactions R4, R5 and R6 being relevant (Diaz et al., 2015). At high temperatures and high steam fractions, soot (carbon) does not form resulting in the last two reactions R8 and R12 to be dominant (Diaz et al., 2015).

Table 3: The main gasification reactions' name, chemical reaction and enthalpy

Name	Reaction	ΔH°r (kJ/mol)	Reaction Number
Devolatilization			
Fuel + heat → volatiles ($CO+CO_2+H_2+CH_4+N_2$+light hydrocarbons) + tar + char		>0	R1
Heterogeneous Reactions			
Char Combustion			
Oxidation	**$C + O_2 \rightarrow CO_2$**	-394	R2
Partial oxidation	**$C + 1/2\ O_2 \rightarrow CO$**	-111	R3
Char Gasification			
Boudouard reaction	**$C + CO_2 \rightarrow 2CO$**	172	R4
Water gas reaction	**$C + H_2O \rightarrow CO + H_2$**	131	R5
Hydrogenation or hydrogasification	**$C + 2H_2 \rightarrow CH_4$**	-75	R6
Homogeneous Reactions			
Methanation reaction	$CO_2 + 4H_2 \rightarrow CH_4 + 2H_2O$	-165	R7
Methane reforming reaction	$CH_4 + H_2O \rightarrow CO + 3H_2$	206	R8
Steam Reforming Reaction			
Dry reforming reaction	$CH_4 + CO_2 \rightarrow 2CO + 2H_2$	247	R9
Methane oxidation	$CH_4 + 2O_2 \rightarrow CO_2 + 2H_2O$	-283	R10
Methane partial oxidation	$CH_4 + 1/2O_2 \rightarrow CO + 2H_2$	-36	R11
Water gas-shift reaction	**$CO + H_2O \leftrightarrow CO_2 + H_2$**	-41	R12
Carbon monoxide oxidation	**$CO + 1/2O_2 \rightarrow CO_2$**	-284	R13
Hydrogen oxidation	**$H_2 + 1/2O_2 \rightarrow H_2O$**	-242	R14
Tar Reactions (tar assumed C_nH_m)			
Tar partial oxidation	**$C_nH_m + (n/2)O_2 \rightarrow nCO + (m/2)H_2$**	*	R15
Tar steam reforming	**$C_nH_m + nCO_2 \rightarrow (2n)CO + (m/2)H_2$**		R16
Tar dry reforming	**$C_nH_m + nH_2O \rightarrow (m/2 +n)H_2 + nCO$**		R17
Tar hydrogenation	$C_nH_m + (2n-m/2)H_2 \rightarrow nCH_4$		R18
Thermal cracking	$C_nH_m + (m/4)CH_4 \rightarrow (n-m/4)C$		R19
*R16 - R19 is highly exothermic and therefore 200 - 300			
Reference	(Couto et al., 2013 **;** Mountouris, et al., 2006 and Fabry et al., 2013)		

Gasification Reactor Configurations

Presently there are several different types of gasification processes: Rotary Kiln, Moving Grate, Entrained Flow, Bubbling Fluidized Bed, Circulating Fluidized Bed, Updraft Fixed Bed and Downdraft Fixed Bed reactors (Fabry et al., 2013). The three main configurations are the Updraft Fixed Bed, Downdraft Fixed Bed and the Fluidized Bed reactors (Fabry et al., 2013).

Oxidants

Pure O_2 as an oxidant produces syngas with the highest lower calorific value (LCV); however, a high flow rate of pure O_2 on an industrial scale is very expensive (Fabry et al., 2013). Air as oxidant and O_2 source, leads to a large fraction of N_2, diluting the syngas due to the excess nitrogen contained in the air and results in the product syngas to have a lower LCV (Fabry et al., 2013; Diaz et. el., 2015). Steam as oxidant is generally preferred as all the desired reactions take place and it leads to a syngas with a higher H_2 content. When compared to air gasification, the H_2 yield through steam gasification can be three times higher. This is due to steam converting the residual carbon and tar yields to syngas through gasification, water–gas shift, and reforming reactions (Sikarwar and Zhoa 2017).

Hydrocarbons (tars)

Hydrocarbons are produced during thermochemical conversion from organic matter, and refers to a complex mixture of, heavy, condensable, organic compounds which have a molecular weight higher than that of benzene C_6H_6 (Fabry et al., 2013; Materazzi, et al., 2014) and mixed oxygenates (Hrabovsky, 2011; Materazzi, et al., 2014). The difference in tar quantity and the nature of the tar mixture can be defined as a function of the processing conditions, the technology applied, and the nature of the waste feed material (Fabry et al., 2013; Materazzi, et al., 2014). For the gasification of biomass, the amount of tar produced, 1–10%, and the performance of the cleaning process are the main influencers for technical feasibility and economic viability (Fabry et al., 2013). The design and operation of a reactor need to ensure adequate control of reaction conditions, as such, the presence of tar constituents which are an indicator of overall reactor design and performance (Fabry et al., 2013). In any industrial gasification process, high levels of tar are deemed the most problematic parameter (Fabry et al., 2013; Materazzi, et al., 2014). It is problematic in downstream processes such as catalytic stages for hydrogen separation or chemical synthesis, tars damage end-use devices due to problems associated with condensation, tar aerosol formation and to polymerization (Materazzi, et al., 2014). Tar constituents should be reduced, converted, or destroyed in the gasification process (Fabry, et al., 2013). Tar removal is achieved through physical processes, and tar conversion is achieved through thermochemical and catalytic processes (Fabry et al., 2013; Materazzi, et al., 2014). Different methods to reduce the tar levels are available and must have a high tar removal efficiency, be economically feasible and environmentally acceptable, and not affect the formation of useful gaseous products (CO and H_2) (Materazzi, et al., 2014). These methods include steam, partially oxidative, thermal,

catalytic and/ or plasma processes, where the decomposition of tar can be divided into two methods, primarily the decomposition of tar occurs inside the reactor and secondarily downstream of the reactor (Fabry et al., 2013). Rather than consequent loss of syngas due to the removal of tars from the syngas, the ideal process aims at a high tar conversion rate within the gasification process itself (Materazzi, et al., 2014). The decomposition of tar inside a reactor is accomplished through optimizing the process parameters, *i.e.* temperature, pressure, oxidizing agent to waste ratio, and residence time, by adding a catalyst or by means of plasma gasification (Fabry et al., 2013). Thereby the decomposition of tar inside the reactor is achieved by catalytic or thermal cracking (Materazzi, et al., 2014). Thermal plasma, as a reforming agent, completely decomposes the input feed into a tar-free and H_2 rich gas, and an inert, environmentally stable, virteous material (Materazzi, et al., 2014). The effect that the operating parameters have on the tar constituents contained in the crude syngas and reactor are as follows: High temperatures minimize the tar quantity and destroys aromatics without the addition of a catalyst (Fabry et al., 2013), at T ≥ 1000°C and reasonable residence times refractory unsubstituted aromatics are destroyed (Materazzi, et al., 2014). Due to thermal decomposition at high temperatures, preheating the gasification agent reduces the tar content significantly (Fabry, et al., 2013). The influence of temperature on the conversion and physicochemical transformation of tar, which occurs during gasification, can be seen in Table 4.

Table 4: The decomposition of tar by increasing temperature for waste

Temperature (°C)	**Tar (dry wt %)**	**Process**	**Hydrocarbon Type**
400	24	Primary	Primary vapours (H_2O, CO_2, CO)
450	31		
500	38		Paraffines, light hydrocarbons and mixed oxygenates
550	40		
600	35	Secondary	Olefins, armoatics, phenols
650	27		
700	20		Phenols, PAHs, C_2H_2, CO, CO_2,H_2O, H_2
750	15		
800	14		
850	12	Tertiary	
900	9		Aromatics, CH_4, CO, CO_2, H_2O, H_2, Soot
950	7		
1 000	<5		
Reference		(Materazzi, et al., 2014)	

The temperature that delivers the maximum tar conversion depends on the chemical structure of the waste and parent substrate (Materazzi, et al., 2014). Therefore depending

on the waste, a slight deviation might occur from that presented in Table 4. Above the maximum tar yielding temperature, gas yield rises while tar amount decreases: suggesting cracking is taking place (Materazzi et al., 2014). To optimize tar reforming at high temperatures, catalysts, *i.e.* dolomite, olivine sand, limestone, lanthanum, alumina, aluminate, nickel, cobalt and natural clay minerals and iron minerals ca be utilized (Fabry et al., 2013). Other parameters such, as the residence time, have little influence on tar level; however, it does have a significant impact on the tar composition, whereas the increase in oxidant ratio results in a decrease in the tar yield (Fabry et al., 2013). As a parameter, pressure can be directly related to the formation of tar and can be attributed to the formation of naphthalene (Mayerhofer, et al., 2012) and increasing pressure is indirectly related to the decomposition of tar (Tuomi, et al., 2015). Auto thermal processes deliver a gas output with a tar content exceeding 1000 ($\frac{mg}{m^3}$), whereas thermal plasma processes deliver a gas output with a tar content in the order of 1 ($\frac{mg}{m^3}$) (Fabry et al., 2013). Since the tar content for plasma gasification is 1000 times less, the cleaning of the syngas downstream will be less costly and tar concentration requirement for biofuel production of 0.1 ($\frac{mg}{m^3}$) can be readily obtained (Fabry et al., 2013). The product gas from low temperature gasification processes, produce CO, H_2 and CH_4 as the main energy containing products (Hrabovsky, 2011). Typically, 50% of the energy is contained in the CO and H_2 gas, the rest is contained in the CH_4 and any other higher aromatic hydrocarbons produced (Hrabovsky, 2011). The quality control of the produced syngas' composition is limited due to the dilution by CO_2 through the partial oxidation that takes place at these process conditions (Hrabovsky, 2011). Waste materials that form are usually discarded in landfills which are an environmental concern (Young, 2010). Due to technical limitations, gasification of high moisture-containing biomass is ineffective by conventional gasification technologies (Sikarwar and Zhoa, 2017), as the steam reforming reaction requires temperatures of 800<T<1430 °C (Fabry et al., 2013). At the low operating temperatures, the generally used thermal processes cannot decompose the materials fed sufficiently and the product gas will contain soot, tar and char (Mountouris, et al., 2006). Given the technical limitations of general auto thermal processes, plasma gasification is considered as one of the best alternative processes to produce a syngas that has both a high purity and high LCV (Fabry et al., 2013).

2.2 Plasma Gasification

2.2.1 Introduction and Background

Plasma is known as the fourth state of matter (Valmundsson & Janajreh, 2011; Diaz et al., 2015) and can be defined as a collection of free-charged particles, a quasi-neutral gas, consisting of both charged and neutral particles that is on average electrically neutral moving in random directions, and which exhibit collective behavior (Byun et al., 2012; Diaz et al., 2015). When gaseous molecules and charged electrons are forced into high energy collisions it results in the plasma state (Valmundsson & Janajreh, 2011). Thermal plasma is generated when an electric current is passed through gas, utilizing the gas's electrical resistive nature to dissipate energy, leading to high temperatures (Valmundsson & Janajreh, 2011). Plasma is classified into either non-thermal or thermal plasma. Classification is done according to the degree of ionization that occurs in the atoms, and the temperature difference between heavy particles and electrons (Byun et al., 2012). The presence of active species, *i.e.* radicals, charged particles, electrons, ions, and excited atoms and molecules, results in the high chemical activity of thermal plasma (Diaz, et al., 2015). The high chemical activity reduces the number of larger molecules by breaking the chemical bonds in biomass, generating small molecules such as H_2, CO, CO_2 and CH_4 (Diaz, et al., 2015). Since electrically generated, thermal plasma can reach temperatures of $T \geq 10{,}000$ °C (Byun et al., 2012), and electron ejection occurs at high enough temperatures, resulting in an ionized gas stream (Valmundsson & Janajreh, 2011). It is thus a thermal process that takes place in a partial oxidizing environment and at high temperatures (Valmundsson and Janajreh 2011). Thermal plasma gasification incorporates a hot plasma with a general temperature range of $4000 \leq T < 7000\ ^{o}C$ (Young, 2010). The O_2 within the system is strictly controlled and gasification occurs after the material has gone through a pyrolysis step, producing tar and char when incomplete oxidation takes place (Byun et al., 2012; Fabry et al., 2013). The produced tar and char then decompose into elemental components during gasification (Byun et al., 2012; Fabry et al., 2013), since chemical bonds are essentially destroyed by the extreme temperatures of the plasma (Janajreh et. el., 2013), and therefore limiting the tar amounts in the produced syngas. The organic fraction is completely decomposed into its constituent elements and the inorganic fraction results in a vitrified, non-leachable slag (Valmundsson and Janajreh 2011; Byun et al., 2012; Janajreh et. el., 2013). Thermal plasma has received attention as a waste treatment method, addressing the contemporary problem of

increasing environmental pollution problems associated with waste and waste management (Byun et al., 2012). Plasma processes were developed during the 19th century to provide high temperature furnaces for the metalworking industry (Fabry et al., 2013). During the early 20th century, plasma processes were used to produce acetylene (C_2H_2) from natural gas in the chemical industry (Fabry et al., 2013). Since the early 1980's thermal plasma processes are considered highly effective for the treatment of municipal wastes, hazardous and toxic waste materials such as asbestos, radioactive waste and chemicals (Fabry et al., 2013), other solid nuclear waste, air pollutant control (APC) residues and medical wastes (Byun et al., 2012). Thermal plasma technology has also been incorporated in varied industrial applications which include: cutting, welding, spraying, mass spectroscopy, powder spheroidization, metallurgy, nano-sized particle synthesis and waste treatment (Byun et al., 2012). Thermal plasma technology is considered one of the most probative technologies for waste gasification (Fabry et al., 2013) and shows great potential as an effective waste-to-energy method, for solid waste treatment and energy recovery (Valmundsson & Janajreh, 2011). A wide range of materials can be utilized as feedstock (including solids, liquids, and gases) and result in near destruction of any kind of waste due to the high temperatures (Valmundsson & Janajreh, 2011). There are three kinds of thermal plasma processes for solid waste treatment (Byun et al., 2012):

1. Pyrolysis - the pyrolysis of gaseous, liquid, and solid waste in a thermal plasma furnace in the absence of O_2 with plasma torches.
2. Gasification – the gasification of solid waste containing organic compounds, in an O_2 starved environment, to produce syngas (H_2 + CO).
3. Vitrification – the vitrification of solid wastes by transferred, non-transferred, or a hybrid arc plasma torch which is determined by the electrical conductivity of the substrate.

Thermal plasma has the advantage of, and is characterized by, high energy density and high temperatures (Valmundsson & Janajreh, 2011), resulting in substantially lower plasma flow rates to be required, to supply efficient amounts of energy for the conversion of carbonaceous material into syngas (Hrabovsky, 2011). The high radiation intensity and active species increase the rate of reactions which allows otherwise hard to achieve reactions to take place (Janajreh, et al., 2013). Traditional processes that incorporate burning fossil fuels operate at an upper temperature limit of $T \leq 2{,}000$ °C (Byun et al., 2012). Chemically, thermal plasma advantageously accelerates the kinetics and improves high temperature cracking of impurities contained in the syngas (Fabry et al., 2013). The

high operating temperature, the high energy density of the plasma and the fast reaction time allows a higher throughput with a smaller reactor size, and compared to conventional combustion processes, thermal plasma reactors produce less gas stream volume since combustion itself is absent (Janajreh et. el., 2013; Byun et al., 2012). Thermodynamically, plasma provides enthalpy that can be manipulated by timing the electrical power supplied, resulting in process independence from the O/C ratio and the nature of the plasma medium (reducing, oxidizing or neutral atmosphere) (Fabry et al., 2013). Due to the steep temperature gradient that exists in the reactor, the reformation of pollutants, such as dioxins and furans, can be minimized by quenching the gas exiting the reactor (Janajreh, et al., 2013). Due to the high heat flux densities at the reactor boundaries, steady state conditions, fast start-up and shutdown are modifiable and obtained without compromising the refractory performance (Janajreh, et al., 2013).. The high electric power usage of the plasma torch and the low operational pressure of the reactor are considered the main disadvantages of the thermal plasma process (Valmundsson & Janajreh, 2011; Janajreh et. el., 2013). The thermal plasma process is considered environmentally friendly and a closed treatment system, due to the fact that controlled disposal is not required (Hrabovsky, 2011) and minimal air pollutants are produced (Byun et al., 2012). Due to the energy recovery and reduction of waste volume, gasification and vitrification are the two thermal plasma processes considered for the treatment of solid wastes (Byun et al., 2012). The main outcome of using thermal plasma is the production of fuel rather than merely waste decomposition alone, and therefore an energy balance of the process is important (Hrabovsky, 2011).

2.2.2 Fundamental Processes

A plasma gasification plant consists of a number of unit processes and for each process to efficiently connect with the other, total process control and safety management is necessary (Byun et al., 2012). Based on the two fundamental systems of total process control and safety management, the following systems are put in place: waste treatment, feeding system, plasma torch, power supply, plasma reactor or furnace, waste heat recovery, slag handling equipment, power generation, gas emission control and syngas utilization, monitoring and control systems (Byun et al., 2012; Janajreh et. el., 2013). The plasma gasification process typically consists of a reactor chamber that is connected to a plasma torch that produces the plasma (Valmundsson & Janajreh, 2011; Janajreh et. el., 2013) and a power supply using AC or DC power, a gas supply for the arc, gas supply of the oxidant, and control and data acquisition equipment (Byun et al., 2012; Surov, et al.,

2017). The chamber is made of refractory materials enabling it to tolerate the high temperature associated with plasma gasification (Janajreh, et al., 2013). As the waste enters the reactor, the thermal plasma decomposes it into a gas and a molten slag stream. The gas stream results in the form of syngas which mainly consists of CO and H_2 and trace amount of pollutants (Janajreh et. el., 2013). The syngas is cleaned and subjected to heat recovery (Janajreh et. el., 2013). The reactor chamber includes a metal and slag collection point at the bottom (Byun et al., 2012; Valmundsson & Janajreh, 2011). A fan is incorporated to generate sub atmospheric pressure in the entire system (Byun et al., 2012). The entire process is monitored and controlled, ensuring optimal performance with regard to the temperature, plasma power, feeding rates and slag removal (Janajreh, et al., 2013).

i) Pre-treatment and Feeding System

Pre-treatment generally involves drying, crushing, milling or grinding of the material prior to being fed to the reactor (Byun et al., 2012; Janajreh et. el., 2013). When working with wastes that have high moisture content, the heating value of the feed is increased by either installing a burner to dry the material or by adding additives like coke to aid in the gasification process (Byun et al., 2012).

ii) Plasma Torch

Two control parameters of the plasma gasification process are the plasma gas, by which the reaction environment can be manipulated, and the torch power, by which the reactor temperature can be regulated since it is an independent heat source (Janajreh et. el., 2013). To generate a plasma column, two arc attachment points are required, one located at the solid gas interface, the cathode electrode, and the other at the gas solid interface, the anode electrode (Byun et al., 2012). Resistance from the plasma is used to convert electricity into heat energy (Byun et al., 2012). Eorosion occurs when elevated temperatures encountered at the attachment points exceed the melting point of the materials used, resulting in vaporization of the electrode material. Water cooling is implemented to minimize the rate of vaporization to extend the life cycle of the electrodes (Byun et al., 2012).

Thermal plasma can be obtained by either of the following methods:

- Arc discharges: DC or AC
- Frequency/wave: RF or MW

RF and MW plasmas do not have electrode erosion, as does the arc discharges, but have lower energy efficiencies. RF/MW plasma have an energy efficiency of 40 – 70 % and arc torches have an energy efficiency of up to 60 - 90 % (Fabry et al., 2013). The varying characterization of plasma torches depend on the whether the plasma is in local thermodynamic equilibrium (Diaz et al., 2015). Arc plasma torches are classified according to electrode geometry as a rod or well type cathode (Byun et al, 2012). The electric arc can be generated by either a DC or AC plasma torch, where the downside to DC torch is considerable erosion of the electrodes, especially the cathode. The AC torch generators have a longer life cycle, since each electrode is an anode and cathode alternatively, however an AC torch is more difficult to produce (Surov, et al., 2017). A low current and high voltage drop increases the torch life cycle (Rutberg, et al., 2013). In this study a DC arc will be utilized. The DC plasma arc generates plasma; a gaseous electrical conducting element, as an electrical discharge is created between two electrodes, and plasma gas flows between them (Byun et al, 2012; Valmundsson & Janajreh, 2011). The ionized plasma gas flows beyond the two electrodes, resulting in a hot, high energy density plasma jet (Valmundsson & Janajreh, 2011). In DC plasma torches, high collision frequencies lead to local thermodynamic equilibrium for thermal plasmas (high energy density plasmas) (Diaz et al., 2015). In thermal plasma, the kinetic energy of the involved particles, i.e. electrons, ions, and neutral gas, can be described using a single temperature value (Diaz et al., 2015). The DC plasma arc is generated and maintained through a combination of electrical and mechanical stabilization mechanisms built into the plasma torch hardware (Byun et al., 2012). DC plasma arcs can suffer from fluctuations due to the undulation of 3-phase rectified power supply, arc voltage and current variations, radiation, and acoustic pressure effect (Diaz et al., 2015). Thermal plasma torches are categorized into transferred and non-transferred types based on whether the arc is directly attached to a substrate or not (Valmundsson & Janajreh, 2011). The DC torch can either be a transferred arc type, which has one electrode inside the torch and the other outside, or a non-transferred arc type, where both electrodes are inside the torch body. Non-transferred arc torches are usually water-cooled to reduce erosion from high temperatures. However, the water cooling can affect efficiency. (Valmundsson & Janajreh, 2011). There are three torch configurations used in the thermal plasma process (Byun et al., 2012):

- The torch is positioned at the top of the reactor, while the reactor itself has an ash recovery area at the bottom. The feed material is injected near the plasma plume,

and this material can be solid, liquid, derived from a pyrolysis process, or in crushed form.

- The torch is located close to the inorganic compound catchment area, and it is mainly used for industrial processes that discard wastes like asbestos or radioactive wastes to enhance the melting of the inorganic faction contained in the waste, the plasma torch can be installed at the bottom of the reactor.
- A hybrid process incorporating plasma technology integrated with another thermal processing technology where the auto thermal zone, pyrolysis zone and the plasma zone, reduction zone, are separated. The process is similar to a two-stage gasifier, where syngas tar concentration is reduced in the thermal plasma zone. Two stage gasifiers can reduce the tar content up to forty times compared to a single stage gasifier with the same operating conditions. Plants that incorporate this technology include: CHO power, Plasco Energy group and AlterNRG.

Thermal plasma characteristics, *i.e.* the plasma flame volume, the input power, the velocity distribution, the range of temperatures, and the chemical composition, can be customized to suit specific applications (Byun et al., 2012).

iii) Plasma Reactor

Multiple designs for plasma gasification reactors exist, but typically, a plasma gasification reactor consists of a reactor chamber; imbedded with a plasma torch that supplies the energy required for gasification (Valmundsson & Janajreh, 2011). The plasma reactor or furnace is a type of vertical shaft, generally used in metal foundries, where the solid waste is introduced from the top of the plasma reactor (Byun et al., 2012). Appropriate refectory lining is used internally that enables the reactor to withstand diffused and convected heat (Valmundsson & Janajreh, 2011) of temperatures ($T > 1200°C$) resulting from the plasma torch, corrosive operating conditions and reactions that take place within the reactor (Byun et al., 2012). A new concept is adding a second combustion chamber to allow for sufficient residence time to ensure complete reaction and gasification (Byun et al., 2012).

iv) Heat Exchanger

A heat exchanger is installed to quench the produced gas before it is purified. The heat recovered from the gas can be used to warm other systems or to power a steam turbine to produce energy (Byun et al., 2012).

v) Gas Purification

Depending on the waste utilized, the implementation of the following purification measures can vary for the gas stream: A water quench chamber to remove dioxins and furans, a scrubber for the removal of acidic gases and a hydrogen sulfide absorber (Byun et al., 2012). For particle removal a cyclone or bag house, high efficiency filters and/or precipitators for small particulates are implemented (Byun et al., 2012). An activated carbon filter is used to remove heavy metals (Byun et al., 2012). Non-catalytic reduction and selective catalytic reduction, typically used for removing NO_x emissions, are not required for plasma gasification because the O_2 starved process does not emit NO_x emissions. (Byun et al., 2012).

vi) Slag Collection and Treatment

The reactor chamber includes a metal and slag collection point at the bottom. The molten slag can be periodically or continuously tapped/removed (Janajreh, et al., 2013). The slag can be quenched in water, where it forms granules that can be reused, for further processing or disposal. The slag can also be cast into molds to create ingots or bricks, valorizing the slag as a recycled material (Byun et al., 2012; Valmundsson & Janajreh, 2011; Janajreh et. el., 2013).

vii) Electricity Generation

Steam turbines can be implemented to generate electricity by combusting syngas to produce steam, which in turn is injected in a steam turbine (Byun et al., 2012; Janajreh et. el., 2013). Alternatively, a gas turbine can be implemented where gas purifiers and compressors will be required along with additional equipment (Byun et al., 2012; Janajreh et. el., 2013).

viii) Other Products

Plasma gasification can be integrated with other technologies to recover energy from the produced syngas, this includes: IGCC (Byun et al., 2012), in the Fischer-Tropsch process for the production of liquid fuels, in a gas turbine or a fuel cell in the production of electricity and to produce chemicals such as NH_3, CH_4 and H_2 (Byun et al., 2012; Fabry et. el., 2013). High value chemicals can be produced by implementing chemical processes and manipulating operating parameters. Chemical wax can be produced by implementing the Ficher-Tropsch process, CH_4 can be produced through utilizing the methanization process and H_2 can be generated by introducing more steam or moist feed into the

system and used in fuel cells. Integrating these processes with the plasma gasification process can widen its applicability (Byun et al, 2012).

2.2.3 Process Performance

The plasma gasification process is subject to performance variability where the main sources of process variations can be attributed to (Diaz, et al., 2015):

- Flow rate fluctuation due to feedstock size and composition variability.
- A back pressure that reduces the arc discharge length due to the non-uniform expansion of gases inside the reactor.
- Electrode consumption rate variability.
- Irregular residence times.
- Thermochemical decomposition rate and syngas production variability, due to changes in temperature inside the reactor.

Chemical Conversion

The various reactions that take place during plasma gasification are the same as the reactions illustrated in Table 3 ascribed to the gasification process. The mass ratio of H_2 in the syngas (H_{syn}) per total mass of H_2 introduced to the system (H_{input}) is defined as the H_2 yield. Similarly, the mass ratio of C atoms in the produced CO (CO_{syn}) per the total mass of C originally contained in the waste or biomass (C_{waste}) (Fabry et al., 2013). The H_2 and CO yield presented below as equations, Eq 1 and Eq 2, and are directly related to the composition of the waste, oxidizing agent and the feed materials moisture content (Fabry et al., 2013).

$$H_2 yield = \frac{H_{syn}}{H_{input}} \qquad \text{Eq 1}$$

$$CO\ yield = \frac{CO_{syn}}{C_{biomass}} \qquad \text{Eq 2}$$

The carbon conversion efficiency (CCE) can be obtained by replacing the ratio of C in the product syngas (C_{syn}) with CO_{syn} (Diaz et al., 2015). The CO yield provides information on the conversion rate, the mass balance and the gasification performance. The H_2 in the crude gas is directly related to the oxidizing agent injected and the initial water content in the waste feed (Fabry et al., 2013). The cold gas efficiency (CGE) is determined by the proportion of the chemical energy contained in the syngas to the combined sum of the

chemical energy in the fuel and the electric power consumed by the plasma torch (Agon, et al., 2016). Where the mechanical gas efficiency is defined as the ratio of the chemical energy content in the generated syngas to the chemical energy present in the fuel (Agon, et al., 2016). The (CGE) and (MGE) are given in Eq 3 and Eq 4 respectively (Agon, et al., 2016) as follows:

$$CGE = \frac{LHV_{syn}F_{syn}}{LHV_{WHW}\dot{m}_{WHW} + P_{plasma}} \qquad \text{Eq 3}$$

$$MGE = \frac{LHV_{syn}F_{syn}}{LHV_{WHW}\dot{m}_{WHW}} \qquad \text{Eq 4}$$

Where LHV_{syn} is the LHV of the syngas, F_{syn} is the flow rate of the syngas (kg/h), $\dot{m}_{WHW}$ is the WHW mass flow rate (kg/h) and P_{plasma} is the torch power input

Reactor Performance Parameters

High process efficiency can be attributed to low moisture content, a high syngas flow rate, a high syngas CV compared to the feedstock and low torch energy consumption (Janajreh, et al., 2013). Different gasification reactor parameters used to evaluate performance of a plasma gasification system, *i.e*., waste pretreatment, feedrate, LCV_{waste}, LCV_{syn}, P_{gas} (bar), $P_{reactor}$ (bar), $T_{reactor}$ (°C), T_{gas} (°C), oxidant type, the equivalence ratio (O:C), steam to carbon ratio (H_2O:C), CO yield, H_2 yield, P_{plasma} (kW), CCE, PSR (plasma power to syngas production ratio), and the type of plasma gas is used (Fabry et al., 2013; Kuo et al., 2020).

2.2.4 Plasma Gasification as a Waste-to-Energy Process

Plasma gasification has been incorporated as a method to dispose, treat and valorize a wide variety of wastes, and is currently in the commercialization stage for feedstocks (such as municipal solid waste (MSW), industrial waste, ash residues, biomass and low grade coal), to produce high valued (HCV>20 MJ/kg) syngas at low operating costs (Marquesi, et al., 2015). The physical and chemical changes, which occur during the gasification of biomass, are like carbonaceous decomposition that takes place during a thermochemical process (drying, devolatilization, fissuring, heat conduction, densification, and fragmentation) (Asfar, 2014). To evaluate different materials and waste as potential feedstock for plasma gasification systems, and gain insight into the best suited gasification parameters, a van Krevelen diagram can be plotted which illustrates: 1) the

elemental characteristics of a material, and 2) depicts change in physiology due to the loss or gain of integral amounts of elemental composition (Poudel, et al., 2018). As the amount of H and O decreases, the relative amount of C increases (Poudel, et al., 2018). A higher O content indicates that a lower amount of oxidizing agent is necessary for the gasification process and air, as oxidizing agent, is preferred to reach operating temperatures (Janajreh, et al., 2013). As the H_2O content increases so does the O:C and H:C ratios; the ratios depend on waste type and sample preparation method, such as torrefaction, which decrease the H:C and O:C ratios (Poudel, et al., 2018). The H_2O in the product gas is directly proportional to the H_2O concentration in the feedstock, while the CV of the gas is inversely proportional to the H_2O concentration. Additionally, the H_2 concentration in the product gas increases when steam is utilized as an oxidant (Janajreh, et al., 2013). The electrical energy requirement on the plasma torch has been reported to be directly proportional to the amount of moisture in the process, whether due to a high steam or initial moisture content in the feedstock (Janajreh, et al., 2013). When steam is used as oxidizer, higher fractions of H_2 is generated and more O_2 will become available for conversion to CO, however, more electrical energy will be drawn by the torch due to the absorbed latent heat of evaporation (Janajreh, et al., 2013). Three plasma gasification case studies are evaluated: 1) the effects of oxidant type (steam and air) on the syngas composition based on the type of feed, input plasma energy and process efficiency, 2) the effects of torrefaction on the biomass, of ER, S/C and CO_2-to-carbon ratios on the syngas yield, syngas LCV and PGE were analysed (Kuo et al., 2020), and 3) Steam gasification of biomass using a two stage plasma gasification process (Diaz, et al., 2015).

Case study 1: In a study by Janajreh, et al., 2013, the organic fraction is modeled as a non-stoichiometric, chemical equilibrium that is solved by using Gibbs free energy minimization methods and the inorganic fraction is modeled as an inert non-conventional and non-reacting solid stream. The model was verified using experimental values and the applied to different feedstocks: RTC coal, tire, MSW, low ash algae, treated wood, untreated wood, pine needles and plywood, where the ultimate and proximate composition and CV of the feedstocks represent the model inputs (Janajreh, et al., 2013). The waste material was chosen as to represent a wide range of solid waste available (Janajreh, et al., 2013). The plasma gasification process model parameters were as follows: a single-stage plasma gasification with air and steam as oxidant, the plasma gas to feedstock mass ratio of 0.782:1, $T_{injected\ gas}$ = 4000°C, $T_{reactor}$ = 2500°C, DC torch with 86% efficiency, T_{syn} = 1000°C (Janajreh, et al., 2013). The simulation results obtained for the syngas yield, CV_{syn}, flowrates, torch energy requirement, reactor outlet temperature

and gasification efficiency for both plasma and air gasification were compared (Appendix E.2, Table E.2.1 and E.2.2). The maximum gasification efficiency was obtained when complete carbon conversion was obtained and the organic part of the feedstock was completely gasified (Janajreh, et al., 2013). The energy required for gasification was supplied by the plasma torch for plasma gasification and the combustion reaction in conventional gasification. Due to this, both instances delivered a low CO_2 concentration whereas plasma gasification delivered a negligible amount of CO_2 (Janajreh, et al., 2013). Tire waste showed incomplete gasification with solid carbon still present, and for maximum efficiency, 100% steam as plasma gas had to be used. However, due to reactor temperature constraints, insufficient steam could be injected which resulted in the incomplete gasification of the feedstock (Janajreh, et al., 2013). Low inherent H_2O content resulted in low H_2O content in the syngas, such as was the case for both RTC coal and tire waste. Even though these two feedstocks are similar in composition, the syngas yield varied due to the amount of plasma gas injected (Janajreh, et al., 2013). RTC coal had a maximum efficiency; a total conversion of carbon, when 70% steam-to-air ratio was injected (Janajreh, et al., 2013). The syngas from both tire waste and RTC coal had a high CV value due to high amounts of steam injected as oxidant, resulting in H_2 rich syngas. The CV values for these two waste types were higher than the other wastes but the efficiencies are on the same level due to the high energy demand of the torch when steam was used as oxidant (Janajreh, et al., 2013). Due to the high amount of ash in MSW waste, the mass flow of syngas was decreased and thereby the efficiency also. The high H_2O content in algae results in it delivering the lowest efficiency, due to large amounts of heat being absorbed from the plasma. High torch power and plasma gas flow requirement, to complete the gasification process, yield low efficiencies such as in the case for plywood (Janajreh, et al., 2013). High plasma gas (N_2) input also diluted the syngas, lowering its CV value (Janajreh, et al., 2013). A high efficiency is obtained as a result of low inherent H_2O content, when $CV_{syn}>CV_{waste}$, high syngas flow rates and low torch energy consumption (Janajreh, et al., 2013). The efficiency for plywood was the highest for all the waste types evaluated, *i.e.* 47%, followed by MSW and tire (Janajreh, et al., 2013).

Case study 2: According to (Diaz, et al., 2015) a two-stage plasma gasification process was applied to a variety of biomass types to obtain experimental data for hydrogen production. The experimental results were compared to a mathematical thermodynamic model. The reactor consists of two separate reactors coupled together; the first stage was an electrolytic cell with the purpose of generating steam (Diaz, et al., 2015). The generated steam (and a small fraction of non-condensable gases) was sent to the second reactor as oxidizing agent. The second reactor was fitted with a DC electrical arc, and the discharge was put in contact with biomass (Diaz, et al., 2015). The plasma power (35 kW each) that allow a maximum voltage 380 V and current 150 Amps was used (Diaz, et al., 2015), and the power input for the first reactor was 11-12 kW and for the DC arc was 13 - 25 kW. The steam flowrate was between 10-12 kg/h, and the resulting syngas temperature 600–900 °C was obtained (Diaz, et al., 2015). The chemical composition and energy content of six different types of biomass were analysed (Diaz, et al., 2015) (Appendix. E.1, Table E.1.3). An average feed rate of 3.5 kg/h and LCV of 20.4 MJ/kg were fed to the steam plasma gasification process and resulted in high fractions of H_2 gas, with the average syngas mol% values of the 6 biomass species: 59.3% H_2, 12.9% CO, 20.3% CO_2, 3.3% CH_4, 3% N_2 and 0.7% O_2 with a LHV_{syn} of 9.4 MJ/kg. An average of 10.2 kWh/kg, a 58.7% conversion , and 41.6% efficiency can be seen for the process (see Appendix. E.2, Table E.2.3) (Diaz, et al., 2015). Low quantities of higher hydrocarbons, *i.e.* ethane, propane, butane, pentane, and hexane, with fractions < 0.4% were produced by the steam plasma gasification process (Diaz, et al., 2015). Increasing the biomass feed rate did not translate into a significant H_2 increase. However, increasing the feed rate without either adding more oxidizer or increasing the power from the plasma torch, will decrease the conversion rate and result in the production of biochar (Diaz, et al., 2015). The excess (unreacted) steam can be utilized to preheat first reactor's input stream, therefore inhibiting the loss of heat energy and increasing the efficiency of the overall system (Diaz, et al., 2015).

Chapter 3 Hyacinth Preparation and Characterization

3.1 Materials

N_2 (99.9%) and dry air (99.9%) were used in the TGA analysis and supplied by Afrox.

3.2 Sample Preparation

Sample

Water hyacinth was harvested manually, on the 5th of September 2019, on the North-Western banks of the Hartbeespoort Dam in the North West Province, South Africa. Roughly 500 kg fresh hyacinth were harvested. Once harvested, the hyacinth was placed outside on sloped, concrete slabs that provided a relatively clean surface to dry. The area was shielded from all sides, limiting dust contamination. The hyacinth was left uncrushed and allowed to dry atmospherically for 5 weeks. The drying process is depicted in Figure 1. Picture (a) shows the freshly harvested hyacinth on day 0, (b) shows the hyacinth after being manually turned, allowing the material at the bottom to dry, on week 2, and (c) shows the dry hyacinth on week 5. A total of 125 kg dry mass was obtained after drying.

Figure 1: The drying process for the harvested hyacinth. (a) day 0, (b) 2 weeks and (c) 5 weeks

Sample Preparation

A 2 m^2 area of the dried bulk sample was sectioned out and separated into the three main physiological parts, which is shown in Figure 2. Picture (a) the roots (WHR), (b) the stems (WHS) and (c) the leaves (WHL). Due to the brittle nature of the dry hyacinth, handling of the material was kept to a minimum. The separated samples and bulk material were stored separately, and transported to the NWU labs to be weighed and prepared for further analysis. A TRF600 Trapp hammer-mill was used to reduce the particle size of samples WHR, WHS, WHL and whole hyacinth WHW, the samples were then reduced

further for TGA analysis to a particle size ≤ 10 mm. The samples were then cone and quartered for proximate and ultimate analysis. The rest of the sample bulk was placed in polypropylene woven bags, each full bag weighing between 4.5 – 6.5 kg and transported to the NECSA sight.

Figure 2: Hyacinth structurally consist out of three parts (a) roots, (b) stems and (c) leaves

The bulk of the dried hyacinth was prepared for the plasma gasification process. In total, roughly 73 kg were chipped using a Muffin Monster Model 3000 chipper, to reduce the particle size to <70 mm, Figure 3: (a). After the hyacinth was chipped, the cone and quarter method was applied to the bulk sample and the remaining quarter was sieved; the gasification system requires a particle size >4.5 mm to prevent smaller particles <4.5 mm from causing problems downstream. The oversized particles >70 mm were handpicked from the sample to prevent and minimize clogging, and retrained material 4.5 mm<WHW<70 mm, is shown in Figure 3(b).

Figure 3: (a) Bulk sample, (b) Final sample

The prepared, bulk, hyacinth material (WHW) was then stored in polypropylene woven bags and used for XRF analysis, and used as the feedstock for the PlasWEn experiments to simulate industrial application. The undersized material was discarded. The difference in chemical characterization between the hyacinth and its parts was analysed and reported in the following sections.

3.3 Experimental Method

Proximate Analysis

Proximate analyses were conducted, at Bureau Veritas, on the hyacinth samples (WHW, WHR, WHS and WHL). The sample was prepared using the standard procedure based on ISO 13909-4:2001. The moisture content (%) was determined based on the ISO 11722:1999 standard, the ash yield (%) was determined based on the ISO 1171:2010 standard and the volatile matter content (%) was determined based on the ISO 562: 2010 standard. The Fixed carbon (%) was determined by difference.

Ultimate Analysis

Ultimate analyses was conducted, at Bureau Veritas, to determine the chemical composition of the hyacinth samples (WHW, WHR, WHS and WHL), determining the C, O, H, N and S content. The sample was prepared using the standard procedure based on ISO 13909-4:2001. The total S was determined based on the ISO 19579:2006 standard, The O was determined by difference and the C, N, H analysis was determined based on ISO 12902 - CHN Instrumental method.

CV Analysis

CV analyses was conducted, at Bureau Veritas, to determine the potential energy of the water hyacinth samples (WHW, WHR, WHS and WHL), The samples were prepared using the standard procedure based on ISO 13909-4: 2001 and the CV obtained by the standard ASTM method. The LCV were determined theoretically using Eq 5 (Bergier, et al., 2012), where w is the moisture content.

$$LCV = HCV\left(\frac{1-w}{100}\right) - 2.447\left(\frac{w}{100}\right) - \left[(22.047)\left(\frac{w}{100}\right)\left(\frac{1-w}{100}\right)\right] \qquad Eq\ 5$$

XRF Analysis

XRF analysis (ASTM D4326-13) was used to quantify the proportion of inorganic elements contained in the water hyacinth's ashes. The XRF analysis was conducted at the NWU labs.

Thermogravimetric Analyzer (TGA)

The thermal analysis of water hyacinth, samples whole hyacinth (WHW), and its parts: leaf (WHL), stem (WHS) and root (WHR), conducted at the NWU, using a TGA Instrument SDT-Q600 thermogravimetric analyzer. To create an inert atmosphere, N_2 gas was flushed through the instrument (furnace and sample), using a constant 100 Ncm^3/min flow rate. A sample size of approximately 200 mg was loaded into a 90 µL alumina crucible. The furnace was heated to the desired temperature of 950 °C, under a constant flow of N_2 gas (100 cm^3/min), with a heating rate of 5 °C/min. When the TGA reached 950 °C, the gas flow was switched to dry air with a constant 20 Ncm^3/min flow for 60 min to allow for complete combustion. The mass and temperature were logged in real time every 0.75 s.

3.4 Results and Discussion

3.4.1 Physiological Structure

The hyacinth in this study was harvested as new growth started after winter, yielding physiological ratios for WHW of 46% WHR, 42% WHS and 12% WHL, and according to Rezania, et al., (2016), hyacinth on a dry basis consist of 23% roots, 37.5% stems and 38.8% leaves. However, according to Sukarni, et al., (2019), the physiochemical properties of hyacinth are influenced by the environment the hyacinth grows in. Therefore the difference between the two studies can be attributed to environmental factors and the season the hyacinth was harvested in.

3.4.2 Proximate Analysis Results

The moisture and ash free chemical composition for the hyacinth samples is presented in Table 5, along with air dried moisture composition. Sample WHL has the highest VM and FC content, and the lowest ash yield, whereas WHS and WHR show relatively similar values. These values correlate to the chemical composition for water hyacinth, on a dry basis obtained from literature, *i.e*., 56-74% VM, 10-30%, FC and 11-26% ash (Zhang et

al., 2020; Promdee, et al., 2012; Su, et al., 2018; Rezania, et al., 2015; Sukarni, et al., 2019). It can be deduced that dry hyacinth contains approximately 74-89% organic matter.

Table 5: Water hyacinth chemical characterization results

Characterization of Water Hyacinth				
Parameter	**WHS**	**WHR**	**WHW**	**WHL**
Moisture (air dried basis %)				
H_2O	6.1	5.1	5.3	5.1
Physiochemical Results (TGA) (dry basis %)				
VM	70.1	67.9	68.5	70.1
FC	16.8	14.7	16.3	19.0
Ash	13.0	16.3	15.2	10.9
Physiochemical Results (Prox) (dry basis %)				
VM	65.8	67.0	67.7	70.9
FC	18.3	17.7	18.8	20.2
Ash	15.9	15.3	13.5	8.8
Elemental Composition (Ult.) (ash and H_2O-free basis, %)				
C	45.8	45.1	45.0	47.5
O	45.4	44.3	45.6	43.3
N	2.7	3.9	3.3	3.1
H	5.9	5.9	5.8	6.0
S	0.2	0.8	0.4	0.2
Molar Ratios (ash-free basis)				
H:C	1.6	1.5	1.6	1.5
O:C	0.7	0.7	0.8	0.7
CV (MJ/kg)				
HCV	13.8	13.9	14.3	16.3
LCV	12.4	12.5	12.9	14.8

3.4.3 Ultimate Analysis Results

The elemental composition results obtained are presented in Table 5. The WHL sample shows the highest C, H and O content. The WHS and WHR samples have similar C, H and O content, where the WHR sample has the largest S content, and WHS and WHL have the same S content. The elemental composition of hyacinth, obtained from literature, consists of 18-46.5% C, 5.3-6.6% H, 27.5-34% O, 0.7-4.3% N and 0.025-0.6% S (Bergier et al., 2012; Zhang et al., 2020; Su et al., 2018; Li, et al., 2021), which are comparable to the values presented in Table 5.

The four hyacinth samples are plotted on a van Krevelen diagram, together with different waste types, see Figure 4.

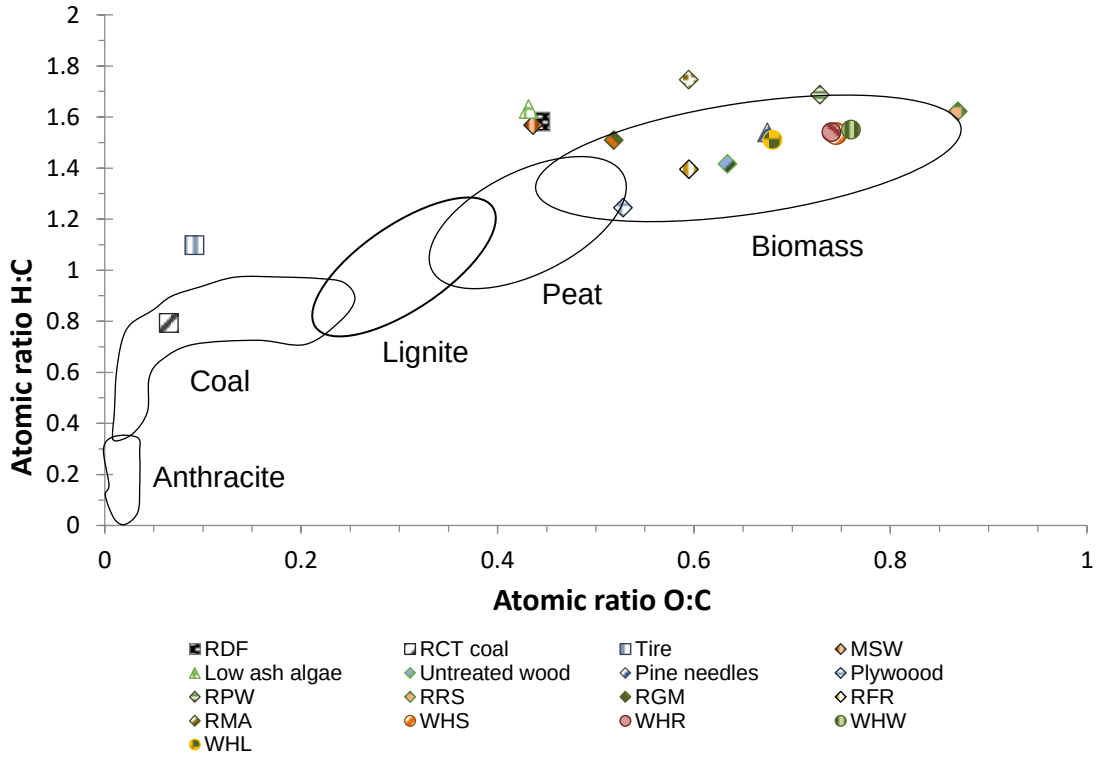

Figure 4: van Krevelen diagram WHW, WHS, WHR, WHL and other biomass and waste types

A van Krevelen diagram provides insight about the feedstock quality based on its O:C and H:C ratios. The first aspect to note from Figure 4 is that WHW, WHR, WHS and WHL fall inside the biomass area, and WHW, WHR and WHS are clustered together. Since WHW consists of 46% WHR, 42% WHS and 12% WHL (Section 3.1.2), it can be assumed that WHW will more closely resemble WHR and WHS, as seen in Figure 4. In general as the ratios approaches the origin (0,0), the energy potential increases. According to Janajreh, et al., (2013), as the O:C and H:C ratios decreases, higher amounts of oxidant is required. Therefore as the O:C ratio increases, and less oxidant will be needed for gasification. Additionally, the molar ratios of hyacinth, presented in Table 5 are similar to the molar ratios of water hyacinth obtained from literature, *i.e.* 1.6-1.9 H:C and 0.6-0.7 O:C (Huang, et al., 2020; Zhang et al., 2020). The experimental results indicate a higher O:C and a slightly lower H:C. Based on the relative positions in Figure 4, it can be expected that WHL will have the highest CV, followed by WHR, WHS and WHW. The hyacinth samples are compared to that of different biomass types, *i.e.*, low ash algae, untreated wood, pine needles, plywood, raw pine wood (RPW), raw rice straw (RRS), raw grape marc (RGM), raw forest residue (RFR), raw macro algae (RMA) biomass. And non-biomass waste

types, *i.e*., refuse derived fuel (RDF), River-Trading-Company (RTC) coal (similar to Kentucky bituminous grade), tire and municipal solid waste (MSW) (Kuo et al., 2020; Janajreh et. el., 2013). Since these waste types can be considered for co-gasification, it is important to analyse each waste's chemical composition, which will give insight as to how the gasification process will be affected. The chemical and elemental composition of the different waste types used are sourced from Kuo et al., (2020) and Janajreh et el., (2013) (Appendix E.1, Tables E.1.1 and Table E.1.2).

3.4.4 CV Results

The HCV for the hyacinth samples: WHW, WHS, WHR, and WHL were obtained experimentally and are presented in Table 5, along with the calculated LCV values. The WHL sample show the highest CV result, whereas WHS and WHR delivered similar CV values, affirming the results found in the Table 5. The CV values show that the ash content is the strongest indicator for the energy potential of a material, followed by the C, O and H content. According to Li, et al., (2021), dry hyacinth has a CV value between 13.1-18.4 MJ/kg, whereas Zhang, et al., (2020) and Sukarni, et al., (2019) obtained values of 14.5 and 14.7 MJ/kg. These values correlate with the experimental value of 14.3 MJ/kg for WHW. However, the CV values obtained for WHL, WHS and WHR deviate from that which was obtained in Rezania, et al., (2016), *i.e.,* 14.9 MJ/kg leaves, 13.5 MJ/kg stems and 8.5 MJ/kg roots. The HCV values given in Table 5 and the respective biomass and non-biomass waste types (presented in Figure 4) are plotted together in Figure 5. The CV range for hyacinth, obtained from Li, et al., (2021), is indicated in Figure 5 (between the two lines). It is seen that the hyacinth samples fall inside, on the lower boundary, of this region. As expected from analyzing the molar ratios in Figure 4, the HCV values are as follows WHL>WHW>WHR≥WHS. The hyacinth and its parts have relatively low CV values in relation to other biomass and waste types. It is seen that untreated wood, pine needles, plywood, RPW fall inside the hyacinth CV region, and RPW is similar to WHL. It is clear from the CV values, presented in Figure 5, that biomass have a general CV value < 22 MJ/kg, and the hyacinth samples of this study yield CV values significantly lower when compared to non-biomass wastes. If co-gasification is required, the analysis done in Figure 4 and Figure 5 will assist in choosing the waste type required based on the PlasWEn plant constraints and the wanted product.

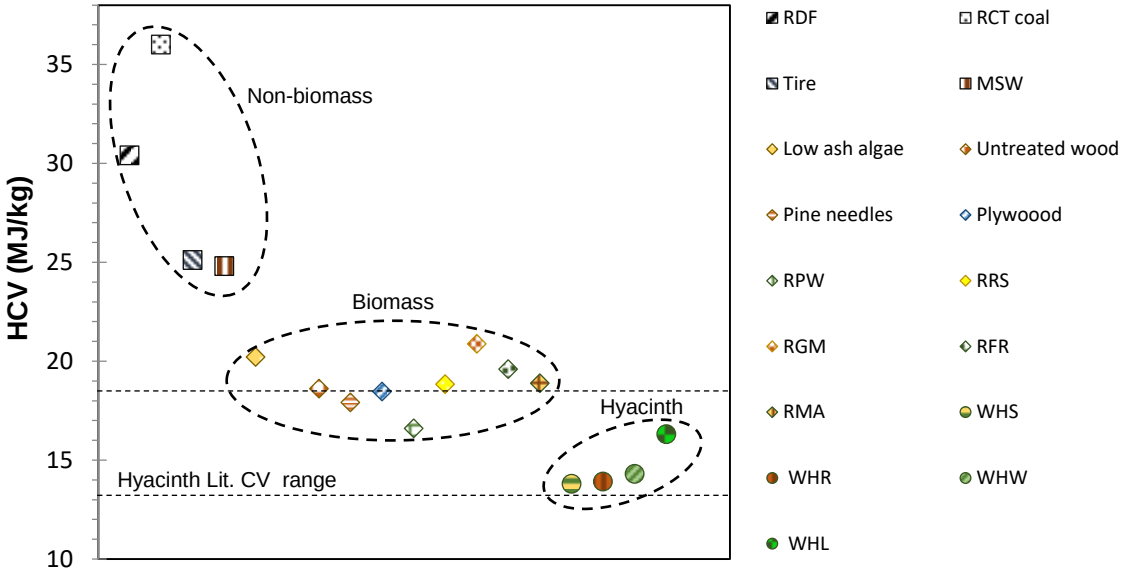

Figure 5: The HCV of WHW, WHS, WHR , WHR and other biomass types from literature

3.4.5 XRF Results

The major elements present in the inorganic fraction of WHW, are presented in Table 6, along with values obtained from literature. The XRF analysis of WHW shows that the major elements contribute 95% of the inorganic fraction. According to Newete, et al., (2016), water hyacinth can survive in the presence of heavy metals, however, prolonged exposure to excess heavy metals result in the adaptation of different physiological and molecular mechanisms. And since the Hartbeespoort dam is continually fed by the Crocodile River, it can be assumed that the influx of metals and pollutants are continuous (Atta, et al., 2020). The hyacinth's survival mechanisms increases the tolerance for metal toxicity, *i.e*. excluding heavy metals from specific, binding them in cell walls and vacuoles, or preventing their entry into the entire plant (Newete, et al., 2016), limiting the amount of metals that the plant can assimilate and translocate to the stems and leaves. Therefore, the concentrations of metal oxides and heavy metals in root tend to be higher than those in shoot or leaves (Mahani, et al., 2018). Therefore, the higher inorganic content for WHL in relation to WHS and WHR seen in Table 5, can be expected.

Table 6: The major elements that WHW 's ash is composed of determined by XRF analysis

Element		WHW Ash %	WHR1	WHSh1	WHR2	WHSh2	WHR3	WHSh3
			Biomass (moisture free basis) %					
Na_2O	Na	2.97	1.40	0.12	1.40	0.70	0.67	1.38
MgO	Mg	8.78	1.20	0.42	0.78	0.54	0.46	0.23
Al_2O_3	Al	1.55	3.92	0.11	1.20	0.09	1.58	0.03
SiO_2	Si	4.98	11.95	0.33	3.31	0.30	4.29	0.13
P_2O_5	P	11.93	1.20	0.68	2.05	0.83	2.40	0.50
SO_3	S	4.33	0.99	0.18	2.05	0.34	2.71	0.49
K_2O	K	18.24	4.02	5.30	2.40	3.81	2.40	4.01
CaO	Ca	31.33	3.32	2.65	4.73	2.94	2.73	2.20
TiO_2	Ti	0.10	0.66	0.04	0.23	0.03	0.29	-
V_2O_5	V	0.02	-	-	-	-	-	-
Cr_2O_3	Cr	0.07	-	-	-	-	-	-
MnO	Mn	0.94	0.70	0.05	1.11	0.16	0.48	0.03
Fe_2O_3	Fe	9.46	6.02	0.21	2.45	0.19	3.98	0.07
Total		94.60	35.40	10.10	21.70	9.90	22.00	9.10
Reference		This study	(Osama, et al., 2010)					

According to Atta, et al., (2020), the high K and P fractions, seen in Table 6, can be attributed to the high levels of K and P trapped in the Hartbeespoort Dam due to the influx of sewage and fertilizer. Since water hyacinths absorb pollutants from the water (Santos, et al., 2018), the inorganic composition of WHW can be related to the eutrophic condition of the Hartbeespoort Dam. This highlights the importance of proper management of continuously harvesting the hyacinth from the Hartbeespoort Dam. This can alleviate the eutrophication process by limiting the re-entry of metals into the water, through the decomposition of dead plant matter and the removal of absorbed pollutants. The XRF analysis, obtained from Osama, et al., 2010, for WHR1 WHSh1, WHR2, WHSh2, WHR3 and WHh3 and are presented in Table 6. Where WHR1, WHSh1, WHR2, WHSh2, WHR3 and WHSh3 report the difference of the root and shoot (stem and leaves) absorption of heavy metals and oxides (Osama, et al., 2010), on a moisture free basis. However, from the proximate results shown in Table 6, it can be seen that the inorganic fractions of WHS≥WHR which slightly deviates from literature; and contributed to the season and experimentation. It has been made evident in Section 3.2 by comparing the WHW sample with that of literature that the chemical composition of hyacinth is dependent on the present environmental conditions it grows in.

3.4.6 TGA Results

The TG and DTG analysis results for WHW, illustrate the mass loss as a function of temperature for WHW and is presented in Figure 6 (refer to Appendix A.1, Figures A.1.1 – A.1.3 for TG and DTG graphs for WHR, WHL and WHS). The mass loss temperature peaks and the temperature ranges are indicated on the DTG curve and the corresponding mass loss is indicated on the TG curve. When evaluating Figure 6, it can be seen that both the WHW1 and WHW2 lines for the TGA and DTG curves are on top of each other, therefore no significant difference between the two runs. The TGA and DTG graph can be divided into three main stages, and the results on a dry basis are given in Table 5. In the first stage (I), a mass loss of 8% can be observed between the temperature range 20<T<115 °C. At this point it is assumed that all the H_2O% contained WHW, *i.e.*, contained in the cells and the external water limited by surface tension, was released (Huang, et al., 2020). As seen in Table 5, the proximate analysis results showed a smaller H_2O% content than the TGA results, and therefore corroborates that stage (I) corresponds with the loss of moisture and light volatile matter (Sukarni, et al., 2018).

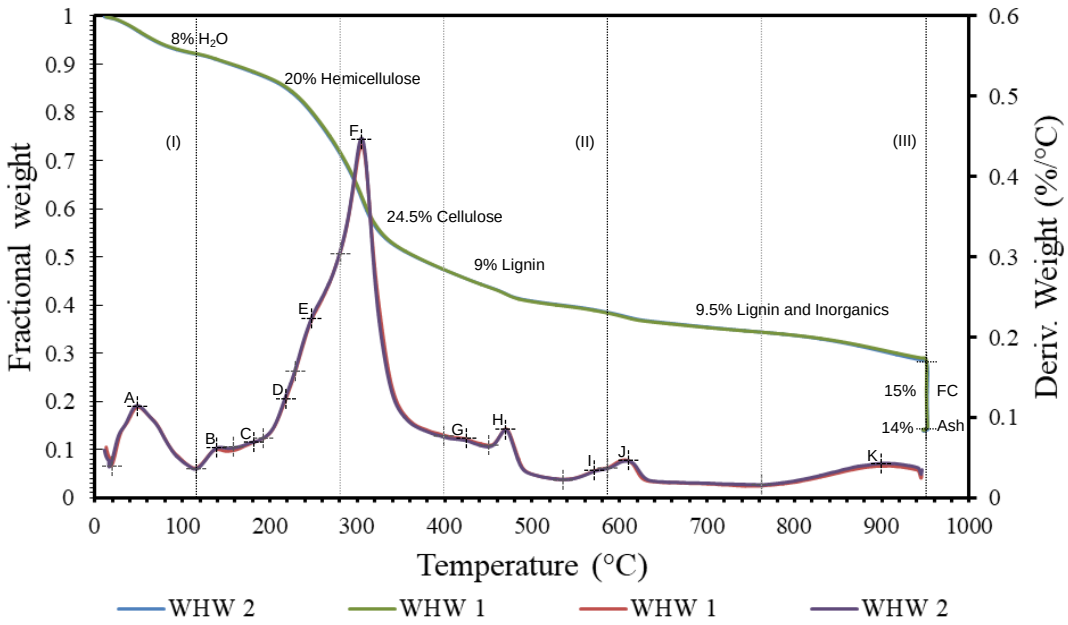

Figure 6: Experimental TG and DTG curves illustrate the non-isothermal behavior of WHW

Stage (II), the devolatization stage, occurs at 115<T<585 °C, and can be subdivided into three divisions where a significant amount of the hyacinth's organic fraction is decomposed and released as volatile matter (Sukarni, et al., 2018). The first division is observed at 115<T<280 °C, with a mass loss of 20%. A steady mass loss occurs between 115<T<160 °C and 160<T<230 °C, followed by an accelerated mass loss seen as the

sharp slope occurring between 230<T<280 °C with a mass loss peak (E) at 250 °C. The second division is observed at 275<T<400 °C, with a mass loss of 24.5% with a mass loss peak (F) at 305 °C. The primary mass loss occurs between 230–400 °C and indicated by a sharp slope on the TG curve and peaks (E) and (F) of the DTG curve. According to Huang, et al., (2020), stage (II) is the decomposition of lignocellulose components and a complex process whose reaction mechanism involves the interaction of multiple reactions, making it difficult to predict. A total of 53% of the WHW mass was decomposed during stage (II). Even though overlapping decompositions of hemicellulose and cellulose may occur, Peak (E) and (F) can be distinguished and corresponds to the mass loss of hemicellulose and cellulose (Huang, et al., 2020). Hemicellulose, comprising short-chain heteropolysaccharides with low polymerization and susceptibility to hydrolysis, exhibits increased activity during thermal decomposition. In contrast, cellulose, a linear macromolecular polysaccharide consisting of D-glucosyl groups with high polymerization and resistance to hydrolysis, exhibits more difficulty in thermal degradation compared to hemicellulose (Huang, et al., 2020). The third division is observed at 400<T<585 °C with a mass loss of 8.5% that corresponds to the decomposition of a greater fraction of lignin (Huang, et al., 2020). The thermal decomposition of lignin proves more difficult than the hemicellulose and cellulose decompositions due to lignin comprising of an aromatic matrix and is present in the cross-linking of cellulose and hemicellulose (Huang, et al., 2020). Stage (III) occurs at 585<T<950 °C with a mass loss of 9.5% and can be contributed to further decomposition of lignin and inorganic components (Sukarni, et al., 2018). At 950 °C it can be considered that most of the volatile matter (VM) has escaped, leaving fixed carbon (FC) and ash. Upon combustion at 950 °C, seen in Figure 6, the mass loss of 15% can be attributed to the loss of FC and any remaining VM, and 14% ash remains. It should be noted that the mass loss peaks (H), (J) and (K) and the consequent mass loss that occur at 420, 610 and 900 °C could be contributed to the decomposition of inorganic matter contained in the hyacinth structure, such as sulfur, potassium, and sodium found in the XRF analysis, refer to Table 6. The mass decomposition of hyacinth obtained from Figure 6 and the corresponding temperatures of the three primary lignocellulose compounds it can be assumed that WHW roughly consists of 20% hemicellulose, 24.4% cellulose and 9-18% lignin. According to literature, hyacinth biomass typically consists of 18-31% cellulose and 18-43% hemicellulose and 7-26% lignin content (Bergier, et al., 2012; Gaurav, et al., 2020). The moisture loss occurs at 20<T<170 °C, and the three primary lignocellulose components in hyacinth typically decompose at the temperatures: Hemicellulose at 170<T<285°C, cellulose at 285<T<400 °C and lignin at 400<T<950 °C

(Huang, et al., 2020). However due to the complex structure of lignin, decomposition can occur between 150<T<1000°C (Diez, et al., 2020). It can be seen that both the consistencies and temperature ranges for the three lignocellulose fractions found in WHW can be correlated to that found in literature. The TGA results, on a dry basis, are normalized and the chemical composition of WHW and its parts are summarized in Table 5. As seen in Table 5, WHL has the highest FC and the lowest ash content, which would indicate a high CV value can be expected. WHR delivered the lowest VM and FC, and the highest ash content, as can be expected according to literature discussed in Section 3.3.5. Whereas WHS and WHR delivered similar VM and FC values, but WHS has a lower ash content. A TGA done by Sukarni, et al., (2018), show air dried sample with 4.9% H_2O, and on a dry basis, 64.4% VM, 14.5% FC and 21.1% ash, with TGA parameters: at a constant heating rate of 10 °C/min with a N_2 flowrate of 100 ml/min and 25<T<1000 °C. It is noted that the hyacinth harvested from the Hartbeespoort dam has a lower ash content and a slightly higher FC and VM content.

Chapter 4 Experimental

4.1 Materials

The following gases O_2 (99.9% purity), N_2 (99.9% purity) and Argon (99.9% purity) supplied by Afrox were used. Sample WHW is used for the plasma gasification experiments, due to the various parts having similar CVs and when considered for commercial application, the whole hyacinth will be used as feedstock, refer to Ch 3, Section 3.3 and Table 5 for characterization results.

4.2 Experimental

4.2.1 Plasma Gasification Process Equipment: H-PlasWEn

The batch asWEn laboratory setup is illustrated in Figure 7.

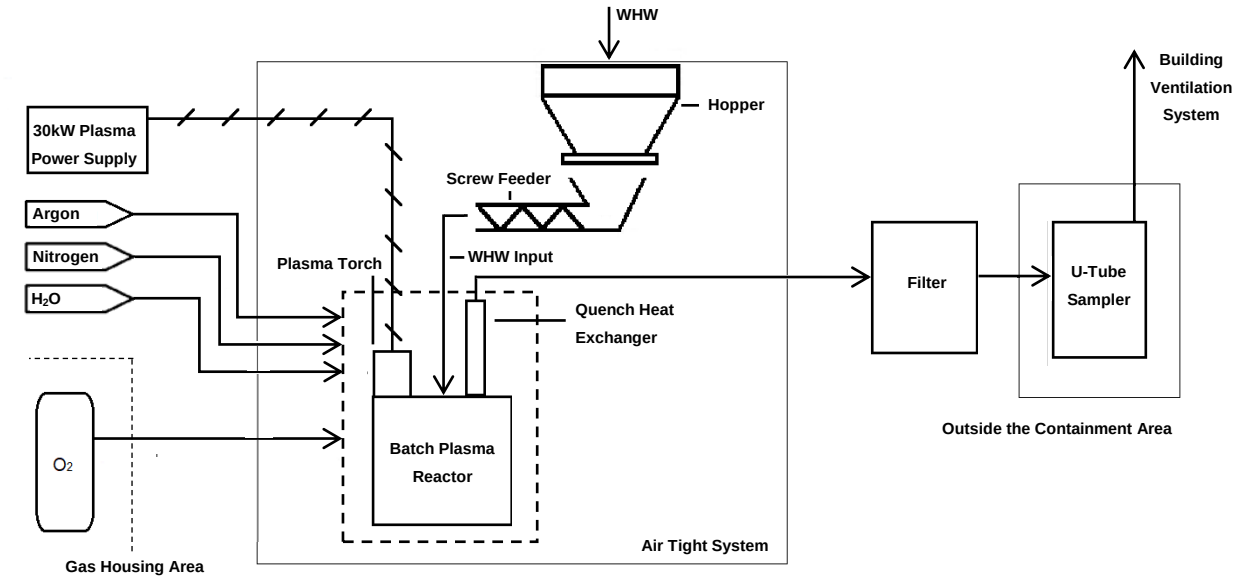

Figure 7: Schematic presentation of the Plasma gasification rig, PlasWEn at NECSA

4.2.2 Process Description

The 25 L hopper is filled with 2.5 kg WHW and the feed rate was calibrated (Appendix B, Table B.2.1). After the sample preferred feed rate was determined, the hopper was refilled, the hopper inlet closed and sealed, and the hopper outlet was connected to the reactor and sealed. After the pre start-up and start-up procedures are completed

(Appendix B.3 and Table B.3.1) and the plasma reactor has reached a temperature of 900 °C, the feed screw was started at the calibrated setting, and hyacinth material started to feed into the plasma reactor. The chemical bonds in the hyacinth feed were decomposed upon contact with the plasma flame, resulting in the conversion of the material into gaseous form or free elements. The plasma generated elements is then rapidly cooled by a quench heat exchanger, w here the rapid cooling facilitate the recombination of the free elements to form synthesis gas (syngas). In the PlasWEn laboratory setup, the cold gas was then passed through a bag filter to remove any entrained solids. The remaining gas was safely vented through the building ventilation system along with excess air to attain a H_2 concentration below LEL (4 vol. %) in the ducting of the ventilation system. Air, in excess of 110 Nm^3/h, was introduced into the gas stream at the entry to the ventilation system. In order to collect samples, a U-tube bypass sampler was mounted downstream of the filter and syngas flows through a bypass stream, driven by a compressor and controlled by a valve. Samples were taken every 15 minutes, and the syngas filled U-tube samples were sent to NECSA's laboratory to perform GC analysis on the syngas. The solid residue was removed after the experiments were concluded from the batch reactor, and the quench heat exchanger, pipes and bag filter once the system has cooled to room temperature. A continuous record of the measured system variables, i.e., temperatures of the cathode, anode, the heat exchanger, reactor, gas stream and cooling water streams (in and out), was kept; starting from the initial conditions prior to switching on the 30 kW power supply, and throughout the sample collection process.

Gas Chromatography (GC) Analysis

A gas chromatography (GC) was used to analyse the produced syngas composition. The analyses were done off-line internally by NECSA at Pelindaba Analytical Lab, and were reported in ppm and %_Norm (mol %). The GC system used was an Agilent 7890 GC coupled with a RGA system with six columns, six valves, and three detectors, *i.e*., one detector was a flame ionization detector and two were thermal conductivity detectors.

4.3 Experimental Plan

The plasma gasification experiments were piloted at varied feed rates, and oxidant type (O_2 and H_2O). Fluctuations in the current and voltage were observed, due to the current (Amp) being adjusted by hand to control the temperature, and due to the voltage (Volt) being a function of the quantity of plasma gas (N_2) and the physical state of the torch. Fluctuations can be observed in the reactor temperature and pressure, depending on the feed type and feed rate, due to the use of a feedscrew, where the feed enters the reactor continuously in a pulsed manner. This can have an impact on the waste conversion since O is fed into the reactor continuously and at a fixed rate. For this reason and due to the general circular design of the research gasification reactor, unreacted O_2 could be observed in the product gas (syngas). The system operated at a pressure slightly over 1 bar, ±0.05 bar in relation to the pitch of the feedscrew. Due to the position of the quench probe it can be assumed that $T_{reactor}$= T_{gas}. Steady state was reached when the current and voltage stabilizes, see Table 7. The PlasWEn system's base and average parameters and input values for each experimental run are given in Table 7.

Table 7: PlasWEn system experimental parameters and input values

PlasWEn Experimental Parameters						
Run	**Unit**	**A**	**B**	**C.1**	**C.2**	**C.3**
Gas Input (4.5 bar)						
N_2	mol/h	151.6		71		
O_2	mol/h	-	-	12.8		
Hyacinth Input (1 bar)						
$\dot{m}$	kg/h	0.87		1.05	1.25	1.50
T_{in}	° C	20.0				
H_2O	%	5.3	30.3	5.3		
Total O to C Input ratio						
O:C	mol ratio	0.9	1.2	1.7	1.5	1.4
Plasma Reactor (1 bar)						
Current	Amp	141-157	156	137-143		
Voltage	Volt	95-100	99-108	64		
P_{plasma}	kW	13.8-15.4	15.4-15.6	8.8-9.0	9.1-9.2	9.1
$P_{plasma}/\dot{m}$	(kWh/kg)	15.9-17.7	17.8-17.9	8.8-9	7.3-7.4	6.1
T_{gas}	° C	1182-1227	1096-1222	1075-1100	1123-1128	1130-1144

4.3.1 Plasma Gasification Experimental Parameters

Reactor Conditions and Sample Input Experimental Setup

Each experimental set, *i.e*., Run A, Run B, Run C (C.1, C.2 and C.3) evaluates the effect of a variation in O:C ratio, plasma gas (N_2) feedrate, O_2 or H_2O oxidant, the power input (kW) and how it relates to temperature, feed mass flow ($\dot{m}$) and the specific power input (kWh/kg) on the plasma gasification of WHW. The hyacinth samples are compared to different waste types that are suitable for plasma gasification such as those briefly discussed in Section 3.3.3 and 3.3.4.

Run A: Plasma Pyrolysis Gasification

To determine a base experiment, plasma pyrolysis experiments were piloted at system conditions as presented in Table 7. Run A is chosen as the baseline for the Techno-Economic Evaluation (TEE) because the O:C ratio of 0.9, nearing 1, indicates that there is sufficient inherent O to facilitate the conversion of C in the feedstock. In Run A, and according to past experimental experience from NECSA, the data aligns with what can typically be anticipated in a run where there is a 10% excess of O supplied to the system. The primary distinction is that the CO_2 content would be slightly larger, and the unreacted C fraction in the residue would be slightly smaller. The changes in CO are minimal, with a slight increase in CO_2 formation, while the H_2 content remains constant. This is sufficient for a TEE applied for industrial scale.

Run B: Plasma Gasification with H_2O as Oxidant:

To determine the effect of H_2O as an oxidant and to vary the O:C ratio, and since a steam line to the PlasWEn system was not part of the lab setup, a total of 25% H_2O was added to WHW (refer to Appendix B.1, Table B.1.3 for batch calculation) resulting in a sample containing 30.3% H_2O. The plasma steam experiments were piloted at system conditions as presented in Table 7. The additional mol/h of O and H due to the additional H_2O for the continuously fed PlasWEn system (Appendix B.1, Table and B.1.4) will simulate a steam plasma gasification experiment, and increase the O:C and H:C ratios.

Run C: Plasma Gasification with Varied Feed Rate.

To evaluate the effect feed rate has on the syngas quality, and therefore residence time, the feed rate was increased incrementally. The PlasWEn system feeder was upgraded by NECSA to account for hyacinths physiology, and then recalibrated (refer to Appendix B.2,

Table B.2.1 and Figure B.2.1). A constant O_2 flow for each feed rate was also used, the experiments were piloted at system conditions as presented in Table 7 used.

4.4 Thermodynamic Process Simulation

For the thermodynamic modelling of the H-PlasWEn process, the simulation package, FactSage was used to evaluate and compare the experimental results to the theoretical. To determine and simulate the conditions for multiphase, multicomponent equilibria under the experimental constraints specific to this study, Gibbs energy minimization was used (Appendix C.1, Figures C.1.1). For accurate thermodynamic calculations, there are two important prerequisites for a given system: 1) the accuracy for the total Gibbs energy minimizing algorithm, with a given set of constraints, and 2) the availability of an accurate thermodynamic database (Jung & van Linde, 2020). For the simulation of PlasWEn process, the FactPS (FACT Pure Substances) database, which contain the thermodynamic data for more than 4900 species (solid, liquid, gas and ionic states) (Jung & van Linde, 2020) was used. Since thermal plasma is used to convert solids into the gas state, the gaseous ions (plasma) for the product gas species were used and the C_xH_y species were limited to x = (0,1,…4) and y = (0,1,…4) with a minimum of 2 solution components. The units for the simulation were predefined and specified as T(°C), Energy (J), Quantity (mol) and Volume (L) (Appendix C.1, Figures C.1.2). The reactant streams were added and the molar inputs, for each experimental condition, Run A–C, are presented in Table 8 and indicated as Streams 1–3 (Appendix C.1, Figures C.1.3).

Table 8: Experimental molar input values for thermodynamic simulation using FactSage

Simulation Molar Input Values (mol/h)					
Run	**A**	**B**	**C.1**	**C.2**	**C.3**
kg/h	1		1	1	2
Stream 1:	**1 bar (abs) and 25 °C**				
C	27		32	38	46
O	20		24	29	35
N	2		2	2	3
H	41		50	59	71
S	0		0	0	0
H_2O	3	12	3	4	4
Stream 2:	**4.5 bar (abs) and 20 °C**				
N_2	152				
Stream 3:	**4.5 bar (abs) and 20 °C**				
O_2	0		13		

A temperature range of 800<T<2000 °C, at increments of 100 °C, were chosen to simulate equilibrium conditions for the PlasWEn process and equilibrium is calculated. (Appendix C.1, Figures C.1.4). Each temperature increment lists the fractional syngas composition (Appendix C.1, Figures C.1.5) which is used to plot graphs where the syngas composition and temperature can be related. Often the syngas composition and information will deviate from chemical equilibrium predictions on account of the kinetic constraints (Sikarwar & Zhoa, 2017).

Chapter 5 Results and Discussion

5.1 Plasma Gasification Results

The averaged mass balance for Run A, given in Appendix B.4, Table B.4.1, delivered a mass difference of 0.05±0.03 kg/h. Where the difference in mass can be attributed to the possible presence of H_2O (not quantified). A 5% error margin was assumed on all values due to the limitations associated with the experimental setup. An important parameter determined by the mass balance was the unreacted C which was used, together with the H_2, CO, CO_2, CH_4, C_2H_2 and O_2 in the syngas, on a kg/kg WHW basis in the TEE. The 0.02 kg/kg unreacted C mass fraction is used to determine syngas yield, composition and theoretical LCV_{syn}, and equates to 6.4% of the total C fraction (see Appendix B.4, Table B.4.2). The experimental results for runs A, B and C.1, C.2 and C.3 are presented in Table 9, on a N_2 free basis, along with the system parameters. By evaluating the results given in Table 9, the uncertainty analysis was done, and the following average values and standard deviations were obtained:

- Run A at 14.1 kW and 16.2 kWh/kg:
  1 209 ±26.2 °C, 49±0.4% H_2, 49±0.9% CO, 2±0.3% CO_2, 0±0.2% O_2, and 0±0.4% C_2H_2.
- Run A at 15.4 kW and 17.7 kWh/kg:
  1 218±8.1°C, 49±3.6% H_2, 47±1.8% CO, 2±2% CO_2, 2±3.0.2% O_2, and 0±0.1% C_2H_2.
- Run B at 15.6 kW and 17.9 kWh/kg:
  1 186 ±51.6 °C, 54±0.1% H_2, 34±2.4% CO, 12±1.9% CO_2, 0±0.1% O_2, and 0±0.1% C_2H_2.

It can be seen that the CO_2 content increases and CO content decreases as the O:C ratio increases, and unreacted O_2 can be seen to increase in the syngas with O:C ratios 1.2-1.6 which can negatively affect the H_2 and CO production. Furthermore, the results for Run A at 1 214 °C show unreacted O_2 which can be attributed to system limitations as described in Section 4.3, and the results obtained for C.3 at 1130 °C is inconsistent. It can be noted that small amounts of C_2H_2 was present in the syngas produced during in Run A and B, and decreases with increasing O:C, leading to no C_2H_2 in Run C. The system parameters are presented in Table 9, along with N_2 plasma gas (kg/h) per $\dot{m}_{whw}$ (kg/h). The plasma torch NECSA developed can function on a 2 kg/h N_2 feedrate, however

optimal conditions are achieved from 3 kg/h N_2 and above. The amount of N_2 available has an impact on the current and voltage, and therefore the torch efficiency.

Table 9: PlasWEn experimental syngas composition as a function of temperature, O:C ratio, feedrate and specific power input (kWh/kg)

Run		Syngas Composition (N_2 free basis)												
	$\dot{m}_{whw}$	H_2O	O:C	H:C	T_{gas}	N_2:$\dot{m}_{whw}$	P_{plasma} (kW)	kWh/kg feed	H_2	CO	CO_2	O_2	CH_4	C_2H_2
	kg/hr	%			°C				mol %					
A	0.9	5.3	0.9	1.6	1 196	4.9	14.1	16.2	48.4	48.1	2.4	0.0	0.7	0.4
					1 145		14.9	17.1	48.2	48.2	2.7	0.3	0.0	0.6
					1 205		13.8	15.9	50.5	47.7	1.5	0.0	0.0	0.2
					1 222		14.1	16.2	48.8	49.4	1.5	0.0	0.0	0.2
					1 182		15.1	17.3	48.8	49.5	1.6	0.0	0.0	0.1
					1 214		15.4	17.7	45.8	47.5	1.5	5.2	0.0	0.0
					1 212		15.4	17.7	52.9	45.0	2.0	0.1	0.0	0.1
					1 227		15.4	17.7	49.5	48.4	1.9	0.0	0.0	0.2
B		30.0	1.2	2.6	1 096		15.4	17.8	53.8	32.6	13.1	0.3	0.0	0.2
					1 149		15.6	17.9	53.6	32.0	13.5	0.3	0.0	0.2
					1 222		15.6	17.9	53.4	35.4	10.8	0.4	0.0	0.1
C.1	1.1	5.3	1.7	1.6	1 075	1.9	8.8	8.8	6.7	14.3	56.7	22.3	0.0	0.0
					1 100		9.0	9.0	10.2	20.7	57.2	11.8	0.0	0.0
C.2	1.3		1.5		1 128	1.6	9.2	7.3	14.2	28.3	32.3	25.2	0.0	0.0
					1 123		9.1	7.3	18.9	32.4	27.0	21.6	0.0	0.0
C.3	1.5		1.4		1 130	1.3	9.1	6.1	8.8	15.6	13.8	61.9	0.0	0.0
					1 144		9.1	6.1	23.8	39.5	23.8	10.5	0.0	0.0

5.2 Thermodynamic modelling

The following result analysis will plot H_2, CO and CO_2 syngas yield on a N_2, O_2, CH_4 and C_2H_2 free basis, and compared based on the system parameters and also with the thermodynamic model.

Run A: Plasma Gasification Pyrolysis

The process results for Run A are presented in Table 9 and plotted as shown in Figure 8.

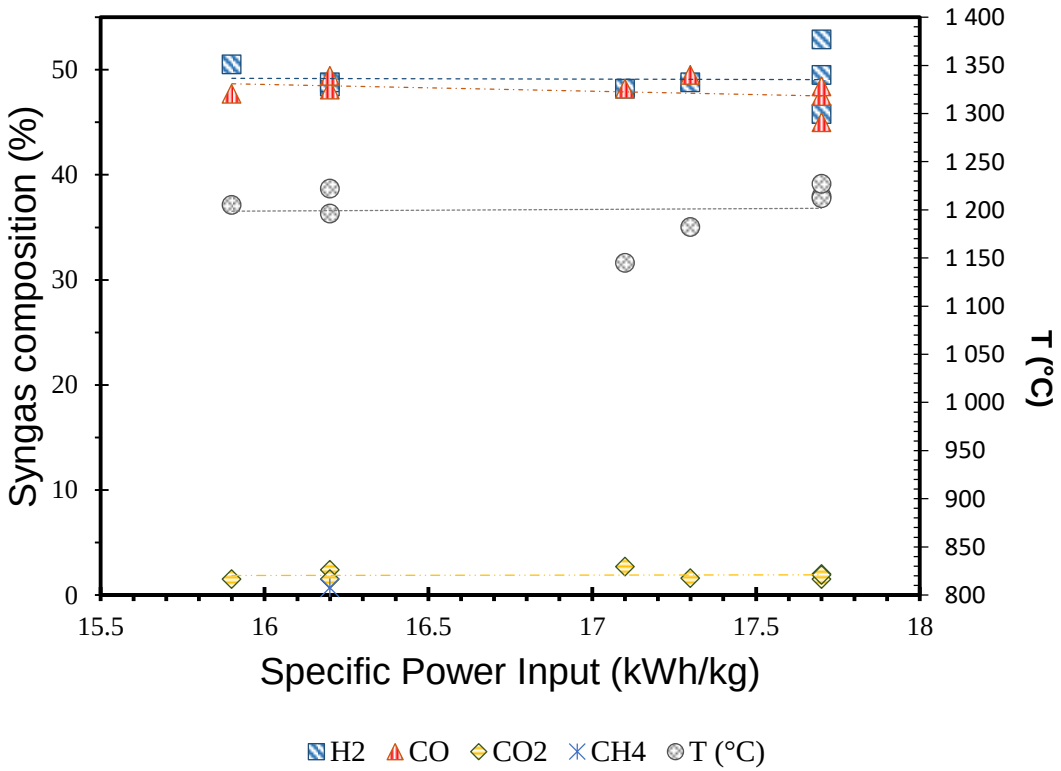

Figure 8: Experimental syngas composition of Run A as a function of specific power input and temperature

The H_2 and CO concentration are nearly 1:1 between 16.4 – 17.4 kWh/kg. The H_2 content increases and the CO content decreases by 17.7 kWh/kg and can be attributed to the 0.9 O:C ratio, which limited the formation of CO. Comparing syngas samples produced across the specific power input range, it is clear that H_2, CO and the CO_2 production were relatively stable, where average H_2:CO ratio of 1.03±0.07 were obtained, with an outliner of 1.18 at 1212 °C. The results obtained from Run A are plotted and compared to equilibrium values shown in Figure 9. The results show that slightly more H_2 and slightly less CO were produced experimentally than what is predicted thermodynamically. The presence of CO_2 indicates a degree of oxidation occurred and deviates from what was

predicted, and no HCN detected as thermodynamically predicted. This could perhaps be due to the formation of H_2 and CO_2 were preferred to that of HCN.

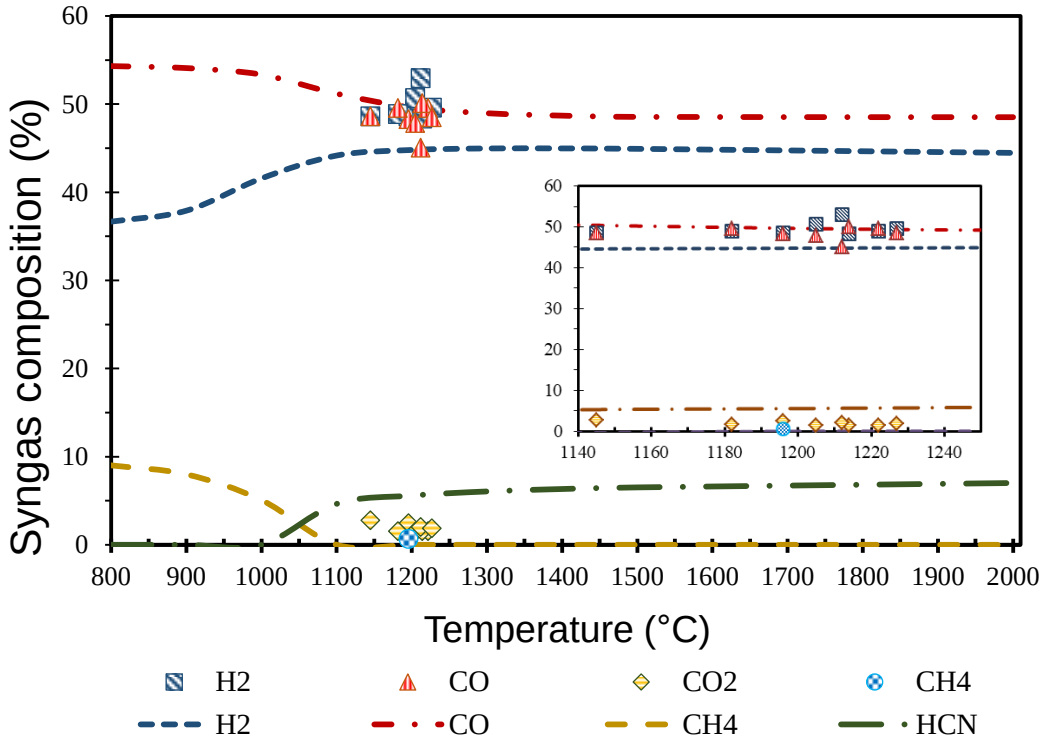

Figure 9: Experimental and simulated values for Run A

Run B: Plasma Gasification with H_2O as Oxidant

The parameters for Run B, presented in Table 9, are similar to Run A with the exception of a 25% increased H_2O content, which resulted in an additional 12.1 mol/h H_2O input (21% O excess), increasing the O:C to 1.21. The syngas composition at the respective specific power input and temperature can be seen in Figure 10, plotted together with the results obtained from Run A obtained between specific power input of 15.5-18.5 kWh/kg. The specific power input and the H_2 production for Run B are practically constant, however with fluctuation in temperature, and a slight CO and CO_2 difference in concentrations are observed. The addition of 25% H_2O resulted in a syngas with an average increase of 5.3% H_2 and 9.2% CO_2, and average decrease of 14.6% CO. On average an 0.59 increase of H_2:CO ratio for Run B from the average Run A can be seen.

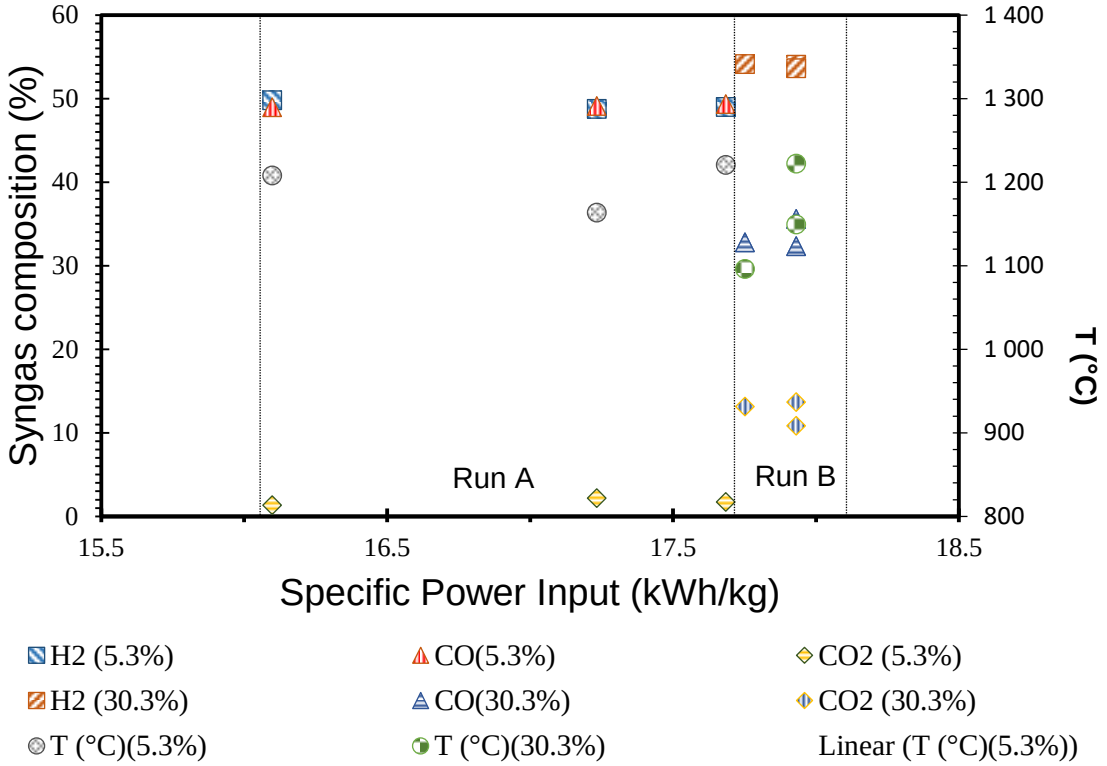

Figure 10: Experimental syngas composition results of Run B as a function of specific power input and temperature

The experimental results are compared to values that can be expected under thermodynamic equilibrium, shown in Figure 11. It can be noted that the experimental composition compared to the thermodynamic modeling results in a higher H_2 and CO_2,

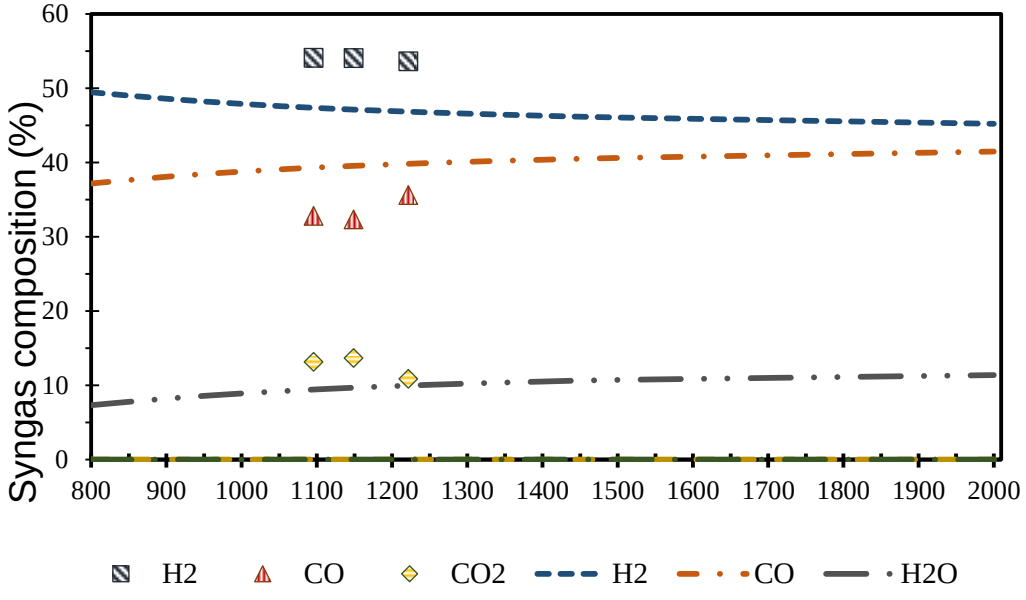

Figure 11: Experimental and simulated values for Run B

lower CO concentrations, and the H_2O fraction was not quantified.

Run C: Plasma Gasification with Excess O_2 and Increasing Feedrate

The results obtain for increased feed rates are shown in Figure 12, and the system parameters for Run C (C.1, C.2 and C.3) are presented in Table 9. A constant 12.8 mol/h O_2 input, resulting in an excess O for each respective feed rate, *i.e.*, Run C.1 (65% at 1.05 kg/h), Run C.2 (52% at 1.25 kg/h) and Run C.3 (41% at 1.5 kg/h). The syngas composition and temperatures for all three feedrates are plotted against the specific power input, and can be seen in Figure 12. It can be noted that the excess O_2 has a greater effect on the concentration of H_2, CO and formation of CO_2, than the specific power input, temperature or feedrate, where a lower feedrate translates into a longer residence time. At a constant P_{plasma}, the specific power input and excess O% decreases with an increasing feed rate.

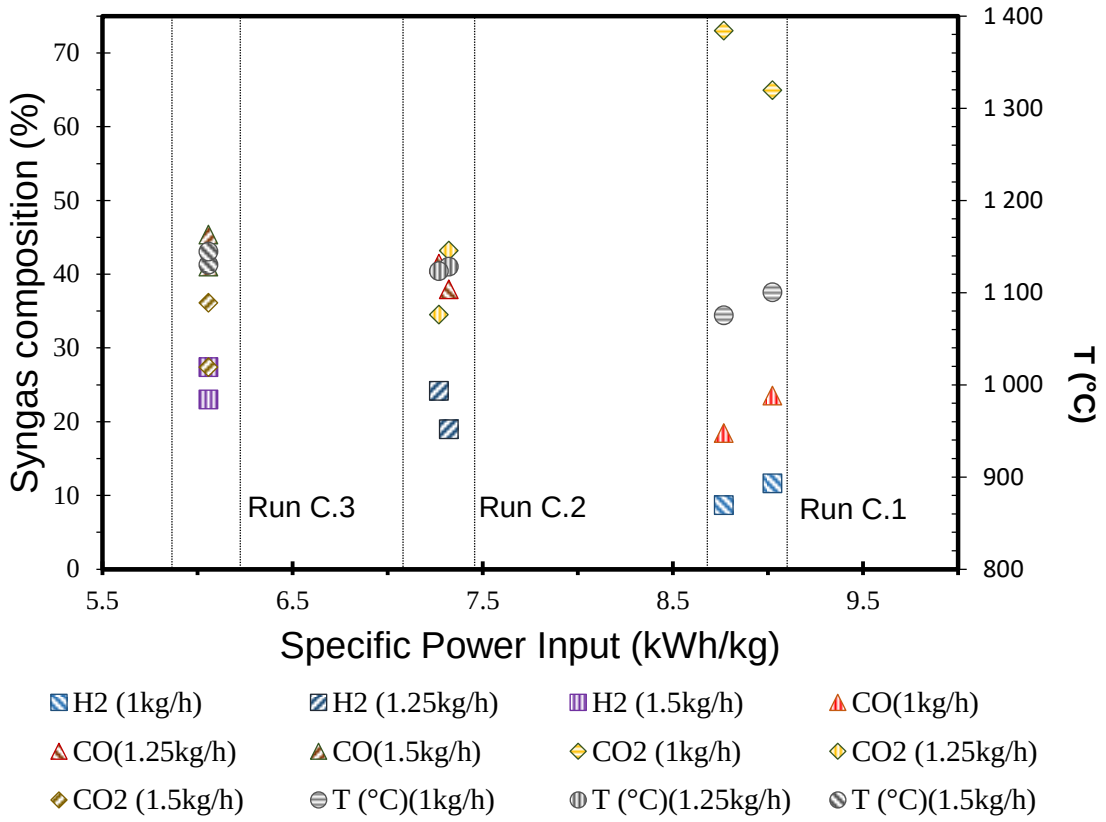

Figure 12: Experimental syngas composition results of Run C.1, C.2 and C.3 as a function of the specific power input and temperature

It is clear that when there is a change in feed rate that temperature is more indicative as a parameter to the syngas composition than the specific power input. The average H_2:CO ratios decrease with an increase in excess O_2, therefore, the values obtained from Run C

reflect the effects of excess O rather than that of increasing feedrate. The experimental results for 1.05 kg/h can be seen in Figure 13.

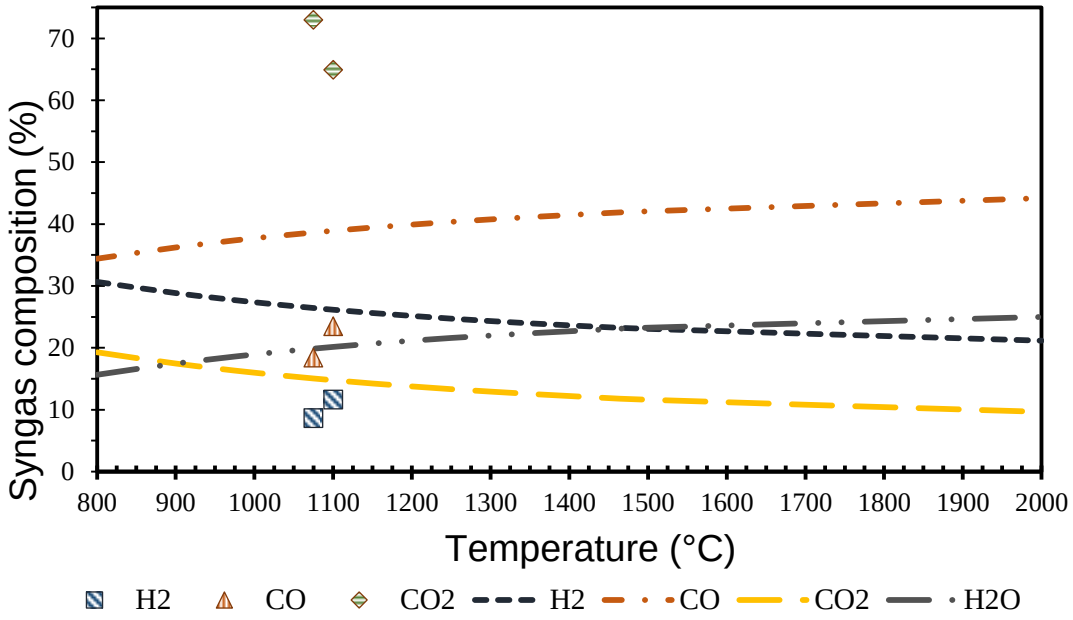

Figure 13: Experimental and simulated results for C.1

The experimental results for 1.25 kg/h can be seen in Figure 14.

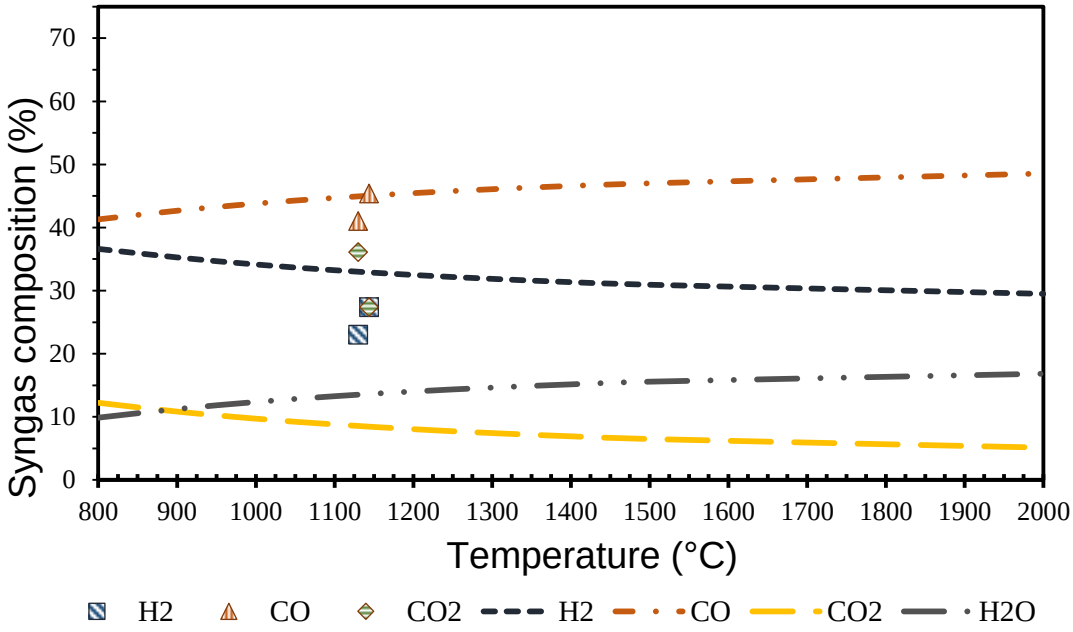

Figure 14: Experimental and simulated results C.2

The experimental results for 1.5 kg/h can be seen in Figure 15.

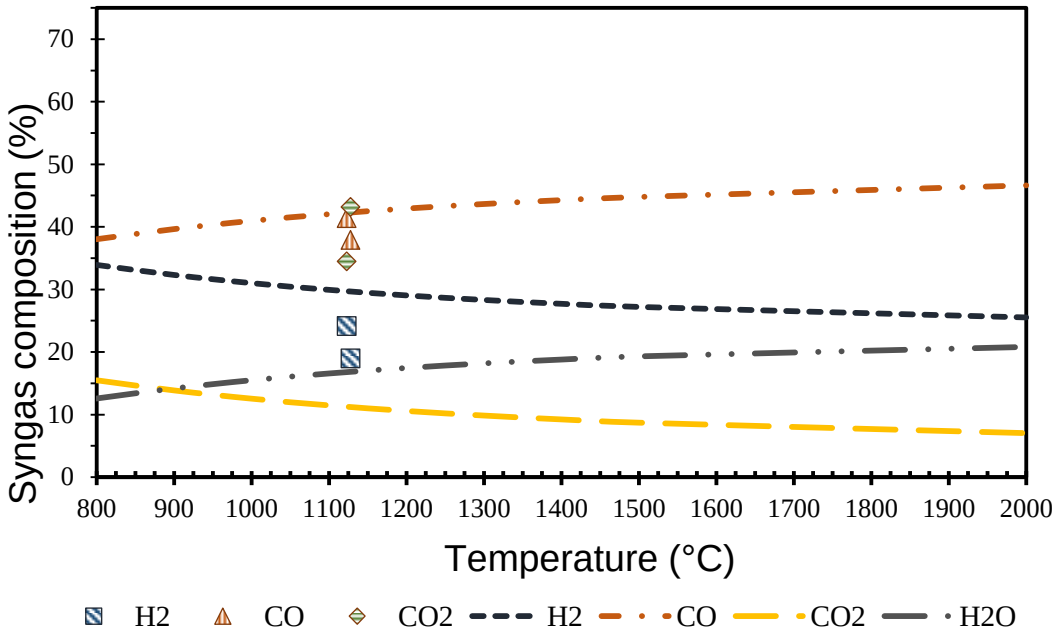

Figure 15: Experimental and simulated results for C.3

Analysing Figure 13, Figure 14 and Figure 15 shows Run C.1 deviates significantly from equilibrium, with ±16% CO, ±18% H_2 and ±54%CO_2. Run C.2 adhere more to equilibrium conditions with a deviation of ±9% CO, ±2% H_2 and ±27% CO_2. Run C.3 adhere more to equilibrium conditions with a deviation of ±8% CO, ±2% H_2 and ±23% CO_2. The H_2O fraction was not measured during experimentation. According to Diaz, et al., (2015), increasing the $\dot{m}$ without increasing the oxidant and P_{plasma} will lead to a decrease in conversion efficiency and may lead to the production of biochar. It can be assumed that the specific power input was too low, which lead to incomplete gasification to occur. The high amounts of CO_2 can be contributed to the excess O, low power input, lower residence times due to the increase in feedrate and a fluctuating feeding mechanism. It can be clearly noted how the excess O influences the equilibrium fractions of H_2, CO, CO_2 and H_2O, and how the system is dependant on temperature to reach equilibrium. As seen in Case study 2, However, according to (Sikarwar & Zhoa, 2017) the syngas composition and information will often deviate from chemical equilibrium predictions on account of the kinetic constraints. Therefore some variation can be attributed to the kinetics of the system.

5.3 Summary

The plasma efficiencies along with the H_2 and CO yields (see Section 2.2.3 Eq 1 and Eq 2) were considered when determining the efficiency of the H-PlasWEn system. From Appendix B.4, Table B.4.2, it can be seen that Run A has the highest conversion for the total C, H and O fed into the H-PlasWEn system. With a 93.6% CCE, 88.5% CO yield,103.2% H_2 yield and a 100.9% O conversion. The O_2 and H_2 yields can be contributed to error margins on the hyacinth feedrate or the gasification of unpredicted water. A error of 4.5% H_2O is determined and can be attributed to the absorption of water from the atmosphere. Despite the small inconsistency, Run A demonstrate the high performance of the PlasWEn system. The derived LCV_{syn} value 14.7 MJ/kg and a syngas density of 0.7107 kg/m^3 was obtained. Run B has a lower CO yield, however, a much lower H conversion is observed in relation to the amount of H input. It can be assumed that the unreacted 44.5% H in Run B remained as H_2O (not quantified). This would increase the H_2O composition in the syngas, and along with a lower C conversion rate lead to a significantly lower LCV_{syn} of 11 MJ/kg. This would suggest that the moisture level in Run B is too much for current system parameters to negate the loss of heat due to the absorption of latent heat for evaporation. Therefore, low reaction rates can be expected and temperatures did not reach the necessary threshold for the water-gas shift reaction to be dominant. The WHW experiments and system parameters are given in Appendix B.4, Table B.4.4 and Table B.4.5, it can be seen that the following is true: A>B>C.3>C.2>C.1 CCE, A>B>C.3>C.2>C1 for the CO yield and A>BC3>C2>C1 for the H_2 yield. Whereas C.1>C.2>C.3>B>A for O:C and B>A>C.3>C.2>C.1 for the H_2:CO. It can also be noted that the average gas temperature in order were A>B>C.3>C.2>C.1. The O:C ratio of a feedstock is indirectly proportional to the energy content of the syngas (Janajreh, et al., 2013). The effect of a high O:C, low plasma power input and therefore low specific power input can be seen in the conversion efficiencies. It is clear between Run A and Run B that if an oxidant is to be added then either the O fed to the PlasWEn is system should not exceed an O:C ratio of 1.1, or for plasma pyrolysis (no O or air fed to the system) the hyacinth should have an inherent H_2O<20%. Relating the PlasWEn experimental results and parameters, see Appendix B.4, Table B.4.4 and Table B.4.5, it can be noted that generally CO%>H_2% when air, O_2 or O_2 and CO_2, and H_2O and CO_2 was used as an oxidant instead of water or steam, and CO%<H_2% when H_2O or O_2 and H_2O are used as oxidant. The gasification temperatures from Table B.4.4 and Table B.4.5 for this study and that obtained from Agon, et al., (2016), Minutillo, et al., (2009), Valmundsson & Janajreh, (2011) and Janajreh, Raza, & Valmundsson, (2013) occur between 1 108–1 554 °C, with

an O:C between 0.2-1.7 where more O was put in the system where O was added when the specific waste type had a low O:C ratio. It can be seen that the H_2:CO ratio is higher for the wastes gasified with H_2O as oxidant. The experimental (and theoretical in brackets) cold gas efficiency (CGE) and mechanical cold gas efficiency (MGE) for the experimental runs (see Section 2.2.3 Eq 3 and Eq 4 and Appendix B.4, Table B.4.3), show that A>B>C.3>C.2>C.1 for GCE and A>B>C.3>C.2>C.1 for MCE. The experimental and theoretical values can be related to values obtained from Agon, et al., (2016). The plasma gasification results from Run A was chosen to be used in the TEE due to the fact that the syngas composition neared thermodynamic equilibrium under the system parameters. it will be used to as the basis for the techno economic study (TEE) done in Chapter 6. The TEE will be built based on the H-PlasWEn system's syngas yield for Run A and use the experimental gas compositions of H_2, CO, CO_2, CH_4, C_2H_2 and O_2 on a kg/kg feed basis and scaled to the plant sizes evaluated in CH 6. The amount of plasma gas, N_2, that will be used in the large scale operation, which is calculated as 10% of total mass fed.

Chapter 6 Techno Economic Evaluation

6.1 Introduction

To estimate the profitability of a project, an estimate of the capital investment and the cost of production are needed. Cost estimation is a specialized subject, however, a rough cost estimate is made to decide between project alternatives and design optimization (Towler & Sinnott, 2008). This techno economic evaluation is done on the profitability, size and necessary capital investment required for economic viability of the H-PlasWEn system. The analysis is done using a financial spreadsheet derived and used in industry. The financial variables and factors used are derived from books such as Peters & Timmerhaus, (1991) and Towler & Sinnott, (2008).

Major project incentives are as follows:

- The management of the hyacinth population.
- Community upliftment.
- Electricity production.
- Environmental protection and awareness.

The major and base assumptions for the projects are listed in Table 10.

Table 10: H-PlasWEn process feasibility assumptions

Product/ Service Selling Price		
Electricity selling price	R/kWh	1.45
Reject Energy selling price:		
Scn1: As electricity	R/kWh	1.45
Scn2: As heat	R/kWh	0.29
Waste management fee	R/t	0
Feedstock price	R/t	0
Ash Selling Price	R/t	800
Time Frame		
Project Lifetime	years	20
Operating days per annum	d/a	330
Hours per day	h/d	24
Maintenance	d/a	35
Grid and Technology Use		
Eskom Grid use charge *Power purchase-local municipality	R/kWh	0.16
*Assumed not applicable because the electricity will be used within the municipal district/ the city, therefore not added to financial calculations.		
Technology royalty (% of sales revenue)	%	1
Finances		
Project financing is assumed to be 30% Equity:70% Debt.		
Nominal WACC or discount factor	%	12.5
Hurdle rate (NECSA)	%	9.6
Equity payment (% of sales revenue), year 2 +	%	1
Production Capacity Ramp-up		
First year	%	50
Second year	%	85
Third year and onwards	%	100
Land		
*The land will not add to the revenue or costs involved in the financial analysis. The assumption is that the project will be built on municipal land based on a a Public Private Partnership (PPP).		
Labour		
The hyacinth harvesting will primarily be done and sponsored by the municipality. However, labour has been included in the feasibility for harvesting and preparation.		
CO_2 Emissions		
Since the feedstock is a biomass the process is deemed carbon neutral, it is assumed there are no cost implications.		

A R1.45kW/h rate was chosen which is 58% less than rate payable by the public and 60% less than the rate payable by the business sector (Eskom, 2023. pp 28-31). The ash or residue price was chosen as an estimated guess based on gravel prices (PMG, 2023).

6.2 Site and Hyacinth Availability Analysis

When estimating certain annual operating costs, the cost for land should not be included in the fixed capital investment since the value of the land rarely decrease with time (Peters & Timmerhaus, 1991). The location influences the cost of the land the facility will be built on, the land surveys and the fees involved in land preparation and building. For the harvesting and drying facility, it is recommended that a site study be done, to take the main wind directions into account, since the wind naturally pushes the hyacinth mats to the shoreline. The South bank of the Hartbeespoort dam has been identified as the location that the wind drives the hyacinth to naturally with access to the shoreline, see Figure 16. The natural shoreline needs to be taken into consideration as it is protected, unfortunately, as it stands this has not been strictly implemented. The drying facility can be built on an open field next to the dam. The Hartbeespoort dam and the main inlet and outlet rivers are depicted in Figure 16.

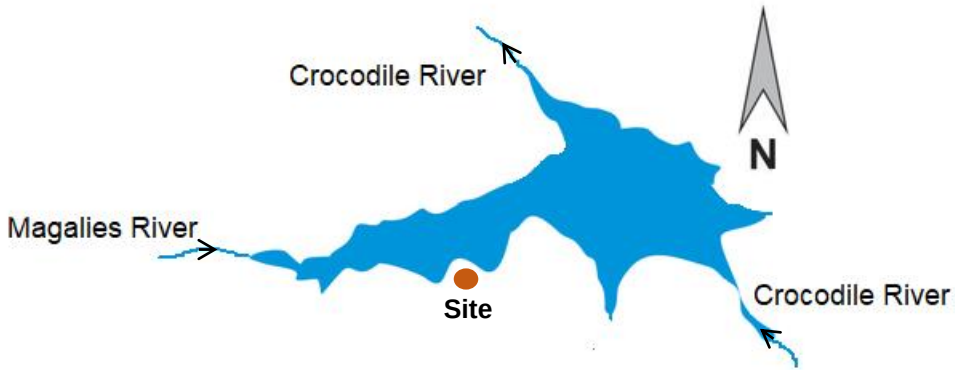

Figure 16: Harvesting and drying facility location at the Hartbeespoort Dam

Since the hyacinth's growth rate depends on environmental factors, the amount available to harvest will fluctuate throughout the year. In South Africa, hyacinth grow and proliferates roughly from September – April and then enters a dormant state from May–August. To estimate how much hyacinth is available to harvest, the amount of fresh hyacinth and dry hyacinth was estimated using the following:

- The Hartbeespoort Dam's surface area of 2062.8 ha (InfoSA, 2013).
- The Hyacinth covers 5 - 80% of the total surface area, depending on the season.
- During the proliferation months 30–80% of the Hartbeespoort Dam's surface area will be covered, and during the dormant months 5 – 20% will be covered.

- According to Simbayi et. el., (2023), 20 dtha can be harvested from the Hartbeespoort Dam. An availability range was determined using 20 dtha and the lower bound of 28.8 - 33.2 dtha from Su et al., (2018).
- Fresh hyacinth is assumed to have an initial moisture content of 80%.

Based on the above assumptions, the amount of fresh hyacinth available for harvesting and corresponding dry material were estimated (Appendix D, Figures D.1.1 and D.1.2). Since there is a variety of variables to consider (a the dry ton/ha/annum (dtha) range, fluctuating surface area covered throughout the year and wind direction and where hyacinth mats in the harvestable vicinity) was considered. The amount of fresh hyacinth, per day and annum, required was determined for each PlasWEn plant size. Also the estimated amount of fresh and dry hyacinth available for harvesting, which is based on 20 dtha and 28.8 dtha, and on a surface area coverage of 5 – 50%. The hyacinth required and what is available for harvesting is shown in Table 11.

Table 11: Hyacinth required per plant size and the estimated amount available for harvesting

PlasWEn Plant	**Required**		
	Fresh	**Dry**	**Fresh**
tpd	**tpd**	**tpa**	
5	25	1 650	8 250
10	50	3 300	16 500
20	100	6 600	33 000
30	150	9 900	49 500
50	250	16 500	82 500
100	500	33 000	165 000
Surface area	**Available**		
%	**tpd**	**tpa**	
5	31 - 45	2 063 - 2 970	10 314 - 14 852
10	63 - 90	4 126 - 5 941	20 628 - 29 704
20	125 - 180	8 251 - 11 882	41 256 - 59 409
30	188 - 270	12 377 - 17 823	82 512 - 89 113
40	250 - 360	16 502 - 23 763	103 140 - 118 817
50	313 - 450	20 628 - 29 704	144 396 - 148 522

A permit to harvest hyacinth needs to be acquired from the Department of Water and Sanitation and currently there are two groups that have permits to harvest for commercialization purposes: 1) The Harties Foundation NPC that sponsors the removal of hyacinth and waste management, and 2) Hya Matla Organics that converts hyacinth into compost. Harvesting hyacinth is an expensive process, where the equipment, fuel consumption, skilled labour and the high moisture content leads to high handling costs (Li, et al., 2021) and can limit potential commercialization. It is suggested that harvesting be

primarily done by manual labour, limiting heavy machinery at the shoreline. One or two decks built for small to medium TLBs to operate from and a small boat or bard can be incorporated. Depending more on manual labour will decrease the use of fuel and skilled labour, and increase the number of jobs provided to the community. As reference, 230 ton of fresh hyacinth/day can be harvested, with a team of 15 labourers, 2 trucks and a boat. From Table 11 it can be seen that the Hartbeespoort Dam can easily sustain up to 50 tpd with surface area coverage of 30-40%. However, to compensate for the seasonal fluctuation and as a safe guard, a harvesting strategy can be implemented. An additional % of hyacinth can be harvested and prepared during the growing season, since this study found that negligible change occurs when the hyacinth is stored in a dry, dark place (refer to Section 3.3.1). Consideration can be given to store the chipped material and then pelletize before use, or to store pelletized material. This will ensure that enough prepared material is available throughout the year. Should any deviation in harvesting occur, co-gasification can be utilized with other waste types, *i.e.* biomass, RDF, and MSW can be considered.

6.3 PlasWEn Process Description

Different PlasWEn plant sizes, *i.e.,* 5, 10, 20, 30, 50 and 100 tpd are evaluated, with special interest in a 20 tpd operation, based on the following two scenarios: A) Both the syngas and the reject energy produced is converted into electricity (Scn1), and B) the syngas produced is converted into electricity and heat energy produced is sold as heat for other process needs or building heating (Scn2). In both scenarios the operational energy required is subtracted from the total electricity produced, 20% heat energy is redirected to the intermediate storage/continuous feeding system and the remaining 80% heat energy is either converted into electricity or redirected as heat energy and sold. The overall process can be described using the simplified block diagram given below in Figure 17.

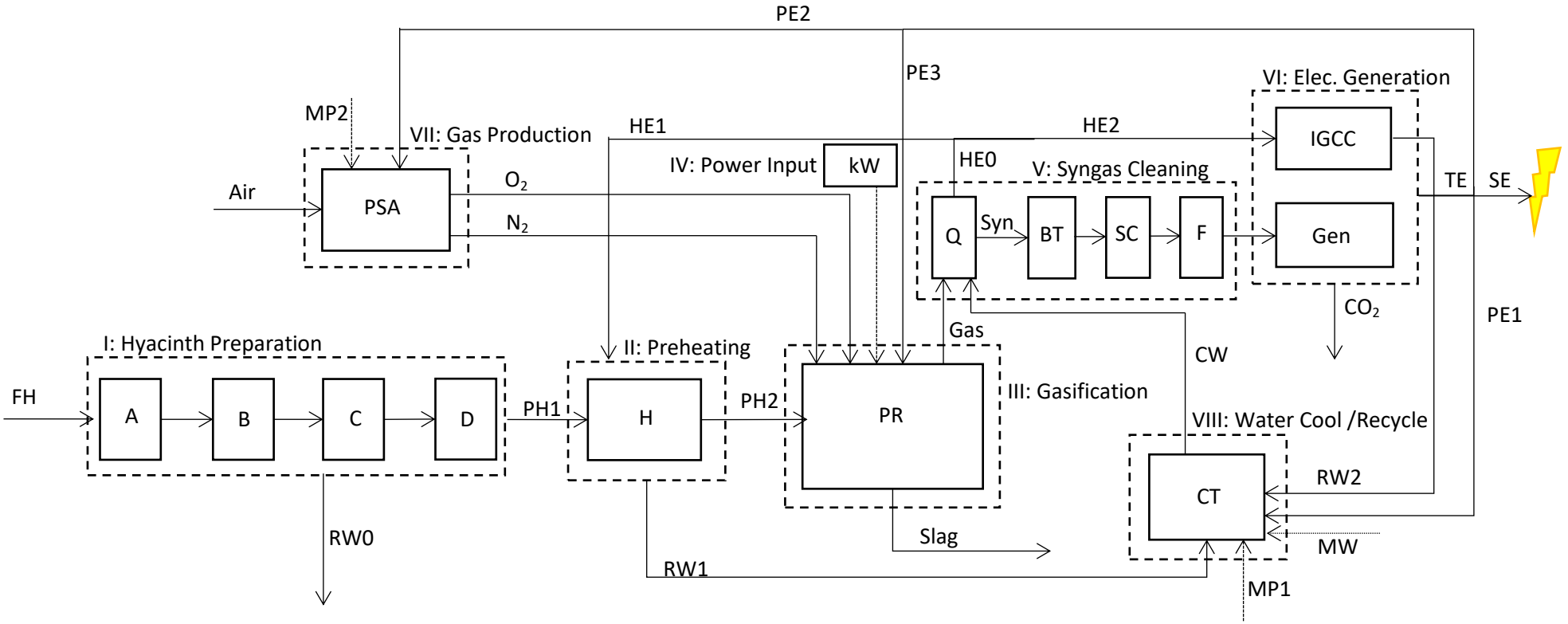

Figure 17: Process block diagrame

The hyacinth preparation (I) will be located at the site indicated in Figure 16, the hyacinth is harvested, and the fresh hyacinth (FH) is immediately fed to a crusher (A). Crushing the hyacinth will allow moisture to escape faster from the cellulose structure, halving the drying time. The crushed hyacinth is then transported by conveyor to the drying facility (B), where the hyacinth will be dried atmospherically. The hyacinth will be laid out on concrete slabs exposed to wind and radiation from the sides, but also protected from rain with roofing. After 1 week, the semi dry hyacinth material (20-40% H_2O content) is transported by conveyor and fed to a chipper (C); chipping semi dry hyacinth will prevent the hyacinth from powderizing, since the stems of dry hyacinth can be difficult to chip due to its sponge like and elastic nature (as noted during experimentation). The chipped hyacinth is then pelletized (D), a biomass needs a moisture content of at roughly 20% for pelletization. The heat due to friction from pelletizing evaporates 5-10% moisture and causes the lignin to act as a binding agent, resulting in a densified feed. Pelletization will lower transportation costs, aid in the prevention of bridging, and clumping in the feedscrew and theoretically result in a smaller reactor volume. Roughly 60–70% initial moisture (RW0) will be removed in the material preparation steps, and it is assumed that all the water is released into the environment via natural evaporation, and without environmental consequence. The pelletized hyacinth (PH1), with a moisture content of 10-15%, is then transported to the intermediate storage and preheating section (II), which consists of a hopper (H) that is preheated between 400-500 °C. Air will be separated by a pressure wing absorption unit (PSA) to provide N_2 and O_2 to the plasma reactor (PR). The preheated pellets (PH2) with is fed to (PR), at a median temperature of 1000 °C, converting the hyacinth into gas (Gas) and inorganic slag (Slag). The (Gas) steam proceed to go through syngas cleaning steps (III); it is firstly cooled rapidly via a quench heat exchanger (Q), forming into syngas (Syn), then flows through a bubble trap (BT), scrubbers (SC) and a filter (F) before it enters the generator, (IGCC) for Scn1 or Gen for Scn2) to be converted into electricity. The heat energy (HE0) resulting from quenching is split into two streams: (HE1) preheats (II) using 20% of (HE0) and the remaining 80% of (HE0), (HE2), and (Syn) are converted into electricity by An itegrated gasification combined cycle gas turbine (IGCC) for Scn1, or only (Syn) is converted into electricity using a single power generator (Gen) for Scn2. The total electricity produced (TE) sustains the plant energy requirements (PE1), (PE2) and (PE3) which powers the cooling tower (CT), the pressure swing absorption (PSA) unit and the PlasWEn reactor (PR). The electricity remaining is available for sale, (SE). The CO_2 from the generator is fed into the greenhouse system, and the rest is released into the atmosphere. The recycled water

streams (RW1) and (RW2) are sent to the cooling tower (CT). For the start-up and after maintenance shutdowns, a power supply (kW) will be used to power the torch, (MP1) and (MP2) are municipal power that will power (CT) and (PSA), and municipal water (MW) connected to (CT) will provide water.

6.4 Capex Development

6.4.1 Introduction and Capital Flow

The conceptual design of the plant is based on laboratory scale developmental studies and experiments done at NECSA, and of literature. To determine if the H-PlasWEn system yields a profit will show if hyacinth is an acceptable feedstock for plasma gasification under the specified operating conditions. The cost of capital is the total cost incurred in order to secure funding a company needs to acquire, develop, produce and maintain its future sources of income (Lilford, 2006). It is important to be aware of the different costs incurred at all steps involved with building and operating the process plant, since the total income minus the expenses equals the net profit (Peters & Timmerhaus, 1991). The capital investment required for any industrial process is an important part of the plant design and includes direct and indirect capital expenses or cost (Peters & Timmerhaus, 1991). In this financial analysis the capital investment, manufacturing, and general expenses, including income taxes, depreciation and inflation indexes, are taken into consideration. Factors affecting costs such as cost fluctuations, wage fluctuations, company policies and governmental regulations (Peters & Timmerhaus, 1991) are up to date and taken into account. Even though an extensive analysis has been done, the results obtained are an estimate and some variation might occur when a more in-depth evaluation is done. A financial flow diagram without the purchase of land is given in Figure 18.

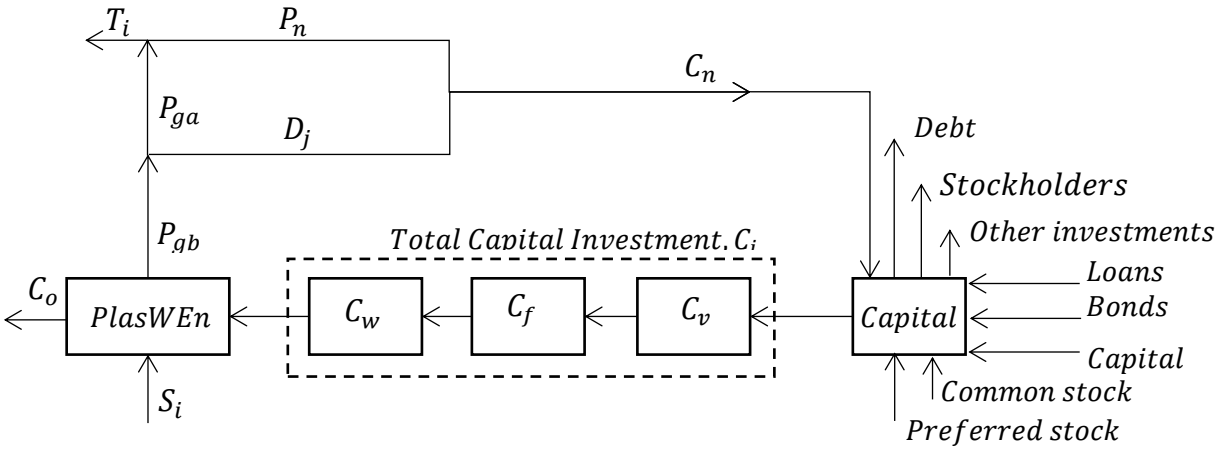

Figure 18: Capital investment and expense flow diagram

The capital needed to finance the project is secured through debt and equity, and depicted as the Capital in Figure 18. The capital invested known as the total capital investment, $C_i, = C_v + C_f + C_w$, consists of the variable cost, C_v, fixed capital cost, C_f, and working capital cost, C_w (Peters, et al., 2003). The C_i covers the equipment acquirement, construction, labour and business overheads…etc costs to construct a functioning H-PlasWEn process plant. Once the plant is operational and in production, then the total sales income, S_i, flowing in and the operational costs, C_o, flowing out can be taken into account of the financial system (Peters, et al., 2003). The gross profit, P_g, is depicted as, $P_{gb} = S_i - C_o$ (before depreciation charge D_j) and $P_{ga} = S_i - C_o - D_j$ when taking the depreciation, D_j, charge of the plant into consideration. The income tax due, $T_i = (S_i - C_o - D_j)T_r$, with the current tax rate, T_r, are deducted from the gross profit resulting in the net profit, $P_n, = P_{ga} - T_i = (S_i - C_o - D_j)(1 - T_r)$ (Peters, et al., 2003). Where the net cash flow, $C_n = P_n + D_j = P_{gb}(1 - T_r) + D_j = (S_i - C_o)(1 - T_r) + D_j$, makes a full circle to the capital source and outflow, and the payments due to loans, stockholder dividends and the like are then paid (Peters, et al., 2003). The C_o, and payments due to banks and stockholders then rely on the total income of the plant to sustain it year to year. The steps involved in developing the techno economic study are described below

6.4.2 Capital Investment

The C_f is the investment necessary for manufacturing and plant facilities and can be subdivided into manufacturing and non-manufacturing fixed-capital investment (Peters & Timmerhaus, 1991). The C_w is the investment necessary for the operation of the plant and

consists of the total investment made into raw materials and supplies, finished and semi-finished products, accounts receivable, cash kept on hand for monthly payment of operating expenses (Peters & Timmerhaus, 1991). The C_e is one of the major costs involved in any industrial process (Peters & Timmerhaus, 1991). Cost data and current cost correlations are difficult to obtain and kept confidential by engineering, procurement and construction (EPC) companies (Towler & Sinnott, 2008). The actual prices for equipment and supplies bought in bulk may differ from catalogue prices since they depend on the purchasing power of a client and discount or sub-charges that are also confidential business information (Towler & Sinnott, 2008). For this study C_e is estimated using Eq 6, for gasification plants between 5–100 tpd, based on the scaling factor, s_f, and cost factor, a.

$$C_e = a^{s_f} \qquad Eq\ 6$$

The cost factors, a, is simplified, resulting in the cost varying linearly with plant size and scaling factor. The scaling factor, $s_{f,}$ is determined by using a 10 tpd size plant cost as reference as seen in Eq 7 below.

$$s_f = (\frac{n_i}{10})^{0.75} \qquad Eq\ 7$$

Where $n_i = 5, 20, 30, 50\ and\ 100\ tpd$.

The scaling factor equation is derived from empirical data on the relationship between plant size and equipment cost. The equation used, Eq 7, is commonly used in industry and a scaling factor of 0.75 is used by NECSA, and is dependent on specific equipment and technology used in a gasification plant. Both Eq 6 and Eq 7 were used to determine the equipment costs for plant sizes 5-100 tpd given in Table 12. The (PSA) unit saves cost on purchasing pure O_2 and N_2 commercially and will be used in both Scn1 and Scn2. All the equipment listed in Table 12 are used in both scenario process designs and therefore part of the fixed capital. The fixed capital cost has both direct and indirect costs that contribute to the building and start-up of the gasification plant. The costs of raw materials, labour, equipment and installation, yard improvements, installation costs (labour and materials), instrumentation, valves and piping, electrical installation, service facilities are examples of direct costs (Peters & Timmerhaus, 1991).

Table 12: Equipment cost analysis

PlasWEn Process Cost (kR)						
PlasWEn Plant Size (tpd)	**5**	**10**	**20**	**30**	**50**	**100**
Solids fed preparation system	714	1 200	2 018	2 735	4 012	6 748
Solids feed system	285	480	807	1 094	1 605	2 699
Chipper	149	250	420	570	836	1 406
Gasification reactors	446	750	1 261	1 710	2 508	4 218
Power Supply	535	900	1 514	2 052	3 009	5 061
Torches	178	300	505	684	1 003	1 687
Quench system	214	360	605	821	1 204	2 024
Refractories	208	350	589	798	1 170	1 968
Filters	59	100	168	228	334	562
Scrubbers systems	51	85	143	194	284	478
Driers	89	150	252	342	502	844
Gas Buffer Vessel	208	350	589	798	1 170	1 968
Blower	178	300	505	684	1 003	1 687
Cooling water supply plus cooling tower	119	200	336	456	669	1 125
PSA for enriched air	446	750	1 261	1 710	2 508	4 218
Argon supply	18	30	50	68	100	169
Flares	446	750	1 261	1 710	2 508	4 218
Control System PLC plus programming	357	600	1 009	1 368	2 006	3 374
Sub-total	4 700	7 905	13 295	18 020	26 432	44 453

Costs for administrative salaries, product-distribution costs, interplant communications, engineering and supervision (construction design and engineering), contractor fees and contingencies (estimates have statistically shown to be of a recurring nature) are examples of indirect costs (Peters & Timmerhaus, 1991). The direct and indirect costs are shown in Table 13.

Table 13: Fixed capital breakdown for the direct and indirect costs investment

Direct Costs (DC) (kR)						
PlasWEn Plant Size (tpd)	**5**	**10**	**20**	**30**	**50**	**100**
Purchased Equipment	4 700	7 905	13 295	18 020	26 432	44 453
Installation costs	564	949	2 659	3 604	9 251	15 559
Instrumentation	705	711	1 329	1 802	2 643	4 445
Valves and piping	705	791	1 994	2 703	5 286	8 891
Electrical	564	791	1 595	2 162	3 965	6 668
Buildings Incl offices, stores etc	470	791	1 994	2 703	5 286	8 891
Yard improvements	235	395	931	1 261	2 643	4 445
Service Facilities	470	316	2 659	5 406	10 573	17 781
Power generators (Scn2)	3 601	6 056	10 185	13 805	20 250	34 057
Power Generators Combined Cycle (Scn1)	5 402	9 084	15 278	20 708	30 375	51 085
Total Direct Costs (Scn1)	13 815	21 732	41 734	58 369	96 455	162 218
Total Direct Costs (Scn2)	12 015	18 704	36 642	51 466	86 330	145 190
Indirect Costs (IC) (kR)						
Engineering and Supervision	940	1 581	2 659	3 604	5 286	8 891
Construction Expenses	235	1 186	1 994	3 604	7 930	13 336
Total Indirect Costs	1 175	2 767	4 653	7 208	13 216	22 227
Total Direct and Indirect Costs (DC+IC) (kR)						
(Scn1)	14 990	24 499	46 387	65 576	109 671	184 444
(Scn2)	13 190	21 471	41 295	58 674	99 546	167 416
Contractors Fees (% of DC+IC)	3 718	3 071	5 697	7 992	13 098	22 028
Contingency (% of DC+IC)	2 789	1 536	2 849	3 996	6 549	11 014
Fixed Capital Investment (kR)						
(Scn1)	21 497	29 106	54 933	77 565	129 318	217 486
(Scn2)	19 697	26 078	49 840	70 662	119 193	200 458

The direct fixed costs can be determined using an estimated factor of either the total capital investment or of the purchased equipment costs (Peters & Timmerhaus, 1991). Standard weighting factors were adjusted to more conservative values, based on the PlasWen's simple installation, in order to provide for the relevant situation (obtained from the JSE business section by NECSA). These factors were calculated based on the purchased equipment costs and presented in Table 14

Table 14: PlasWen weighting standards

Weighting Factors (%)							
PlasWen Plant Size	**5**	**10**	**20**	**30**	**50**	**100**	**T&P**
Purchased Equipment							
Purchased Equipment							
Installation costs	12	12					20-50
Instrumentation	15	9					30-Aug
Valves and piping	15	10					10 - 60
Electrical	12	10					15-Jun
Buildings Incl offices, stores etc	10	10					30-Dec
Yard improvements	5	5					15-Aug
Service Facilities	10	4					15-80
Land	2	2					08-Apr
Power Generators							
Engineering and Supervision	20			20	20		20-40
Construction Expenses	15			20	30		16-40
Direct and Indirect Costs (DC and IC)							
Contractors Fees (% of DC+IC)	20	10					24-Aug
Contingency (% of DC+IC)	15	10					15 - 45
Reference	This study						a
a) Peters & Timmerhaus, (1991)							

In Scn2 a gas turbine generator or a reciprocating engine generator is used which is specifically designed to burn the syngas and convert the energy released into electricity. In Scn1 a CCTG is used to convert the syngas into electricity and the steam is then used to power a steam turbine generator, which produces additional electricity. The CCTG is essentially two generators in one system, but they are still separate components working together to produce electricity. The different costs involved for each generator and the effect it has on the total cost is reflected in Table 13. Therefore indirect costs stay the same for both scenarios however the direct cost varies. Startup expenses can be, but are not necessarily, included in the total capital investment, it can be 8-10% (or up to 12%) of the fixed-capital investment, or be represented as a one-time expense (in the first year of operation) (Peters & Timmerhaus, 1991).

6.4.3 Operational Cost

Operational time, rate of production, and sales demand are interrelated and contribute to an ideal plant operation, where the maximum production rate is obtained while the total cost per unit of production is minimized (Peters & Timmerhaus, 1991). One of the first things that can minimize costs is in the steps taken for the sample preparation. By

choosing to solar dry, up to 70% of the reject or heat energy produced, that would be needed to dry the material to 10% moisture content (Appendix D.1, Figure D.1.3), can be either sold as a product or redirected to save on electricity costs. Pelletizing the hyacinth will not only minimize transport cost, but also act as a means to prevent discontinuous feed and reduces the probability of small particles causing damages downstream. Since the hyacinth will be atmospherically dried. The subtotal variable cost consists of the process water, cooling water, Argon and Nitrogen (kg/MWh) and is shown in Table 15. The scaling equations were applied and factors used for each plant size (Appendix D,2 Table D.2.1).

Table 15: Variable costs

Variable Costs (R/MWh)						
PlasWEn Plant size (tpd)	**5**	**10**	**20**	**30**	**50**	**100**
Subtotal Variable Cost	1.91	3.03	4.95	6.64	9.65	16.09

The labour, production overheads, factory costs, business overheads and repairs and maintenance are part of the fixed operational costs. The labour costs are shown in Table16.

Table 16: Labour costs

Fixed Costs								
Labour (kR/a)								
PlasWEn Plant size (tpd)			**5**	**10**	**20**	**30**	**50**	**100**
Variable	**Fraction**	**Cost/unit**	**Total Cost**					
Plant Supervisor		500	50	100			150	
Process Controller		300	300		600		1 200.00	1 500.00
Process Controller		300	300		600			
Fitter		300	75					
Helper		90	270	450	900	1 350.0		
Overtime	15%	70.5	78	123	129.8	227.3	285.8	286
Sub-total Direct Labour			**799.3**	**1 363**	**2 526**	**3 043**	**3 101**	**3 101**

It can be seen that there is a significant increase in labour expenses with increasing plant size. The work load is divided into shifts and reflects the number of people required with an increased sized plant. Whereas the production overheads and factory costs given in Table 17 and Table 18.

Table 17: Production overheads

Production Overheads (kR/a)							
PlasWEn Plant Size (tpd)		**5**	**10**	**20**	**30**	**50**	**100**
	Cost/unit	**Total Cost**					
SHEQ	275	275					
Plant Overheads	50	50					
Indirect Labour Cost	60	9			18	30	
Sub-total Production Overheads		**86.5**			**95.5**	**107.5**	

Table 18: Factory costs

Factory Costs (kR/a)							
PlasWEn Plant Size (tpd)		**5**	**10**	**20**	**30**	**50**	**100**
Variable	**Cost/unit**	**Total Cost**					
Protective Clothing	2.5	2.5		5	7.5	10	12.5
Operating Supplies	30	9			15	30	
Gas Cylinders	0.5	0.5					
Other Operating Cost	10	5			7.5	10	15
Sub-total Factory Cost		**17**		**19.5**	**30.5**	**50.5**	**58**

The factors used for Table 16, 17 and 18 are based on plant size (Appendix D, Table D.2.2). The business overheads are given in Table 19 and the repair and maintenance cost are given in Table 20.

Table 19: Business overheads

Business Overheads									
Plant size (tpd)				**5**	**10**	**20**	**30**	**50**	**100**
		Fraction	**Cost/unit**	**Total Cost (kR/a)**					
Mangement & Overheads		0.05	1 500	75					
Stationary		0.25	12	3					
Audit Fees		0.05	200	10					
Legal Fees		0.1	400	40					
Office Equipment		0.1	30	3					
Insurance (Assets)		0.50%	% of Capex	125.5	176.6	327.6	459.6	753.1	1 266.6
Insurance (GIT)	**(Scn1)**	0.10%	% of Sales	1.7	3.6	7.6	11.8	20.1	41.4
	(Scn2)			1.4	3	6.5	10	17.1	35.4
Insurance (GP)	**(Scn1)**	0.10%	% of Sales	1.7	3.6	7.6	11.8	20.1	41.4
	(Scn2)			1.4	3	6.5	10	17.1	35.4
Insurance (PBL)	**(Scn1)**	0.25%	% of Sales	3.9	8.3	17.5	26.9	46.1	94.7
	(Scn2)			3.2	6.9	14.8	22.8	39.2	81
Rates and Taxes		5.40%	26.8	25.3	42.7	107.7	146	285.5	480.1
General Expenditure		0.25	50	12.5					
Admin costs		0.02	50	1					
Subtotal business Overheads	**(Scn1)**			**302.6**	**379.3**	**612.6**	**800.5**	**1 269.4**	**2 068.70**
	(Scn2)			**301.3**	**376.8**	**607.5**	**792.7**	**1 256.5**	**2 042.9**

Table 20: Repairs and maintenance

Repairs and Maintenance (kR/a)			
PlasWEn Plant Size (tpd)			**5 - 100**
Variable	**Fraction**	**Cost/unit**	**Total Cost**
Maintenance Labour	0.25	200	50
Maintenance Materials	0.25	200	50
Operating Supplies	0.5	50	25
Sub-total Repairs & Maintenance			**125**

The total operational costs for 5-100 tpd plants are given in Table 21.

Table 21: Total operational costs

Total Costs (kR/a)							
PlasWEn Plant Size (tpd)		**5**	**10**	**20**	**30**	**50**	**100**
		Total Costs					
Total Costs (year 1)	**(Scn1)**	**1 331.3**	**1 975.00**	**3 382.3**	**4 121.5**	**4 720.5**	**5 694.8**
	(Scn2)	**1 330.00**	**1 972.40**	**3 377.20**	**4 113.80**	**4 707.70**	**5 669.10**

It can be seen in Figure 19 that the base fix cost, for both Scn1 and Scn2, increases logarithmically and the base variable cost increases polynomially with increasing size.

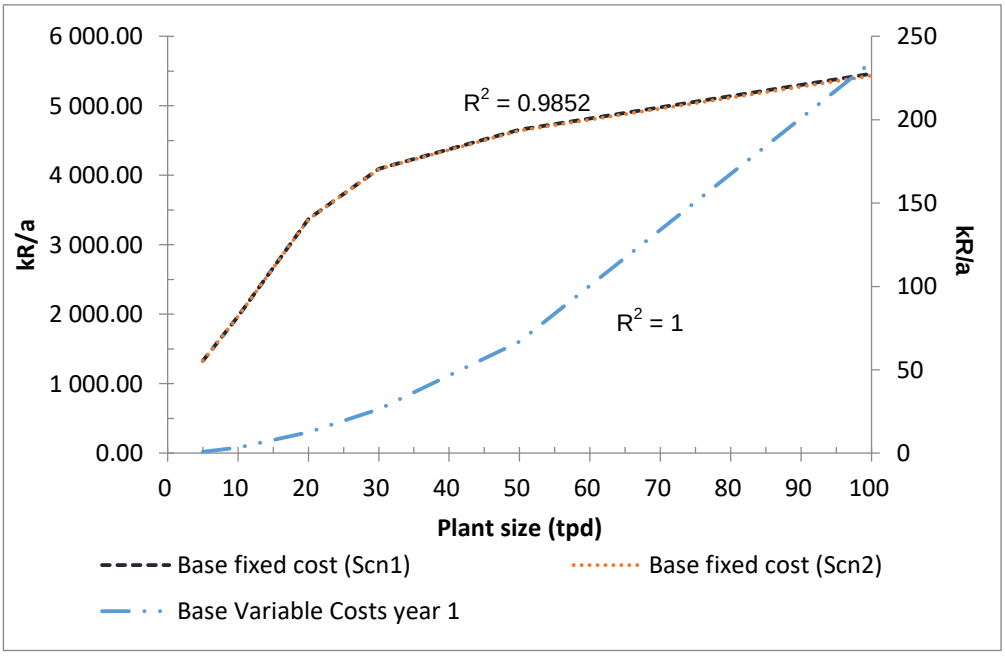

Figure 19: Base and variable fixed costs

By applying indexation from escalation weights (refer to Appendix D.4: Table D.4.1), the inflated operating cost estimation provide a more accurate representation of the costs expected during the plant life time. The annual inflated revenue for Scn1 and Scn2 is shown in Figure 20.

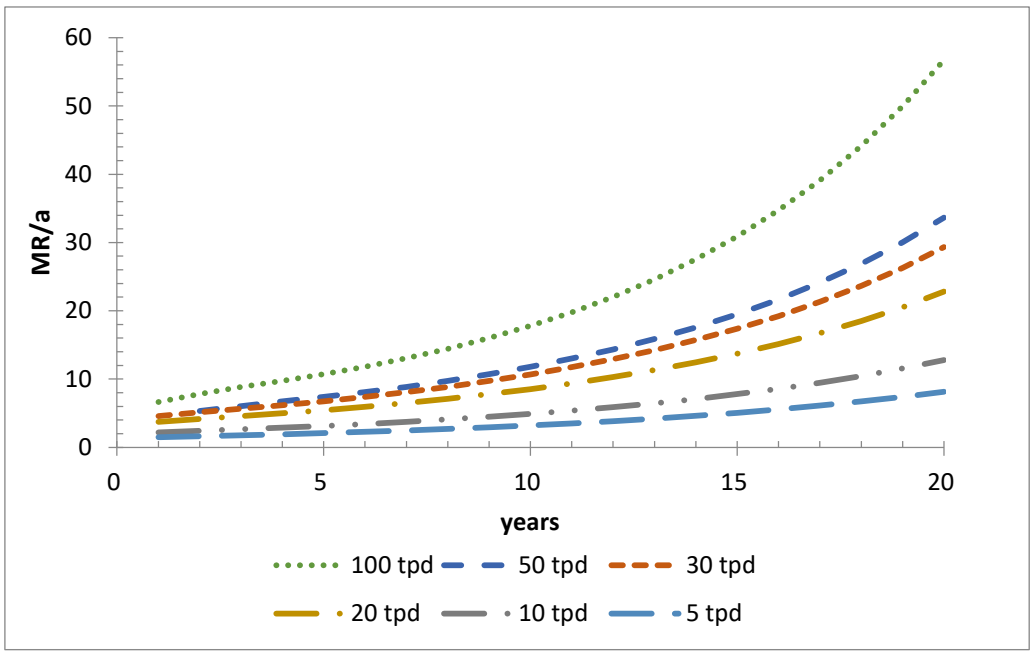

Figure 20: Inflated operating cost estimation for Scn1

The cost to produce electricity for both Scn1 and Scn2 for the first, second and from the third year onwards has a production capacity of 50, 85 and 100%, shown in Figure 21.

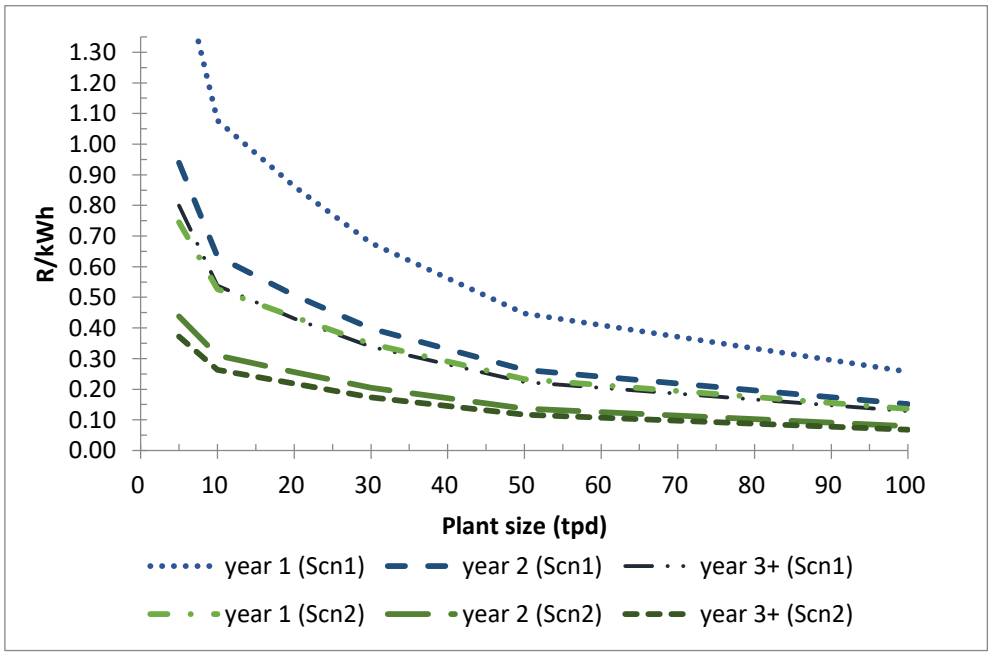

Figure 21: Total cost per kWh

The cost of production decreases linearly, seen in Figure 21, with 4 different decrease rates for plant sizes 5-10, 10–30, 30–50 and 50–100 tpd. The costs at an operational capacity of 85 and 100% for both Scn1 and Scn2 are similar. The cost per kWh for Scn1 is higher than for Scn2, primarily due to more kWh available as heat or loss of kWh due to converting heat to electricity. However, the heat energy is sold at a fraction (20%) of the electricity selling price and will be taken into consideration. The production and operational cost for both scenarios are equivalent and except for a different generator, the capital costs are also the same as seen in Figure 19. Therefore, the amount of kWh available without considering the workability or the selling price of the energy is reflected.

6.5 Plant Production and Sales Revenue

6.5.1 Plant Production

Referring to Figure 17, the total electricity stream (TE), and the plant energy requirement (PE) the total heat energy stream (HE0), as heat and electricity can be seen. The heat stream (HE0) is split into two streams, 20% is redirected to pre-heat the feed material entering the reactor, stream (HE1), and the remaining 80%, stream (HE2), which can either be converted into electricity (Scn1) or sold as heat energy (Scn2). The electricity for sale is the plant energy requirement subtracted from the total electricity produced, seen in Figure 22 is the increasing % electricity available for sale and the decreasing % electricity required for plant operation with increasing plant size.

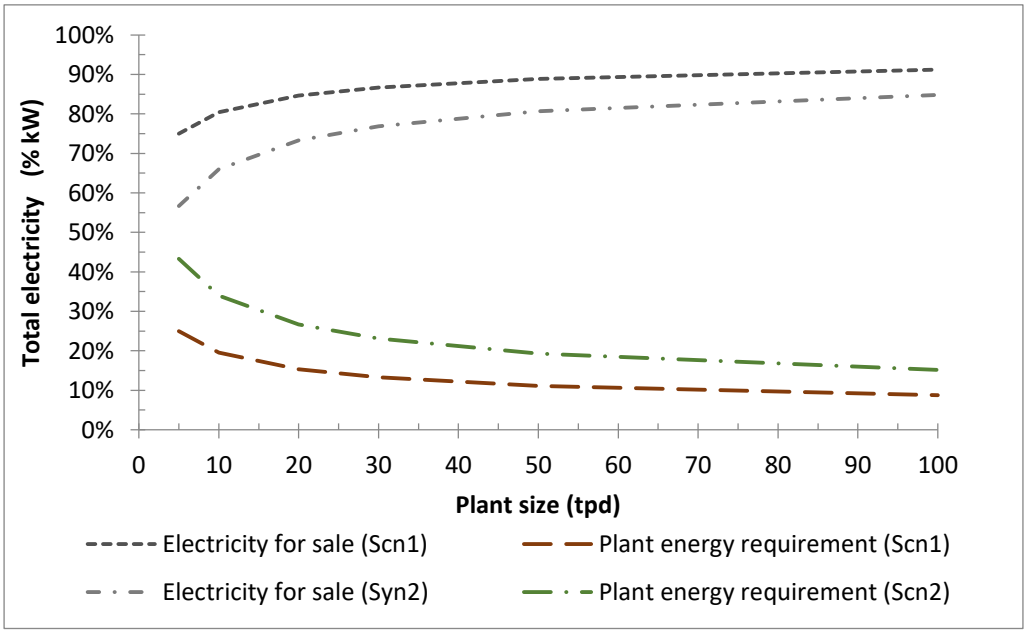

Figure 22: The % electricity available for sale and % required for plant operation

The electricity for sale (SE), from both the syngas and heat streams, along with the redirected heat stream (HE1), the total electricity (TE) and the plant energy requirement (PE) for Scn1, given in kW/d, are shown in Figure 24.

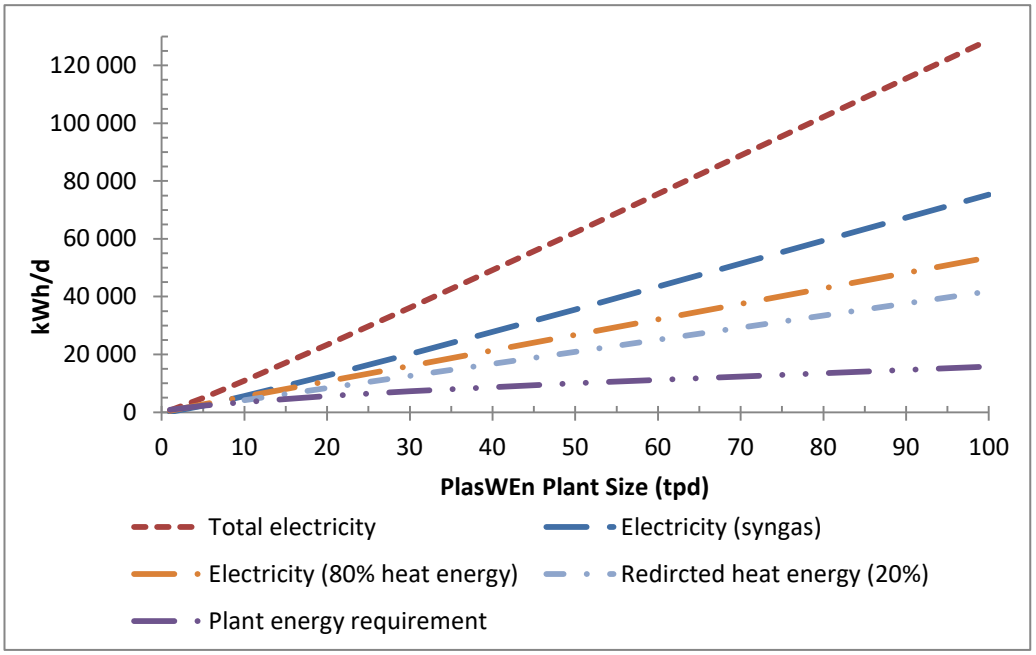

Figure 24: The energy streams for Scn1

The electricity for sale (SE), from the syngas, the heat energy for sale (HE2), along with the redirected heat stream (HE1), and the plant energy requirement (PE) for Scn2 can be seen in Figure 23.

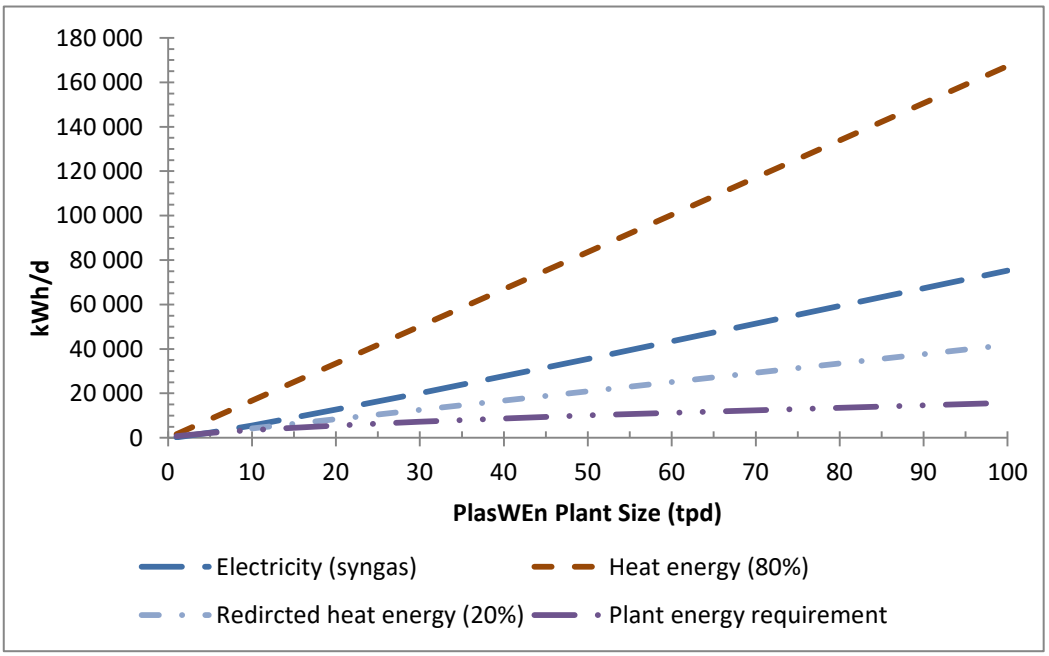

Figure 23: The energy streams for Scn2

From Figure 24 and Figure 23 it is evident that there is roughly a 20–40% increase in available electricity to sell when the heat energy is converted to electricity.

6.5.2 Energy and Ash Available for Sale

The energy available for sale is the energy available after the plant energy requirement and the redirection of 20% of the heat energy are deducted from the total energy streams. The energy for sale for the H-PlasWEn process, for the plant or project life time, is shown in Table 22. Where the production capacities of 50% (year 1), 85% (year 2) and 100% (year 3+) are incorporated. The baseline energy available, (Scn2), before the additional step of converting the heat or reject energy into electricity (Scn1). The ash and CO_2 produced can be sold as a by-product to be used in other industries. The ash will be sold as aggregate and the CO_2 will not be taken into account and seen as negligible since it is produced via the utilization of an invasive biomass as a fuel source.

Table 22: Energy and ash available for sale per annum

Plant Size (tpd)	5	10	20	30	50	100
Conversion of syngas and heat: Electricity (MWh/a)						
year 1	821	1 802	3 856	5 966	10 269	21 253
year 2	1 396	3 064	6 555	10 142	17 457	36 131
year 3 +	1 642	3 605	7 712	11 932	20 537	42 506
Conversion of syngas: Electricity (MWh/a)						
year 1	379	919	2 089	3 316	5 851	12 419
year 2	645	1 562	3 552	5 637	9 947	21 112
year 3 +	759	1 838	4 178	6 631	11 703	24 837
Conversion of heat: Electricity (MWh/a)						
year 1	442	883	1 767	2 650	4 417	8 835
year 2	751	1 502	3 004	4 506	7 509	15 019
year 3 +	883	1 767	3 534	5 301	8 835	17 669
Heat energy (MWh/a)						
year 1	1 380	2 761	5 522	8 282	13 804	27 608
year 2	2 347	4 693	9 387	14 080	23 467	46 934
year 3 +	2 761	5 522	11 043	16 565	27 608	55 216
Ash (t/a)						
year 1	106	211	422	634	1 056	2 112
year 2	180	359	718	1 077	1 795	3 590
year 3 +	211	422	845	1 267	2 112	4 224
CO_2 Generator Emissions ()						
year 1	536	1 073	2 145	3 218	5 363	10 725
year 2	912	1 823	3 647	5 470	9 116	18 233
year 3 +	1 073	2 145	4 290	6 435	10 725	21 450

6.5.3 Sales Revenue

The sales income, in million Rands (MR) per annum for the electricity sold for Scn1 and for Scn2 is given in Table 23. The sales income shown is known as the base income and does not account for the influence inflation will have on future sale prices and therefore the revenue.

Table 23: Base revenue for both Scn1 and Scn2

PlasWEn Plant Size (tpd)	5	10	20	30	50	100
Scn1: Base Revenue (MR)						
year 1	1.3	2.8	5.9	9.2	15.7	32.5
year 2	2.2	4.7	10.1	15.6	26.7	55.3
year 3 +	2.5	5.6	11.9	18.3	31.5	65.0
Scn2: Base Revenue (MR)						
year 1	1.0	2.3	5.0	7.7	13.3	27.7
year 2	1.8	3.9	8.4	13.1	22.7	47.1
year 3 +	2.1	4.6	9.9	15.4	26.7	55.4

By applying indexation from escalation weights, the inflated revenue estimates provide a more accurate representation of the revenue expected during the plant life time. Indexation from escalation weights (refer to Appendix E.D: Table D.4.1), along with the current inflation factors given in Table 24, are used to calculate an inflated revenue in order to account for the impact of inflation over time.

Table 24: South African inflation factors

Inflation Factors	
PPI	10.6%
Labour	8.0%
Power	11.0%
CPI	7.1%
Materials	7.0%

The annual inflated revenue for Scn1 is shown in Figure 25, where there is a steady decrease in the inflated revenue difference between Scn1 and Scn2. Starting with a 17.8%, 16.5%, 15.7%, 15.3%, 14.9% and 14.5% difference for a 5, 10, 20, 30, 50 and 100 tpd PlasWEn plant sizes, with the assumptions for both scenarios as given in Table 10. Other than the electricity available for sale there are financial factors that play an important role in the feasibility of the project and will be discussed in the following section.

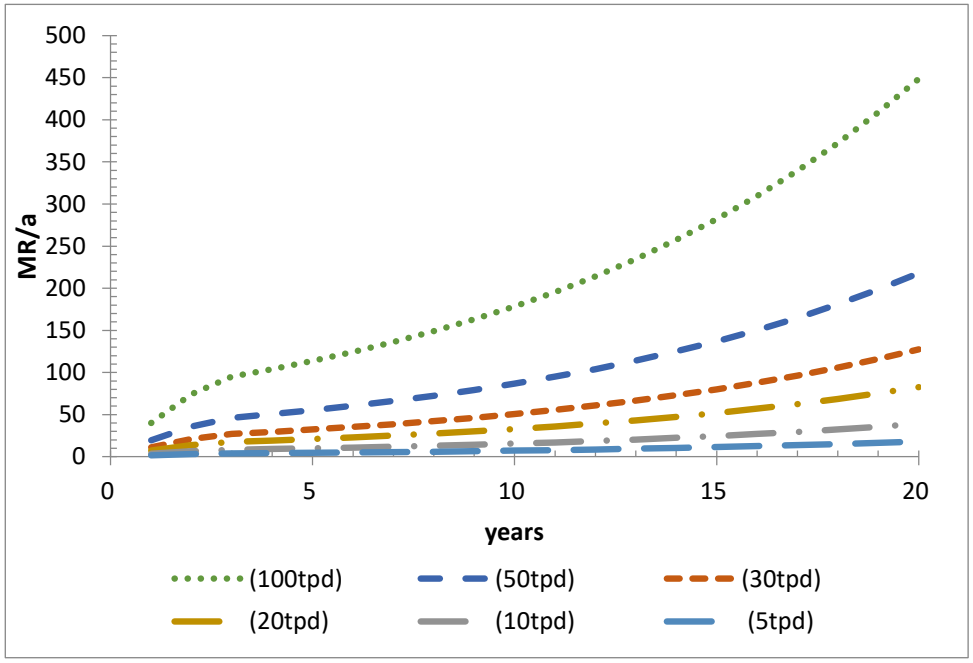

Figure 25: The annual inflated total revenue based on plant size

6.6 Financial Factors

Weighted Average Cost of Capital (WACC): The WACC is the average cost incurred from all sources of financing, and represents the minimum discount rate for a company's cash flows to ensure that the capital they raise generates returns higher than the cost of obtaining that capital. A discount rate is the cost of capital for supplying capital to the company or project, and is the return or consumption power expected by the capital provider for an investment (Lilford, 2006). Therefore, it serves as a discount rate in financial models to calculate the Net Present Value (NPV) of a project. NPV represents the difference between the present value of expected cash inflows and outflows, considering the time value of money (Towler & Sinnott, 2008). WACC reflects the opportunity cost of investment and is used to discount cash flows to their present values (Lilford, 2006). Simply put, WACC is the minimum rate of return required by a company to satisfy creditors and shareholders, while NPV measures project profitability (Towler & Sinnott, 2008). Returns higher than the WACC ensure the viability of existing projects and the development of future projects (Lilford, 2006). In the WACC calculation, the real rate is the inflation-adjusted risk-free rate of return, and accounts for inflation and provide investors with a real return. The real return is calculated by subtracting the inflation rate

from the nominal risk-free rate. The real rate is crucial for determining the cost of debt and equity, which are weighted to calculate the WACC. Therefore, the real rate is the investment's rate of return adjusted for inflation, specific to a country, and reflects the actual purchasing power of the investment returns. The WACC takes into account the balance between equity and debt in a company's capital structure, along with their individual costs of equity (K_e) and debt (K_d). It is used to assess the overall cost of financing for a project, taking into account the relative weight of equity and debt in the capital mix (Lilford, 2006). Debt financing has the advantage of tax-deductible interest payments (Steffen, 2020) and therefore equity shares are kept to a minimum. WACC is applicable for building a project, as well as the operational costs during the project's lifetime. The WACC can be calculated using Equation Eq 8.

$$WACC_{nominal} = [K_e * (\frac{e}{d+e})] + [K_d * (\frac{d}{d+e})] \qquad Eq\ 8$$

Where e is the equity % and d is the debt %, and $(\frac{e}{d+e})$ and $\left(\frac{d}{d+e}\right)$ reflects the equity or debt proportion in the capital structure. Taking inflation into account the real WACC is calculated using the Equation, Eq 9 (Steffen, 2020), below.

$$WACC_{real} = \left(\frac{1 + WACC_{nominal}}{1 + CPI}\right) - 1 \qquad Eq\ 9$$

Cost of equity (K_e): The K_e is the required rate of return for an investor to invest in a company's stock, considering the associated risk (Peters, et al., 2003; Kenton, 2023). It reflects the expense to the company of acquiring funds from equity investors. The K_e is calculated using the following Equation, Eq 10 (Lilford, 2006):

$$K_e = R_f + \beta\, x\, RPM \qquad Eq\ 10$$

Where, Risk-Free Rate (R_f): R_f is the return on an investment without the risk of default. It is often associated with government bonds that guarantee principal and interest payments. The R_f acts as a benchmark for assessing expected returns on other investments, where higher-risk investments are expected to offer higher returns to compensate for the added risk. Beta (Systematic Risk), (β): β measures a stock's sensitivity to market change due to economic, geopolitical and financial factors (Chen, 2023). β = 1 signifies perfect correlation with the market, while a β > 1 indicates higher volatility and a β < 1 suggests lower volatility (Lilford, 2006). Equity Market Risk Premium

(MRP): The MRP is the additional return investors expect from equities compared to R_f. It compensates for the higher risk associated with equity investments and influences the expected return on stocks (Chen, 2020). Small Stock Premium (α): The α is the extra return investors expect from small-cap stocks compared to large-cap stocks. It compensates for the additional risk associated with small-cap stocks, including liquidity and market concentration risk (Maverick, 2022). Cost of debt (K_d): The K_d is the return lenders demand for providing debt financing to a company. It includes the pre-tax cost of debt and the tax benefit derived from the interest payments on debt (Hayes, 2023). K_d can be determined by using the following equation, Eq 11 (Hayes, 2023).

$$K_d = K_t * (1 - T) \qquad Eq\ 11$$

Where Pre-tax cost of debt (K_t): The K_t is the interest rate a company pays on its debt, considering credit risk and market conditions. It begins with the risk-free rate and adds a credit risk premium to account for the borrower's creditworthiness (Hayes, 2023). Tax rate (T_r): The T_r employed in determining the K_d is the company's marginal tax rate, representing the proportion of income paid as taxes. The formula considers the tax shield benefit obtained by deducting interest expenses from taxable income. $K_d < K_t$ because the tax shield reduces the actual interest expense (Hayes, 2023). The formula uses the appropriate marginal tax rate for the specific company or project. Depreciation (D_j): Dj is the process of accounting for the decline in value of an asset or fixed investment over time due to factors like wear and tear, age, and obsolescence. The D_j is recorded on a company's income statement as an expense, reducing taxable income for fixed capital investments only (Towler & Sinnott, 2008; Peters, et al., 2003 & Investopedia, 2023). D_j does not apply to working capital or land purchases, as working capital can be recovered and land is assumed to retain its value (Peters, et al., 2003; Kenton, 2020). The book value of an asset is the difference between its original cost and the depreciation reserve; D_j does not involve any cash outlay or transfer of funds (Peters, et al., 2003). The declining-balance method has been applied to this study and is the accelerated D_j schedule that results in higher charges in the early years, improving project economics by generating higher cash flows initially (Peters, et al., 2003). The financial factors relevant to the South African market are presented in Table 25.

Table 25: Financial factor estimation

Financial Factors				
Deprec Allowance	year 1	40%	**Cost of Equity**	22.3%
	years 2-4	20%	**Risk Free Rate, (R_f)**	9.4%
Inflation Rate		7.3%	**Systematic Risk, (β)**	1.0
Interest Rate		11.3%	**Equity Market Risk Premium (MRP)**	7.9%
Debt Financing, (d)		70%	**Small Stock Premium, (α)**	5.0%
Equity Financing, (e)		30%	**Cost of Debt**	8.2%
$WACC_{nominal}$		12.4%	**Cost of Debt (Pr- tax), (K_t)**	11.3%
$WACC_{real\ rate}$		5.0%	**Tax Rate, (T_r)**	27.0%

Where K_e, K_d, $WACC_{nominal}$ and $WACC_{real}$ are calculated and the inflation, interest and tax (T_i) rates, R_f, β, MRP, α and K_t are values current to June 2023 in the financial market. Both e and d % were chosen as recommended by industry. The discount % that was calculated internally by NECSA is 9.5% and will be related to the $WACC_{nominal}$, and the inflation factors given in For this study the feasibility study uses equity and debt for financing the capital investment to build the H-PlasWEn plant and cover the first year's operational expenses and the operational cost are covered by the revenue generated after year 1. Table 25 represents conservative values with today's economic volatility in consideration.

6.7 Financial Feasibility

The financial model takes into account the two scenarios as stated in Table 10, and evaluates the profitability, payback period and sensitivity to changes in spent capital and sales revenue. The financial model uses different metrics to evaluate the profitability of an investment project over time. In this study the metrics used to analyse the feasibility include the NPV, IRR, RIRR, DPP and SPP.

6.7.1 Net Present Value (NPV)

Net Present Value (NPV): The NPV is used in investment planning and capital budgeting to analyse a project or investment's profitability by comparing the future cash flow's present value to the initial investment cost (Fernando, 2023). Therefore, NPV is the difference between the present value of cash -inflows and -outflows over specific time period, discounted at a predetermined rate (Peters, et al., 2003).

Generally a positive NPV indicates that the investment is profitable, where the reverse is true for a negative NPV value (Fernando, 2023). The NPV for Scn1 and Scn2 are shown in Figure 26 given in million Rands (MR). It is clear that Scn1 has a higher NPV value than Scn2 throughout the plant size range

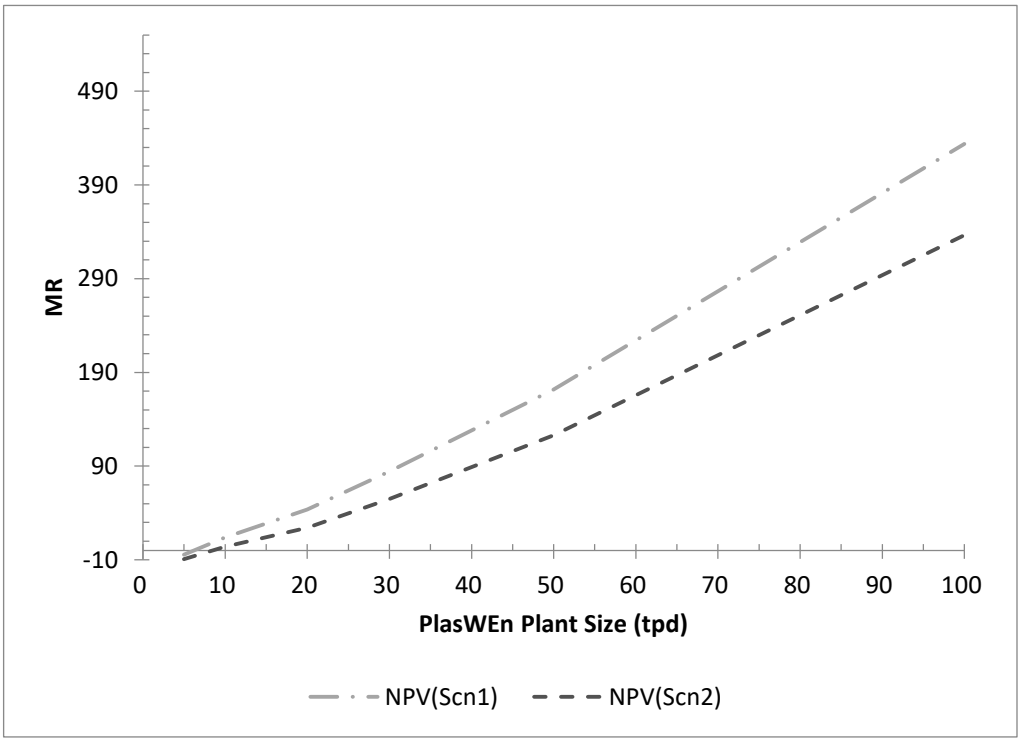

Figure 26: NPV for Scn1 and Scn2

6.7.2 Rate of Return (RR)

Internal Rate of Return (IRR): The IRR is expressed as a percentage and represents the discount rate at which all the investment's cash outflows equal zero, therefore the rate at which the NPV is equal to zero (Peters, et al., 2003; Fernando, 2023). A project is considered profitable if the IRR exceeds 15-20%, and used to rank projects based on their profitability since the IRR is the annual rate of growth generated by an investment. The IRR considers the timing and amount of cash flow only, and does not take into account inflation or the actual purchasing power of returns earned on an investment (Peters, et al., 2003). Real Rate of Return (RIRR): The RIRR is expressed as a percentage, and like the IRR, used to compare investment opportunities. However the RIRR shows the real benefit of an investment by also taking in to account the effect of both inflation and taxes on an investment's return (Hargrave, 2022). Therefore it represents the true rate of return on an investment.

Both the IRR and RIRR for Scn1 and Scn2 are shown in Figure 27 and presented as a percentage. It is clear that Scn1 has both an IRR and RIRR value higher than that of Scn2, throughout the plant size range. In general a project with an IRR value between 15-20% is considered profitable. However, to determine profitability specific to South Africa the RIRR needs to be considered. This can be achieved by using the $WACC_{nominal}$ factor given in Table 25, whereby the H-PlasWEn project is considered profitable for a plant sized 20 tpd and up, operating as Scn1, and a plant sized 30 tpd and up, operating as Scn2. When using NECSA's technology the discount factor of 9.5%, determined inhouse by NECSA can be used. This leads to the H-PlasWEn system to be considered profitable for a 10 tpd plant and up, operating as Scn1 and 30 tpd plant size and up, operating as Scn2.

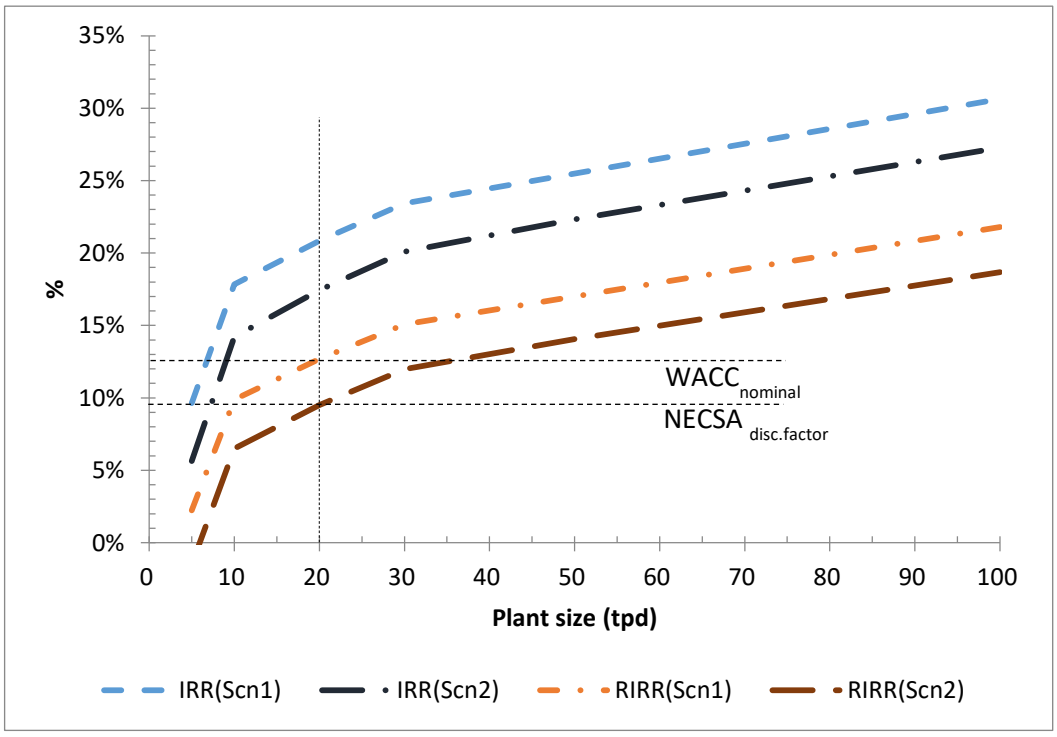

Figure 27: Rates of return for Scn1 and Scn2

6.7.3 Payback Period

Simple Payback Period (SPP): The SPP reflects the time to reach break even on the initial investment, but the time value of money is not taken into account (Kagan, 2023) (Fernando, 2023). Discounted Payback Period (DPP): The DPP is used in capital budgeting to determine the profitability of an investment, by reflecting the time it takes to break even with the initial investment, discounted at a given rate (Kenton, 2020).

It is an important measure of risk and liquidity, by recognizing the time value of money and discounting future cash flow (Kenton, 2020). The discount payback and simple payback periods for both Scn1 and Scn2 are shown in Figure 28. As seen the simple payback period for both Scn1 and Scn2 is significantly lower than the discount period for both Scn1 and Scn2, and that both the simple and discount payback periods for Scn1 are lower than those for Scn2 throughout the plant size range.

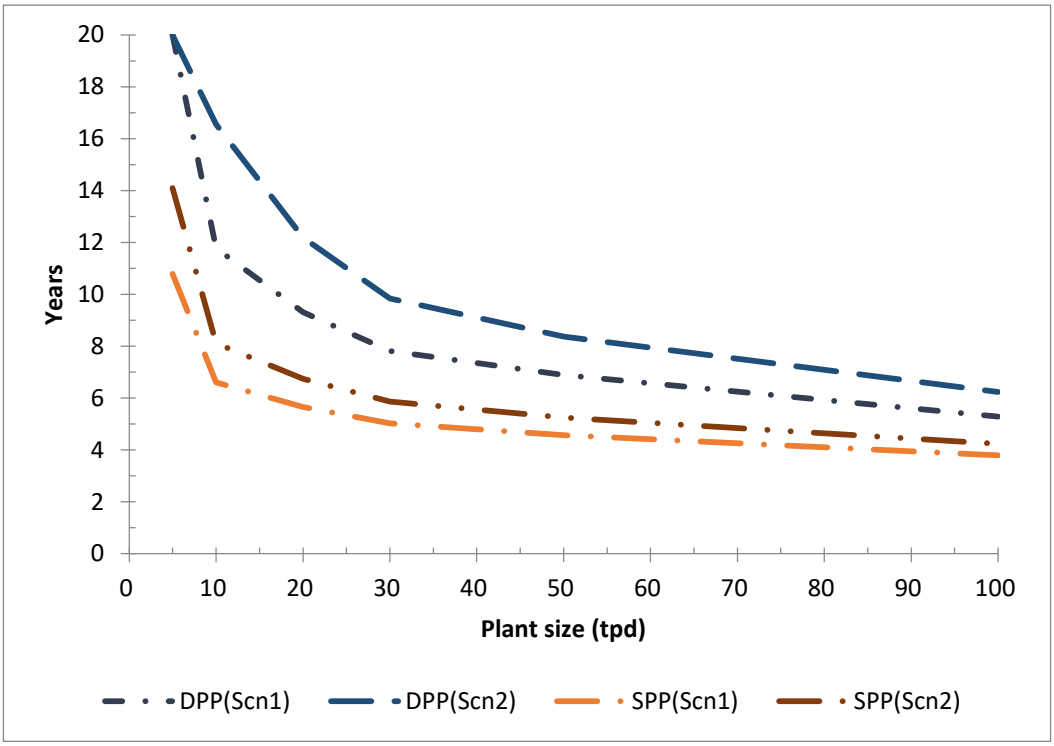

Figure 28: Payback periods for Scn1 and Scn2

6.8 Breakeven and Sensitivity Analysis

To evaluate the H-PlasWEn financial model, a sensitivity and breakeven analysis is done by evaluating the effect fluctuating values of the capital investment, and the fixed and variable revenue has on the on the IRR and NPV values. Given the information shown in Figure 26, Figure 27 and Figure 28, the NPV value for a 20 tpd system, for both Scn1 and Scn2, are 43.6 and 24.1 million Rands (MR). And the RIRR and IRR for a 20 tpd system for Scn1 and Scn2 are 12.7% and 9.5%%, and 20.8% and 17.4% respectively. It is clear that Scn1 is more economically viable than Scn2, furthermore the maximum plasma reactor size currently produced in South Africa is 20 tpd, therefore further analysis will be completed on a 20 tpd plant is chosen for the project, operating under Scn1 conditions. The breakeven point (SPP) shows when the total revenue is equal to total cost, for a 20

tpd system, for both Scn1 and Scn2 are 5.7 and 6.7 years. As stated in Table 10, there is no fixed revenue and therefore it has no effect on the IRR or NPV value. The Project's financial lifetime is presented in Figure 29, where A represents the construction period of one year, B is the breakeven point (SPP), C_n represents the total capital investment, d_j occurs in the first 4 years and P_n represents the net profit, refer to Section 6.4.1, Figure 17 for the capital flow diagram.

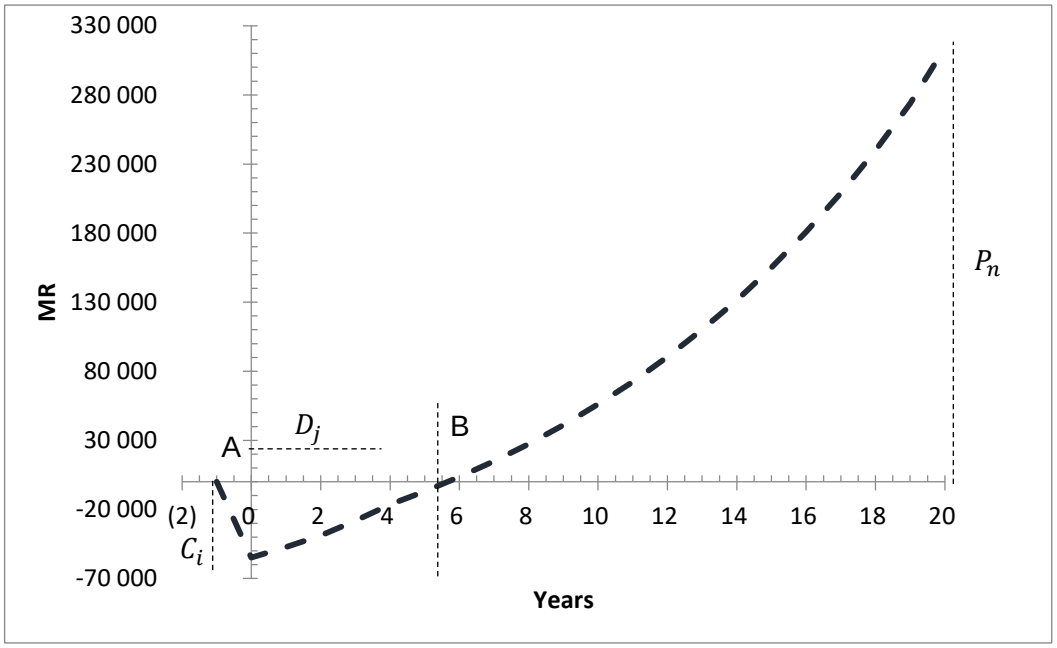

Figure 29: The project life time of a 20 tpd system

The effects on the IRR % and NPV due to varying the above variables are shown in Figure 30 and Figure 31. The capital investment has an indirect influence and the variable revenue has a direct influence on financial viability of the process. The capital investment increases both the IRR and the NPV when a lower %, than that which is estimated is used, and the variable revenue increases both the IRR and NPV values when a larger % be generated than initially estimated. The sensitivity analysis shows that the system is economically robust, considering a project is deemed profitable with an RIRR and IRR is greater than both the estimated $WACC_{nominal}$ and the current $NECSA_{disc.\ factor}$, refer to Figure 27. Upon further analysis of Figure 30, the project will remain economically viable with negative change of 10-20% The project shows very robust financial results at this conceptual stage and the assumptions have all been conservative. There is therefore no reason why from a financial assessment point of view this project should not proceed with full support from all stakeholders.

The project showed very acceptable sensitivities for the main financial input parameters and the plant is expected to operate well above the breakeven point. The soft advantages of the significant extension of the life of the Hartbeespoort Dam remediation and the resulting costs and delays for the earlier establishment of a new site have not been included in this evaluation. The effect on the NPV, IRR, RIRR, simple payback period and discounted payback periods with varying product sales price, for both Scn1 and Scn2, were estimated and plotted (refer to Appendix D.5: Figures D.5.1–E.5.6 and Table D.5.1) and correspond with the PlasWEn system's capital and variable revenue in come sensitivity as shown in Figure 30 and Figure 31.

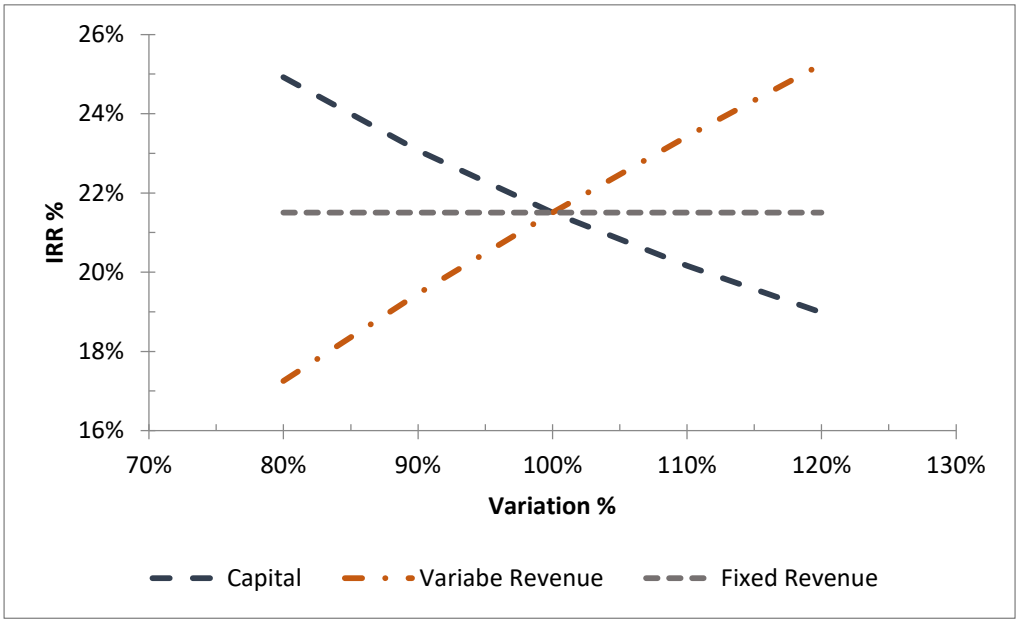

Figure 30: Sensitivity on the PlasWEn-H due to possible change in capital, variable revenue and fixed revenue on the IRR%

Although this can easily be negated by increasing the R/kWh charge. However it is clear from both Figure 30 and Figure 31 that the variable revenue has a larger impact than the capital investment. A 10% variation in the capital investment leads to an average IRR difference of 1.5% and an average NPV difference of 5.2 MR. A 10% variation in the variable revenue leads to an average IRR difference of 2% and an average NPV difference of 14.6 MR.

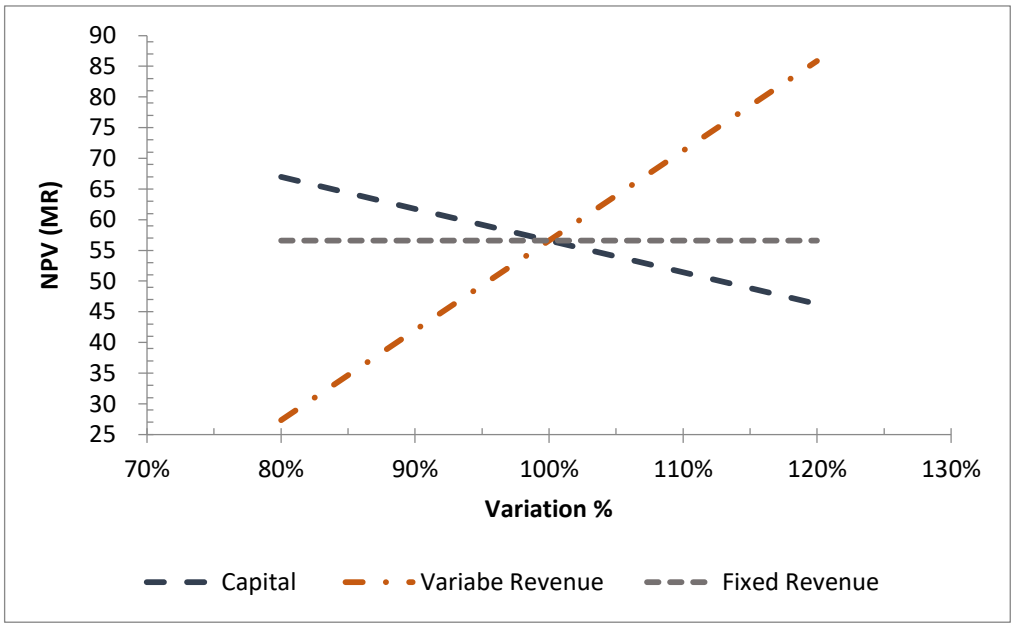

Figure 31: Sensitivity on the PlasWEn-H due to possible change in capital, variable revenue and fixed revenue on the NPV

Chapter 7 Conclusion, Future Work and Recommendations

In conclusion, the PlasWEn system with hyacinth as a feedstock presents a solution to four important sectors, namely water quality, energy (electricity) production, waste management and the protection of the natural environment. The water hyacinth samples were characterized and the WHW sample was chosen as the plasma gasification feedstock due to chemical similarity between the hyacinth and its parts, and for industrial practicality. Various plasma gasification experiments were performed where the O:C molar ratio, specific power input (kWh/kg) and reactor temperature (°C) were varied. The carbon conversion efficiency (CCE) for Run A and Run B were determined to be 95.6% and 63.2% respectively. The experimental results, simulated using FactSage, and the plasma generated gas composition approached chemical equilibrium, specifically at high temperatures. The experimental runs adhered to thermodynamic equilibrium in the following order A>B>C.3>C.2>C1. The plasma gasification results from Run A was chosen to be used in the TEE due to the fact that the syngas composition neared thermodynamic equilibrium under the system parameters. An increase in energy potential can be seen due to $LCV_{WHW} < LCV_{syn,}$ where LCV_{syn} with a value of 14.8 MJ/kg was derived using the experimental gas composition of H_2, CO, CO_2, $CH_{4,}$ C_2H_2 and O_2 on kg/kg feed basis. From the two scenarios considered in the TEE, Scn1 proved to be more economically feasible than Scn2. A PlasWEn plant size of 20 tpd was chosen for further analysis as it is the smallest PlasWen size that is profitable beyond the 20% IRR threshold. The total capital investment of MR 66 is required to build and run the PlasWEn system for the first year. The plant requires 5551.3 kWh/d and is self sufficient once operational, and generates 23 371 kWh/d electricity for sale. A 20 tpd system show an 20.8% IRR,12.7% RIRR, 43.6 MR NPV, 5.7 years SPP and 9.3 years DPP and determined economically viable and a promising waste-to-energy project. Although the techno economic study is conservative, it shows that a 20 tpd H-PlasWEn system can be a profitable business venture. The PlasWEn system presents a sustainable, waste-to-energy system that follows a circular economy principle.

Future work

The produced CO_2 can be incorporated into the TEE as a product aimed at the renewable space involving green liquid fuel production or the beverage industry. Otherwise the H-PlasWEn system can easily be adapted into a methonal production plant.

Recommendation

During the initial experiments it was discovered that the material density caused problems in the hopper, i.e, bridging, and the feedscrew, i.e, clogging in the pipe, and caking together at the output. Therefore the initial feeding mechanism design only allowed a feed rate of 0.87 kg/h at a motor setting of 100 Hz. Higher feed rates resulted in compact cakes being formed, clogging the feed screw. This is attributed to friction between the feed screw, hyacinth and feeder wall. At feed rates higher or lower bridging occurred, attributed to the physiological characteristics of hyacinth**.** To combat bridging, the hopper was caused to vibrate every 5-10 minutes, for 1-2 seconds. The feeding mechanism was disassembled and it was discovered that the feedscrew itself was slightly misaligned contributing to the problem. Densification of the feed material is recommended after as a sample preparation step. An alternative to the densification of the dried material is to implement torrefaction. Torrefaction will allow easier transportation with regards to the feedscrew, and transport if the harvesting site is far from the plasma gasification plant. Furthermore it is recommended that more experimentation be done under various conditions and that both the produced syngas and the residue be analysed.

Bibliography

Agon, N., Hrabovsky, M., Chumak, O., Hlína, M., Kopecky, V., Masláni, A., … & Vierendeels, J. 2016. Plasma gasification of refuse derived fuel in a single-stage system using different gasifying agents. Waste Management, Volume 47 (B), pp. 246-255: http://dx.doi.org/10.1016/j.wasman.2015.07.014

Amdany, R., Chimuka, L., Cukrowska, E., Kukučka, P., Kohoutek, J. & Vrana, B. 2014. Investigating the temporal trends in PAH, PCB and OCP concentrations in Hartbeespoort Dam, South Africa, using semipermeable membrane devices (SPMDs). Water SA, 40 (3), pp. 425-436: http://dx.doi.org/10.4314/wsa.v40i3.5

Ansa, J. R. 2017. Gasification of biomass and solid recovered fuels (SRFs) for the synthesis of liquid. [Online] https://www.tdx.cat/bitstream/handle/10803/450856/TESI_.pdf?sequence=3&isAllowed=y [Accessed 06 Jan 2020]

Asfar, J. A. 2014. Gasification of Solid Waste Biomass. Jordan Journal of Mechanical and Industrial Engineering, 8 (1), pp. 13 - 19: ISSN 1995-6665

Atta, K.P.T., Maree, J.P., Onyango, M.S., Mpenyana-Monyatsi, L. & Mujuru, M. 2020. Chemical phosphate removal from Hartbeespoort Dam water, South Africa. Water SA, 46 (4), pp. 610-614: http://dx.doi.org/10.17159/wsa/2020.v46.i4.9074

Bergier, I., Salis, S.M., Miranda, C.H.B., Ortega, E. & Luengo, C.A. 2012. Biofuel production from water hyacinth in the Pantanal wetland. Ecohydrology & hyrdrobiology, 12 (1), pp. 77-84: http://dx.doi.org/10.2478/v10104-011-0041-4

Bhattacharya, A. & Kumar, P. 2010. Water hyacinth as a potential biofuel crop. Electronic Journal of Environmental, Agricultural and Food Chemistry, pp. 9 (1) 112 -122: ISSN: 1579-4377

Byun, Y., Cho, M., Hwang, S.M. & Chung, J. 2012. Thermal plasma gasification of municipal solid waste (MSW). Fasification for Practical Applications. InTech. pp. 183 -207: http://dx.doi.org/10.5772/48537

Carlini, M., Castellucci, S. & Mennuni, A. 2018. Water hyacinth biomass: chemical and thermal pre-treatment for energetic utilization in anaerobic digestion process. Energy Procedia, 148, pp. 431 -438: http://dx.doi.org/10.1016/j.egypro.2018.08.106

Chamber of Mines. 2018. National coal strategy for South Africa. [Online] https://www.mineralscouncil.org.za/special-features/604-national-coal-strategy-for-south-africa [Accessed 17 Nov 2021]

Chamber of Mines. 2020. Coal 2020 Analysis and forecast to 2025. [Online] https://iea.blob.core.windows.net/assets/00abf3d2-4599-4353-977c-8f80e9085420/Coal_2020.pdf [Accessed 17 Nov 2021]

Chen, J. 2023. Investopedia, Systematic Risk: Definition and Examples. [Online] https://www.investopedia.com/terms/s/systematicrisk.asp [Accessed 28 Sep 2023]

Correa, C. R., Hehr, T., Voglhuber-Slavinsky, A. & Rauscher, Y. 2019. Pyrolysis vs. hydrothermal carbonization: Understanding the effect of biomass structural components and inorganic compounds on the char properties. Elsevier: Journal of analytical and applied physics, 140, pp. 137-147: https://doi.org/10.1016/j.jaap.2019.03.007

Couto, N., Rouboa, A., Silva, V., Monteiro, E. & Bouziane, K. 2013. Influence of the biomass gasification processes on the final composition of syngas. Energy Procedia, 36, pp. 596-606: https://doi.org/10.1016/j.egypro.2013.07.068

Diaz, G., Sharma, N., Leal-Quiros, E. & Munoz-Hernandez, A. 2015. Enhanced hydrogen production using steam plasma processing of biomass: Experimental apparatus and procedure. International Journal of Hydrogen Energy, 40 (5), pp. 2091-2098: http://dx.doi.org/10.1016/j.ijhydene.2014.12.049

Diez, D., Uruena, A., Pinero, R., Barrio, A. & Tamminen, T. 2020. Determination of hemicellulose, cellulose and lignin content in different types of biomasses by thermogravimetric analysis and pseudocomponent kinetic model (TGA-PKM Method). Processes, 8 (9), sp. 1048: http://dx.doi.org/10.3390/pr8091048

EBA. 2019. Biogas Basics, Belgium: European Biogas Association. [Online] https://www.europeanbiogas.eu/wp-content/uploads/2020/01/EBA-AR-2019-digital-version.pdf [Accessed 29 Jan 2020]

Eskom. 2023. pp 28-31. Schedule of Standard Prices 2023/24. [Online] https://www.eskom.co.za/distribution/wp-content/uploads/2023/03/Schedule-of-standard-prices-2023_24-140323.pdf [Accessed 27 Nov 2023]

Fabry, F., Rehmet, C., Rohani, V.J. & Fulcheri, L. 2013. Waste Gasification by Thermal Plasma: A Review. Waste and Biomass Valorization, 4 (3), pp. 421-439: https://doi.org/10.1007/s12649-013-9201-7

Fernando, J. 2023. Investopedia, Internal Rate of Return (IRR) Rule: Definition and Example. [Online] Available at: https://www.investopedia.com/terms/i/irr.asp [Accessed 28 Sep 2023]

Fernando, J. 2023. Investopedia, Net Present Value (NPV): What It Means and Steps to Calculate It. [Online] Available at: https://www.investopedia.com/terms/n/npv.asp [Accessed 28 Sep 2023]

Gaurav, G.K. Mehmood, T., Cheng, L., Klemes, J.J. & Shrivastava, D.K. 2020. Water hyacinth as a biomass: A review. Journal of Cleaner Production, 277, pp. 122214: https://doi.org/10.1016/j.jclepro.2020.122214

Harding, W. R. Thornton, J. A., Steyn, G. & Panuska, J., Morrison, I.R. 2004. Hartbeespoort Dam remediation project: Phase 1, Vol 1 Action Plan: https://doi.org/10.13140/2.1.1392.4486

Hargrave, M. 2022. Investopedia, Real Rate of Return: Definition, How It's Used, and Example. [Online] https://www.investopedia.com/terms/r/realrateofreturn.asp [Accessed 28 Sep 2023]

Hayes, A. 2023. Investopedia, Cost of Debt: What It Means and Formulas. [Online] https://www.investopedia.com/terms/c/costofdebt.asp [Accessed 28 Sep 2023]

Hrabovsky, M. 2011. Thermal Plasma Gasification of Biomass. Progress in Biomass and Bioenergy Production, InTech. https://doi.org/10.5772/18234

Huang, H., Liu, J., Liu, H., Evrendilick, F. & Buyukada, M. 2020. Pyrolysis of water hyacinth biomass parts: Bioenergy, gas emissions, and by-products using TG-FTIR and Py-GC/MS analyses. Energy Conversion and Management, 20, sp. 112552: https://doi.org/10.1016/j.enconman.2020.112552

Ilo, O.P., Simatele, M.D., Nkomo, S.I., Mkhize, N.M. & Prabhu, N. G. 2020. The benefits of water hyacinth (Eichhornia crassipes) for Southern Africa: A Review. Sustainability, 12 (21), sp. 9222: https://doi.org/10.3390/su12219222

InfoSA, 2013. [Online] https://www.infosa.co.za/provinces/north-west/hartbeespoort-dam/ [Accessed 23 Nov 2023]

Investopedia, 2023. Investopedia, How Are Accumulated Depreciation and Depreciation Expense Related?. [Online] https://www.investopedia.com/ask/answers/040215/what-relationship-between-accumulated-depreciation-and-depreciation-expense.asp [Accessed 28 Sep 2023]

Istirokhatun, T., Rokhati, N., Rachmawaty, R., Meriyani, M., Priyanto, S. & Susanto, H. 2015. Cellulose isolation from tropical water hyacinth for membrane preparation. Procedia Environmental Science, pp. 274 – 281: https://doi.org/10.1016/j.proenv.2015.01.041

Janajreh, I., Raza, S. S. & Valmundsson, A. S. 2013. Plasma gasification process: Modeling, simulation and comparison with conventional air gasification. Energy Conversion and Management, 65, pp. 801–809: https://doi.org/10.1016/j.enconman.2012.03.010

Jung, I.H. & van Linde, M.A. 2020. Computational Thermodynamic Calculations: FactSage from CALPHAD Thermodynamic Database to Virtual Process Simulation. The Minerals, Metals & Materials Society and ASM International 2020: Metallurgical and Materials Transactions B, Volume 51, pp. 1851-1874: https://doi.org/10.1007/s11663-020-01908-7

Kagan, J. 2023. Investopedia, Payback Period Explained, With the Formula and How to Calculate It. [Online] https://www.investopedia.com/terms/p/paybackperiod.asp [Accessed 28 Sep 2023]

Kenton, W. 2020. Investopedia, Discounted Payback Period: What It Is, and How To Calculate It. [Online] https://www.investopedia.com/terms/d/discounted-payback-period.asp [Accessed 28 Sep 2023]

Kenton, W. 2023. Investopedia, Cost of Equity Definition, Formula, and Example. [Online] https://www.investopedia.com/terms/c/costofequity.asp [Accessed 28 Sep 2023]

Kuo, P., Illathukandy, B., Wu, W. & Chang, J. 2020. Plasma gasification performances of various raw and torrefied biomass materials using different gasifying agents. Bioresource Technology, 314, sp. 123740: https://doi.org/10.1016/j.biortech.2020.123740

Li, F., He, X., Srishti, A., Song, S., Tan, H.T.W., Sweeny, D.J., … Wang, C. 2021. Water hyacinth for energy and environmental applications: A review. Bioresource Technology, 327, sp. 124809: https://doi.org/10.1016/j.biortech.2021.124809

Lilford, E. V. 2006. The corporate cost of capital. The Journal of The South African Institute of Mining and Metallurgy, Volume 106, pp. 134-146: ISSN 0038–223X/3.00 + 0.00.

Mahani, R., Atia, F., Al Neklawy, M. M. & Fahem, A. 2018. Dielectric spectroscopy study of water hyacinth collected from different media. Spectrochimica Acra Part A: Molecular

and Biomolecular Spectroscopy, 191, pp. 352-356: https://doi.org/10.1016/j.saa.2017.10.024

Mahlangu, M. L. 2009. Waste tyre management problems in South Africa and the possible opportunities that can be created through the recycling thereof. [Online] https://uir.unisa.ac.za/handle/10500/1307 [Accessed 21 Jan 2020]

Marimuthu, T. & Atmakuru, R. 2015. Isolation and Characterization of Cellulose Nanofibers from the Aquatic Weed Water Hyacinnth: Eichhornia crassipes. In: Pandey, J., Takagi, H., Nakagaito, A., Kim, HJ. (eds) Handbook of Polymer Nanocomposiites. Processing, Performance and Application, Springer, Berlin, Heidelberg, pp. 38 – 45: https://doi.org/10.1007/978-3-642-45232-1_55

Marquesi, A.R., Filho, P.G., Gorbunov, A.V., Halinouski, A.A., Essiptchouk, A.M. & Sismanoglu, B.N. 2015. Theoretical assessment of plasma gasification process of low grade coal and biomass feedstock. Advances in Chemistry Research, Nova Science Publishers, 26, pp. 57-76: https://doi.org/10.13140/RG.2.1.2567.4481

Materazzi, M. 2017. Clean Energy from Waste. Fundamental Investigations on Ashes and Tar Behaviours in a Two Stage Fluid Bed-Plasma Process for Waste Gasification. London, UK: Springer https://doi.org/10.1007/978-3-319-46870-9

Materazzi, M., Lettieri, P., Mazzei, L., Taylor, R., Chapman, C. 2014. Tar evolution in a two stage fluid bed–plasma gasification process for waste valorization. Fuel Processing Technology, 128, pp. 146-157: http://dx.doi.org/10.1016/j.fuproc.2014.06.028

Maverick, J. B., 2022. Investopedia, How Small Cap Stocks Differ from Large Cap Stocks in Risk. [Online] https://www.investopedia.com/ask/answers/032615/how-do-risks-large-cap-stocks-differ-risks-small-cap-stocks.asp [Accessed 28 Sep 2023]

Mayerhofer, M., Mitsakis, P., Meng, X., de Jong, W., Spliethoff, H., Gaderer, M. 2012. Influence of pressure, temperature and steam on tar and gas in allothermal fluidized bed gasification. Fuel, 99, pp. 201-209: https://doi.org/10.1016/j.fuel.2012.04.022

Mazaheri, N., Akbarzadeh, A. H., Madadian, E. & Lefsrud, M. 2019. Systematic review of research guidelines for numerical simulation of biomass gasification for bioenergy production. Energy Conversion and Management, 183, pp. 671-688: https://doi.org/10.1016/j.enconman.2018.12.097

Messerle, V.E., Mosse, A.L. & Ustimenko, A.B. 2016. Plasma gasification of carbonaceous wastes: thermodynamic analysis and experiment. Thermophysics and Aeromechanics, 23 (4), pp. 613-620: https://doi.org/10.1134/S0869864316040144

Minutillo, M., Perna, A. & Bona, D.D. 2009. Modelling and performance analysis of an integrated plasma gasification combined cycle (IPGCC) power plant. Energy Conversion and Management, 50 (11), pp. 2837-2842: https://doi.org/10.1016/j.enconman.2009.07.002

Mountouris, A., Voutsas, E. & Tassios, D. 2006. Solid waste plasma gasification: Equilibrium model development and exergy analysis. Energy Conversion and Management, 47 (13-14), pp. 1723-1737: https://doi.org/10.1016/j.enconman.2005.10.015

Murray, K, M Du Preez, en C E Van Ginkel. 2002. South African National Water Quality Monitoring Programmes Series. National Eutrophication Monitoring Program, Implementation Manual. Pretoria. Department of Home Affairs and Forestry (DWAF), 1: [Onlinel http://www.dwa.gov.za/iwqs/eutrophication/NEMP/EutrophicationMonitoringProgramme.pdf [Accessed 03 Sep 2019]

Musingafi, M.C.C. & Tom, T. 2014. Fresh Water Sources Pollution: A Human related threat to fresh water security in South Africa. Journal of Public Policy and Governance, Journal of Public policy and Governance, 1 (2), pp. 72-81

Nel, J.L., Le Maitre, D.C., Roux, D.J., Colvin, C., Smith, J.S., Simth-Adao, L.B., … Sitas, N. 2017. Strategic water source areas for urban water security: Making the connection between protecting ecosystems and benefiting from their services. Ecosystem services, 28 (Part B), pp. 251-259: https://doi.org/10.1016/j.ecoser.2017.07.013

Neuwahl, F., Cusano, G., Benavides, J.G., Holbrook, S. & Roudier, S. 2019. *Best Available Techniques (BAT) reference document for waste incineration – Industrial Emissions Directive 2010/75/EU (Integrated Pollution Prevention and Control)*. European Commission. Joint Research Centre. [Online] https://eippcb.jrc.ec.europa.eu/sites/default/files/2020-01/JRC118637_WI_Bref_2019_published_0.pdf [Accessed 21 Jan 2020]

Newete, S. W., Erasmus, B. F., Weiersbye, I. M. & Byrne, M. J. 2016. Sequestration of precious and pollutant metals in biomass of cultured water hyacinth (Eichhornia crassipes). Environmental Science and Pollution Research, 23, pp. 20805-20818: https://doi.org/10.1007/s11356-016-7292-y

Osama, O., Atia, F., Hakeem, N.A., Neklawy, M.M.A., Fahem, A. 2010. Molecular Spectroscopic Study of Water Hyacinth Collected from Different Media. Australian Journal of Basic and Applied Sciences, 4 (12), pp. 6134-6139: ISSN 1991-8178

Palma, C. F. 2013. Modelling of tar formation and evolution for biomass gasification: A review. Applied Energy, 111, pp. 129-141: http://dx.doi.org/10.1016/j.apenergy.2013.04.082

Panwar, N. L., Kothari, R. & Tyagi, V. 2012. Thermo chemical conversion of biomass – Eco friendly energy routes. Renewable and Sustainable Energy Reviews, 16 (4), pp. 1801 – 1816: https://doi.org/10.1016/j.rser.2012.01.024

Peters, M. S. & Timmerhaus, K. D. 1991. Plant design and economics for chemical engineers. Singapore: McGraw-Hill International Editions, 4: ISBN 0-97-100871-3 ed

Peters, M. S., Timmerhaus, K. D. & West, R. E., 2003. Plant design and economics for chemical engineers. New York: Elizabeth A. Jones, The McGraw-Hill Companies, 5: ISBN 0-07-119872-5 ed

Pavement Material Group. [Online] https://www.pavementmaterials.co.za/products/19mm-crushed-stone-agregate-gravel?variant=13162635690102 [Accessed 27 Nov 2023]

Poudel, J., Karki, S. & Oh, S. C. 2018. Valorization of waste wood as a solid fuel by torrefaction. Energies, 11 (7), sp. 1641: https://doi.org/10.3390/en11071641

Promdee, K., Vitidsant, T. & Vanpetch, S. 2012. Comparative Study of Some Physical and Chemical Properties of Bio-Oil from Manila Grass and Water Hyacinth Transformed by Pyrolysis Process. International Journal of Chemical Engineering and Applications, 3 (1), pp. 72-75: https://doi.org/10.7763/IJCEA.2012.V3.163

Republic of South Africa, 2019. Carbon Tax Act, 2019: No. 15 of 2019. Government Gazette No.42483, Vol. 647, Cape Town: [Online] https://www.gov.za/documents/carbon-tax-act-15-2019-english-afrikaans-23-may-2019-0000 [Accessed 30 Oct 2021]

Rezania , S., Din M.F.M., Kamaruddin, S.F., Shazwin, M.T., Singh, L., Yong, E.L., Dahalan, F.A. 2016. Evaluation of water hyacinth (Eichhornia crassipes) as a potential raw material source for briquette production. Energy, 111, pp: 768-773: http://dx.doi.org/10.1016/j.energy.2016.06.026

Rezania, S., Ponraj, M., Din, M.F.M., Songip, A.R., Sairan, F.M., Chellianpan, S. 2015. The diverse applications of water hyacinth with main focus on sustainable energy and

production for new era: An overview. Renewable and Sustainable Reviews, 41, pp. 943 – 954: http://dx.doi.org/10.1016/j.rser.2014.09.006

Rimayi, C., Odusanya, D., Weiss, J.M., de Boer, J., Chimuka, L. 2018. Contaminants of emerging concern in the Hartbeespoort Damcatchment and the uMngeni River estuary 2016 pollution incident, South Africa. Science of the Total Environment, 627, pp. 1008-1017: https://doi.org/10.1016/j.scitotenv.2018.01.263

Rutberg, P.G., Kunznetsov, V.A., Serba, E.O., Popov, S.D., Surrov, A.V., … Nikonov, A.V. 2013. Novel three phase steam air plasma torch for gasification of high calorific waste. Applied Energy, 108, pp. 505-514: http://dx.doi.org/10.1016/j.apenergy.2013.03.052

Salas-Rulz, A., Barbero-Barrera, M. M., Sanchez-Rojas, M. I. & Asenslo, E. 2020. Water Hyacinth–Cement Composites as Pollutant Element Fixers. Waste and Biomass Valorization, 11, p. 3833–3851: https://doi.org/10.1007/s12649-019-00674-1

Santos, L. O., Silva, F.F., Santos, L.C., Carregosa, I.S.C., Wisniewski, A.Jr. 2018. Potential bio-oil production from invasive aquatic plants by microscale pyrolysis studies. Chem. Soc., 29 (1), pp. 151-158: http://dx.doi.org/10.21577/0103-5053.20170124

Sariatli, F. 2017. Linear Economy Versus Circular Economy: A Comparative and Analyzer Study for Optimization of Economy for Sustainability. Visegard Journal on Bioeconomy and Sustainable Development, 6 (1), pp. 31-34: https://doi.org/10.1515/vjbsd-2017-0005

Sikarwar, V. S. & Zhoa, M. 2017. Biomass Gasification. [Online] https://www.researchgate.net/publication/315849347_Biomass_Gasification [Accessed 08 May 2019].

Steffen, B. 2020. Estimating the cost of capital for renewable energy projects. Energy Economics, 88, sp 104783: https://doi.org/10.1016/j.eneco.2020.104783

Sukarni, Widiono, A.E., Sumarli, S., Wulandari, R., Nauri, I.M. & Permanasari, A.A. 2018. Thermal decomposition behavior of water hyacinth (eichhornia crassipes) under an inert atmosphere. MATEC Web of Conferences,204 (00010): https://doi.org/10.1051/matecconf/201820400010

Sukarni, S., Zakaria, Y., Sumarli, S., Wulandari, R., Permanasari, A.A. & Suhermanto, M. 2019. Physical and Chemical properties of water hyacinth (Eichhornia crassipes) as a sustainable feedstock. IOP Conference Series: Materials Science and Engineering, 515 (012070): https://doi.org/.1088/1757-899X/515/1/012070

Surov, A. V., Popov, S.D., Popov., V.E., Subbotin, D.I., Serba, E,O., Spodobin, V.A., … Pavlov, A.V. 2017. Multi gas AC plasma torches for gasification of organic substances. Fuel, 203, pp. 1007-1014: https://doi.org/10.1016/j.fuel.2017.02.104

Su, W., Sun, Q., Xia, M., Wen, Z. & Yao, Z. 2018. The resource utilization of water hyacinth (Eichhornia crassipes Mart.(Solms) and its challenges. Resources, 7 (46), pp 1-9: https://doi.org/10.3390/resources7030046

Ruiz Téllez, T., López, E., Grando, G., Pérez, E., Morán-López, R. & Guzman, J. 2008. The Water Hyacinth, Eichhornia crassipes: an invasive plant in the Guadiana River Basin (Spain). Aquatic Invasions, 3(1), pp. 42-53: https://doi.org/10.3391/ai.2008.3.1.8

Towler, G. & Sinnott, R. 2008. Chemical engineering design: Principles, practice and economics of plant and process design. ISBN 13: 978-0-7506-8423-1 ed

Tuomi, S., Kaisalo, N., Simell, P. & Kurkela, E. 2015. Effect of Pressure on tar decomposition activity of different bed materials in biomass gasification conditions. Fuel, 158, pp. 293-305: https://doi.org/10.1016/j.fuel.2015.05.051

Valmundsson, A. S. & Janajreh, I. 2011. Plasma gasification process modeling and energy recovery from solid waste. Energy Sustainability Proceedings, Paper No ES2011-54284, pp. 361 – 368: https://doi.org/10.1115/ES2011-54284

van Ginkel, C. & Michael, S. 2007. Temporal trends in total phosphorus, temperature, oxygen, chlorophyll a and phytoplankton populations in the Hartbeespoort Dam and Roodeplaat Dam, South Africaa, between 1980 - 2000. African Journal of Aquatic Science, 32 (1), pp. 63-70: https://doi.org/10.2989/AJAS.2007.32.1.9.146

van Schalkwyk, H., Potgieter, L. & Cang, H. 2017. The Development of a Spatio-Temporal Model for Water Hyacinth Biological Control Strategies. Mathematical and Computational Forestry & Natural-Resource Sciences, 9 (1), pp. 30-42: ISSN 1946-7664

Young, G. C. 2010. Municipal Solid Waste To Energy Conversion Processes. Economic, Technical, and Renewable Comparisons, New Jersey: Wiley. pp. 4- 26: ISBN 978-0-470-53967-5

Zhang, C., Ma, X., Chen, X., Tian, Y., Zhou, Y., Lu, X. & Hauang, T. 2020. Conversion of water hyacinth to value-added fuel via hydrothermal carbonization. Energy, 197, pp. 117193: https://doi.org/10.1016/j.energy.2020.117193

Appendix A – Hyacinth Characterization

A.1 TG-DTG Graphs for WHL. WHR and WHS

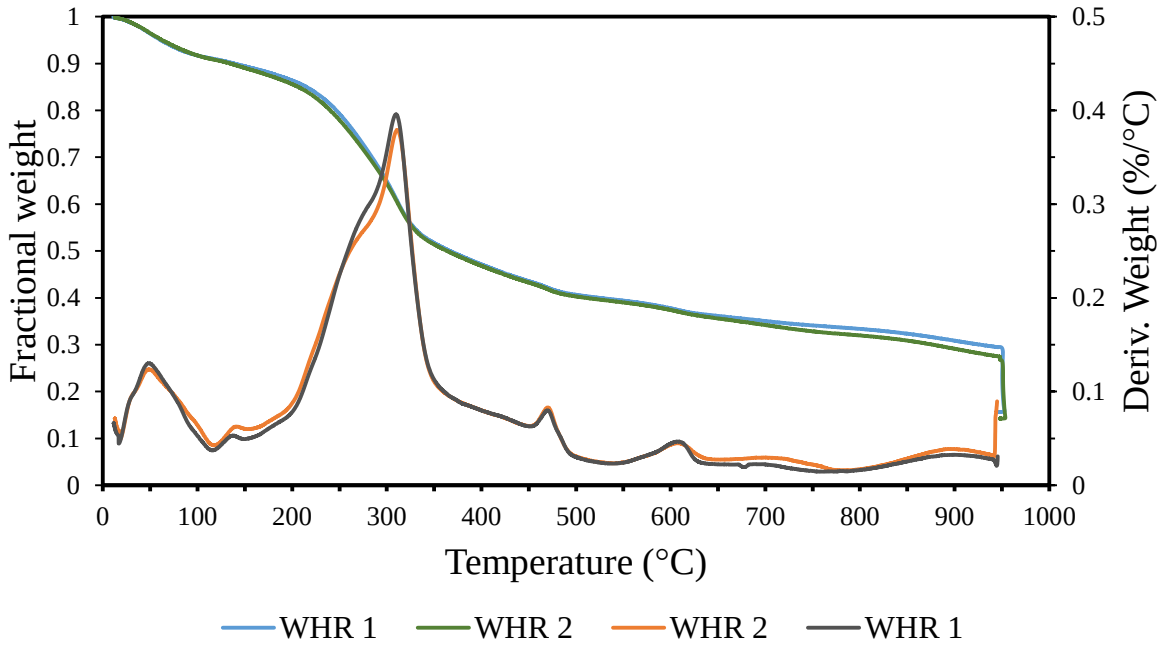

Figure A.1.1: TG-DTG graph for WHR

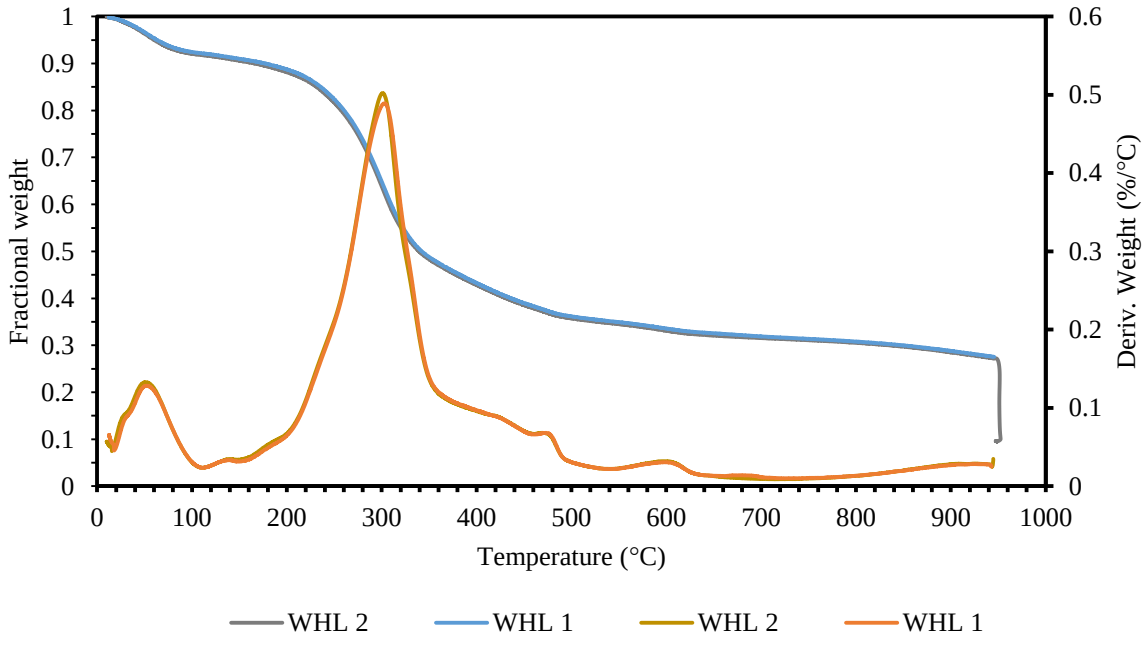

Figure A.1.2: TG-DTG graoh for WHL

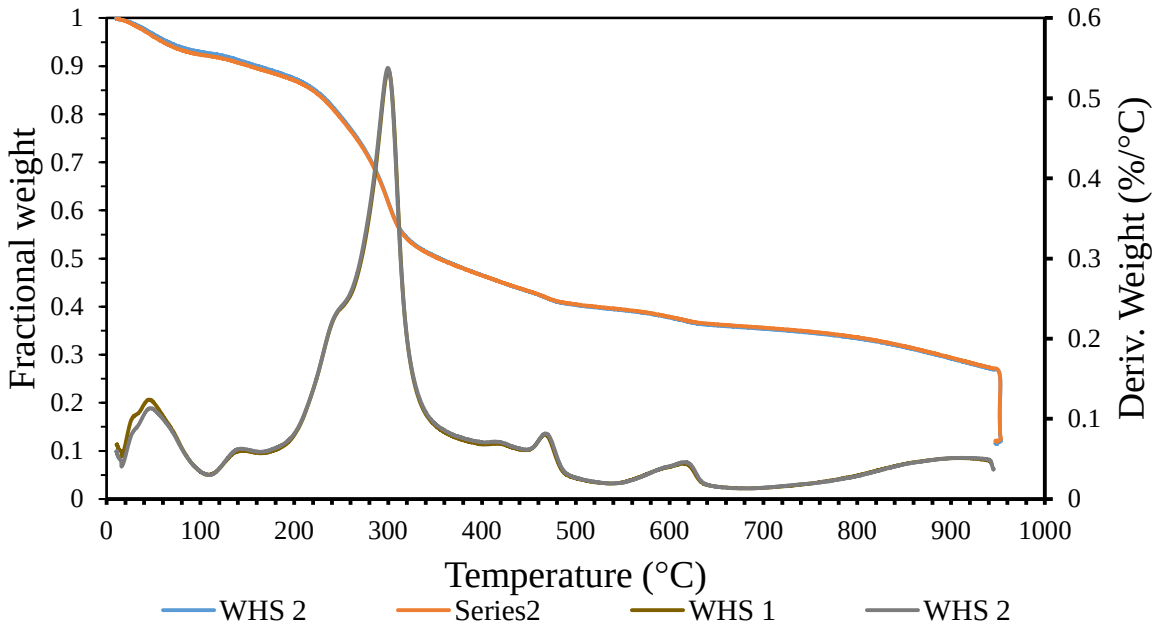

Figure A.1.3:TG-DTG graph for WHS

A.2 Proximate Analysis of Hyacinth after Storage

Table A.2.1: Chemical composition of hyacinth, relating Prox results

Variable	Prox wt (%)		
	1	2	Ave
VM	59.9	60.4	60.2
FC	16.6	15.2	15.9
Ash	13.7	15.1	14.4
H_2O	9.8	9.7	9.8
$H_2O_{absorbed}$	4.5	4.4	4.5

Table A.2.2: Elemental composition of hyacinth

Element	Ultimate. wt (%)		
	1	2	Ave
C	37.2	38.8	38.0
O	32.0	29.7	30.8
N	2.6	2.7	2.6
H	4.5	4.5	4.5
S	0.1	0.1	0.1

Appendix B – Experimental Calculations and Results

B.1 Run B Moisture Calculations

Table B.1.1: Batch H_2O% addition calculation

Moist % Batch Calculation			
Filled Hopper	2	kg	
H_2O Added	0.5	L	
	0.5	kg	
H_2O	**%**	**kg**	**mol**
Initial	5.3	0.11	5.88
Additional	25	0.5	27.75
Total	30.3	0.61	33.64

B.2 Run C Feedrate Calibration

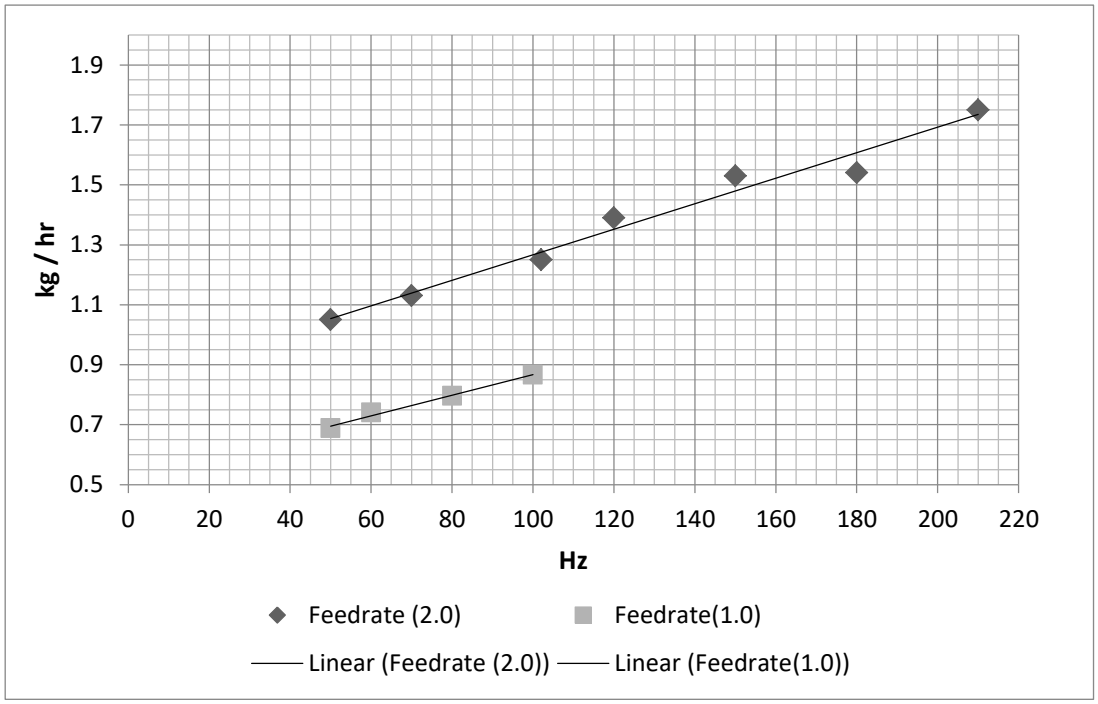

Figure B.2.1 Feed calibration curve

B.3 Start-up Procedure

The feed screw, quench heat exchanger, temperature display board and compressor were switched on and the quench heat exchanger air feed valve was opened. Thereafter both the water supply and cooling tower's pumps were switched on, and all the water valves were opened (for in and outlet for the quench, feeder, reactor..etc) to allow continuous flow. The ventilation system was switched on and then the gas cylinders (Ar, N_2 and O_2) were opened and the regulators were opened at the respective pressures for each gas. The pressure gauge was turned on and N_2 was allowed to flood the system when the N_2 valve, connected directly to the reactor, was opened. When the plasma power was switched on, the N_2 valve connected to the reactor was closed. The start-up procedure see Table B.3.1.

Table B.3.1: Start-up procedure of PlasWEn system

PlasWEn Gas Start-up Sequence						
	Phase	**Time s**	**Argon kg/hr**	**N_2 kg/hr**	**Current A**	**Resistance V**
Start-up	1	10	1.3	0	0	20
	2	10	1.3	0	80	
	3	10	1.3	0	110	
	4	65	1	0.4	120	60
	5	19	0.7	1.3	120	
	6	10	0.4	1.3	120	
	7	10	0.2	2.5	120	
	8	10	0	3.4	130	95

B.4 Plasma Gasification Results

The following was used; the proximate results (the ash and H_2O %) and for the element balance, *i.e*., C, H, N, O and S from the ultimate analysis obtained from Table 5. The N_2 flowrate given in Table 7, and the ash content was assumed to be constant and inert. The average vol % syngas composition of Run A was used to determine the molar feed rate (mol/h) of the different species in the output. Then the mass feed rate (kg/h), and the mass fraction: chemical specie (kg/h) produced per feed mass rate (kg/h), therefore (kg/kg feed) is calculated and can be seen in Table B.4.1

Table B.4.1: PlasWEn Mass Balance on Run A

Input			**Output**			
Element	**kg/h**	**mol/hr**	**Element**	**kg/h**	**mol/hr**	**kg/kg feed**
Gas Input			**Gas Output**			
N2	4.25	151.61	**N_2**	4.27	152.43	-
Feed Input			**H_2**	0.05	23.78	0.06
C	0.32	26.63	**CO**	0.66	23.56	0.76
O	0.32	20.25	**CO_2**	0.04	0.97	0.05
N	0.02	1.65	**CH_4**	0.01	0.11	0.01
H	0.04	40.99	**C_2H_2**	0.00	0.15	0.00
S	0.00	0.08	**O_2**	0.00	0.07	0.00
H_2O	0.05	2.55	**Total Gas**	5.03	201.07	0.878
Total Feed	0.757	92.16	**Solid Output**			
Ash	0.111	-	**Ash**	0.111	-	0.13
Total Input (Solid and Gas)			**Unreacted C**	0.020	1.70	0.02
Total	5.116	244	**Total Solid**	0.132	-	0.15
Missing Mass calculation			**Total Output (Solid and Gas)**			
Unknown	0.05		**Total**	5.165	-	1.029

Table B.4.2: PlasWEn system chemical conversion efficiency of C, H and O (mol%)

Run	A	B	C.1	C.2	C.3
C Conversion					
CO	88.5%	45.6%	2.5%	9.1%	9.1%
CO_2	3.6%	17.0%	7.9%	8.8%	6.2%
CH_4	0.4%	0.2%			
C_2H_2	1.1%	0.4%			
$Total_{Reacted}$	93.6%	63.2%	10.5%	17.9%	15.2%
$Total_{Unreacted}$	6.4%	36.8%	89.5%	82.1%	84.8%
H Conversion					
H_2	103.2% (94.3%)*	55.5%	1.4%	5.7%	6.1%
$Total_{Reacted}$	103.2% (94.3%)*	55.5%	1.4%	5.7%	6.1%
$Total_{Unreacted}$	-3.2% (6.7%)*	44.5%	98.6%	94.3%	93.9%
O Conversion					
O_2	0.6% (0.5%)*	0.6%	3.0%	9.1%	16.8%
CO	92.7% (85.4%)*	34.8%	1.7%	6.0%	6.4%
CO_2	7.6% (7%)*	26.0%	10.7%	11.5%	8.7%
$Total_{Reacted}$	100.9% (93%)*	61.4%	15.4%	26.7%	32.0%
$Total_{Unreacted}$	-0.9% (7%)*	38.6%	84.6%	73.3%	68.0%

Table B.4.3: PlasWEn system MGE % and CGE % calculations

Parameter	Units	A	B	C1	C2	C3
Experimental						
$\dot{m}_{WHW}$	kg/h	0.9		1.1	1.3	1.5
$\dot{m}_{Syn,exp}$	kg/h	5.0	5.3	2.2	2.4	2.4
$LCV_{Syn,exp}$	MJ/kg	3	2	0.13	0.42	0.70
MGE_{exp}		104%	66%	2%	6%	8%
CGE_{exp}		48%	30%	1%	4%	6%
Theoretical						
$\dot{m}_{Syn,theo}$	kg/h	0.8	1.1	0.2	0.4	0.5
$LCV_{Syn,theo}$	MJ/kg	15	11	1	2	4
MGE_{theo}		98%	96%	1%	5%	9%
CGE_{theo}		45%	43%	1%	3%	6%

Table B.4.4: PlasWEn system and Literature performance summary

Parameter	WHW					RDF0	RCT coal	MSW	LAH*	UW*	Pine Needles
	Run A	Run	Run C.1	Run C.2	Run C.3						
Syngas Composition											
H_2	49±1.5	54±0.3	10±2.1	22±3.6	25±3	33.9±4.5	54.7	46.2	40.5	35.9	39.2
CO	48±1.6	34±1.8	21±3.6	40±2.5	43±3.2	46.2±0.7	44.5	36.6	38.8	48.7	51.1
CH_4	0.07±0.2	-	-	-	-	2.7±4.8	0.01	0.01	-	0.8	1.1
CO_2	2±0.5	13±1.5	69±5.7	39±6.2	32±6.2	0.7±0.9	0.1	0.0	0.1	14.6	8.6
H_2O	-	-	-	-	-	16.4±1.6	0.8	0.0	20.6	0	39.2
Syngas Parameters											
O:C	0.9	1.2	1.7	1.5	1.4	-	1.0	0.8	0.5	0.6	0.7
H_2:CO	1.03±0.07	1.61±0.09	0.48±0.01	0.54±0.04	0.59±0.01	0.7±0.1	1.23	1.26	1.04	0.74	0.67
CCE	93.6	63.2	10.5	17.9	15.2	-	100	100	100	100	100
CO yield	88.5	45.6	2.5	9.1	9.1	-	-	-	-	-	-
H_2 yield	103.2 (94.3%)	55.5	1.4	5.7	6.1	-	-	-	-	-	-
LCV_{syn} (MJ/kg)	14.8	10.9	0.4	1.3	2.0	9.6±0.5	15.94	13.44	8.99	8.31	8.71
Plasma Gasification Parameters											
Plasma gas	N_2					Air	Argon				
Oxidant	none	H_2O	O				H_2O			none	
T (°C)	1200±26.6	1156±63.3	1088 ±17.7	1126±3.5	1137± 9.9	1250	1264	1267	1258	1260	1257
P (bar)	1.013 * slightly over atmospheric										
CGE (%)	48%(45%)	30%(43%)	1%(1%)	4%(3%)	6%(6%)	-	-	-	-	-	-
MGE (%)	104%(98%)	66%(96%)	2%(1%)	6%(5%)	8%(9%)	-	-	-	-	-	-
Notes and References											
Reference	This study					a	b and c,				
	a) (Minutillo, et al., 2009), b) Valmundsson & Janajreh, (2011) and c) Janajreh, Raza, & Valmundsson, (2013) * LAH –low ash algae, *UW –untreated wood										

Table B.4.5: Literature performance summary

Parameter	RDF1	RDF2	RDF3	RDF4	RDF5	BM1	RDF6	BM2	RDF7	BM3
Syngas Composition										
H_2	26	26	30	53	53	48	37	40	45	46
CO	43	44.5	46	30	27.5	38.5	42	46.5	37	38.5
CH_4	2.0	2.0	2	4	4	1	3.5	0.5	2.5	1.5
CO_2	18	16	11	3.5	6	2	8.5	2	6.5	6
H_2O	-	-	-	-	-	-	-	-	-	-
Syngas Parameters										
O:C	0.52	0.46	0.43	0.44	0.55	0.19	0.42	0.24	0.43	0.24
H_2:CO	0.60	0.58	0.65	1.77	1.93	1.25	0.88	0.86	1.22	1.19
CCE	84	81	86	83	85	85	83	88	100	93
CO yield	56	58	66	68	61	79	65	83	82	78
H_2 yield	64	63	76	66	59	89	64	73	83	84
LCV_{syn} (MJ/kg)	15.21	15.272	17.325	20.056	20.116	-	19.635	-	19.344	-
Plasma Gasification Parameters										
Plasma gas	Argon									
Oxidant	O_2 and CO_2			H_2O			H_2O and CO_2		H_2O and O_2	
T (°C)	1554	1538	1536	1429	1395	1460	1446	1418	1490	1443
Pr (bar)	1.013 slightly above atmospheric pressure									
CGE (%)	42	42	48	56	56	65-66	54	65-66	53	65-66
MGE (%)	72	72	82	94	95	105-107	92	105-107	91	105-107
Notes and References										
Reference	(Agon, et al., 2016)									

Appendix C – FactSage Simulation

Figure C.1.1: Starting FactSage and select Equilibrium simulation

C.1 Initial program setup

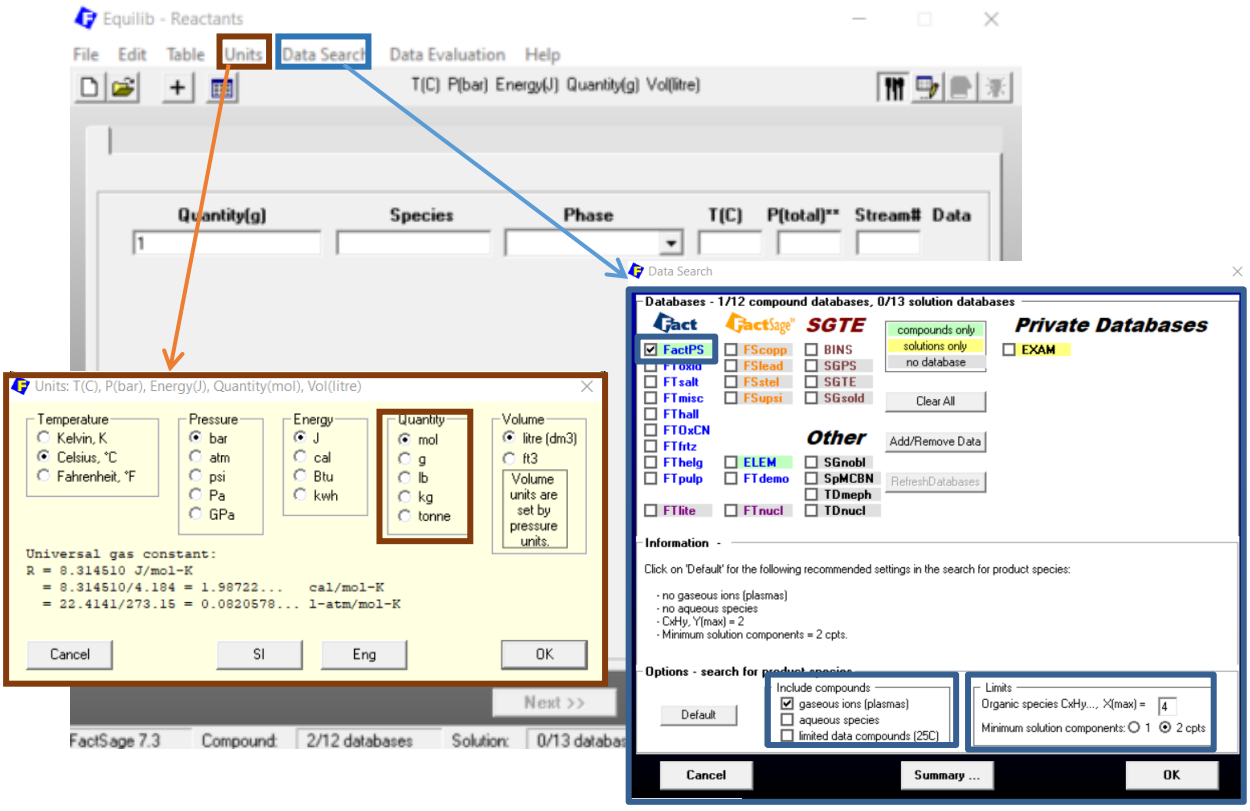

Figure C.1.2: Setting units and selecting databases

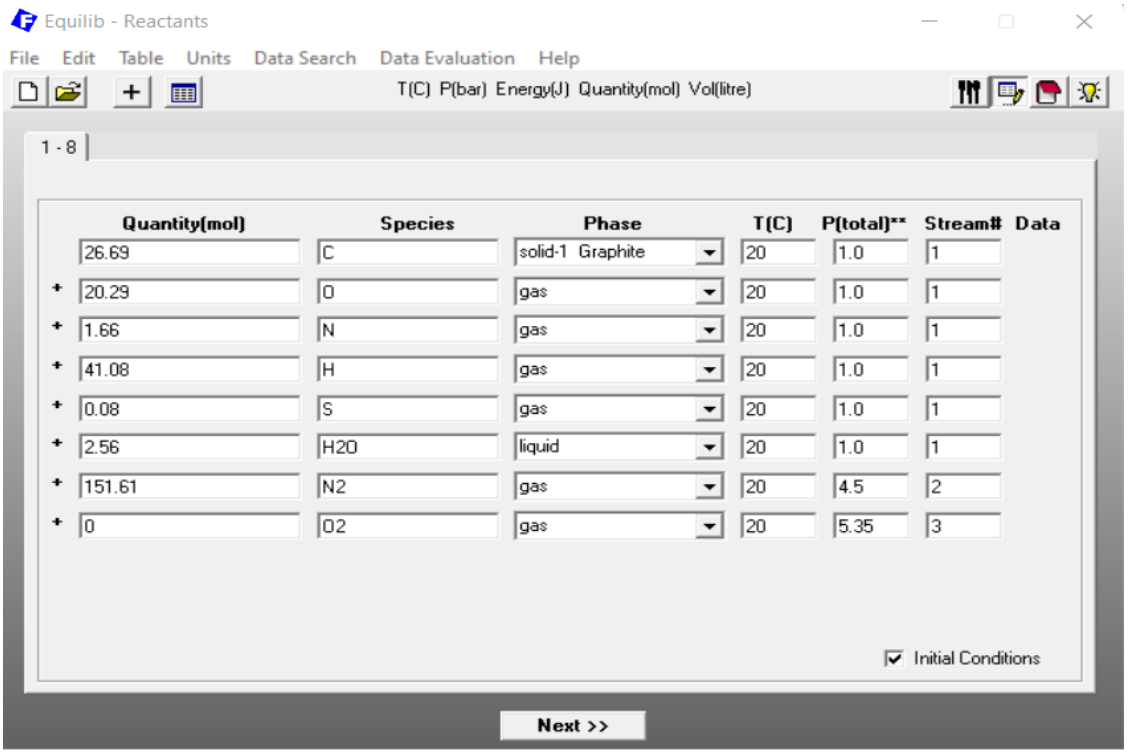

Figure C.1.3: Plug in chemical composition of feedstock

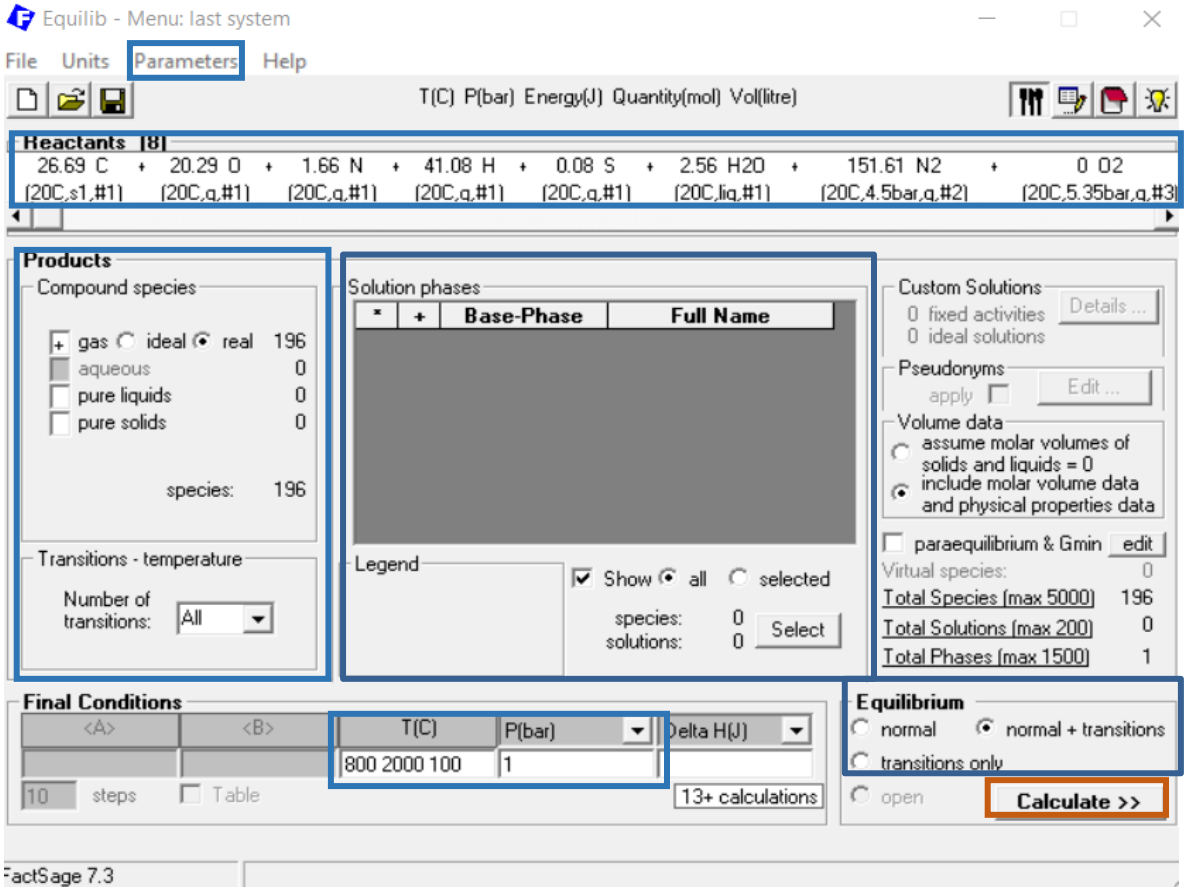

Figure C.1.4: Setting parameters

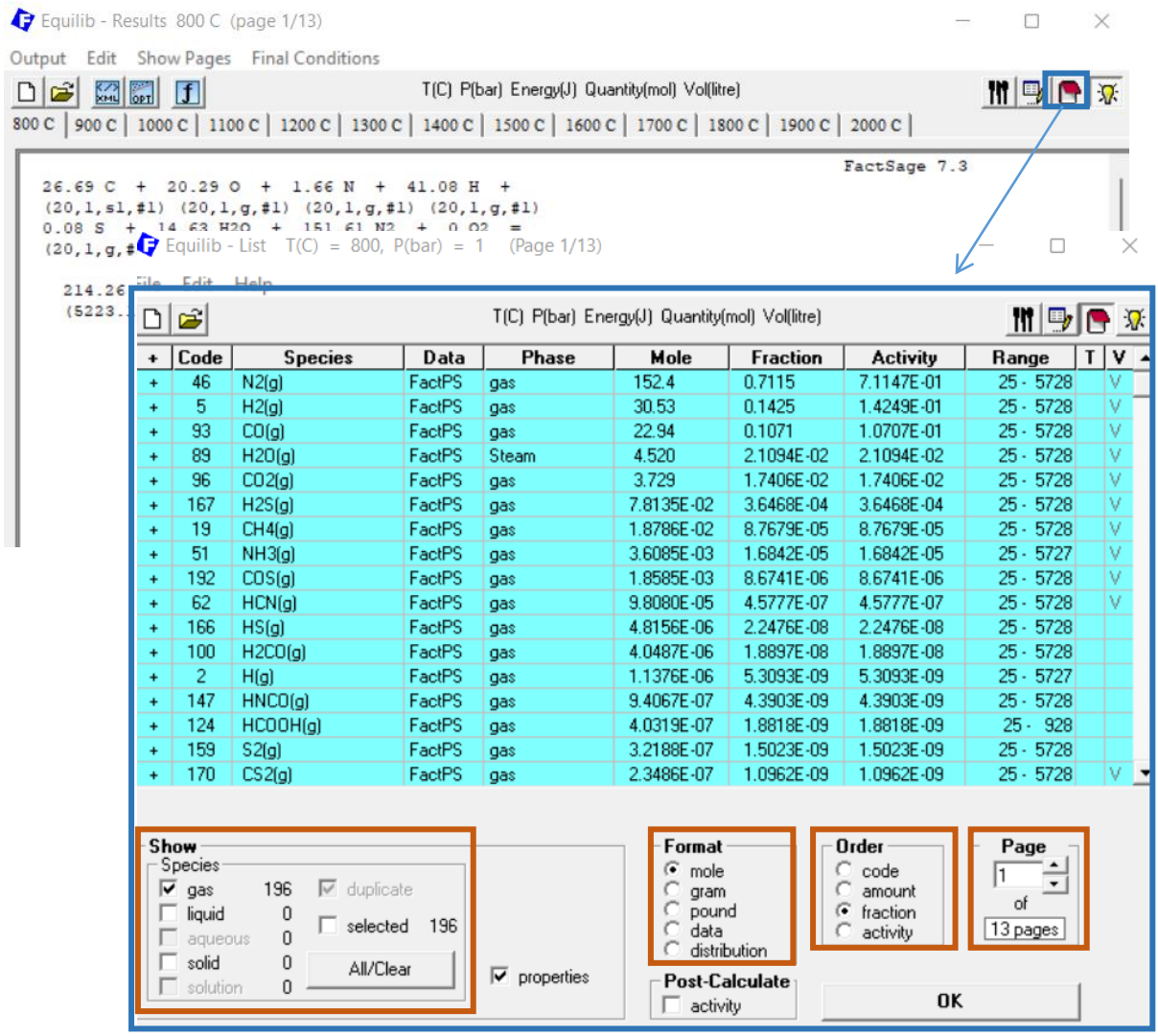

Figure C.1.5: Selecting result format

D.1 Harvesting and sample preparation

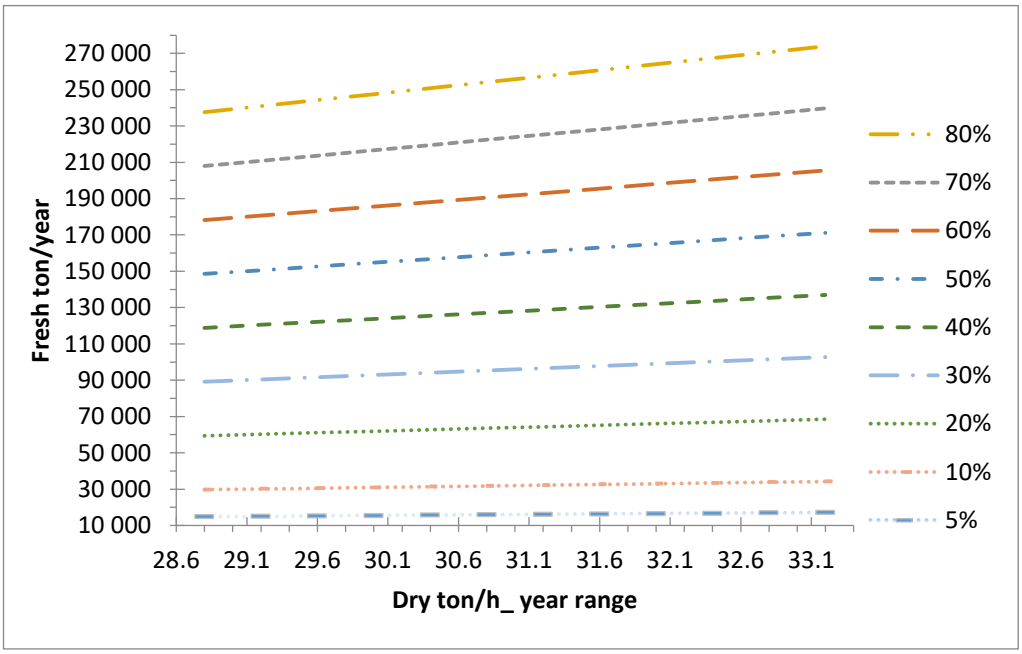

Figure D.1.1: Ton per year hyacinth growing on the Hartbeespoort dam depending on the surface area covered

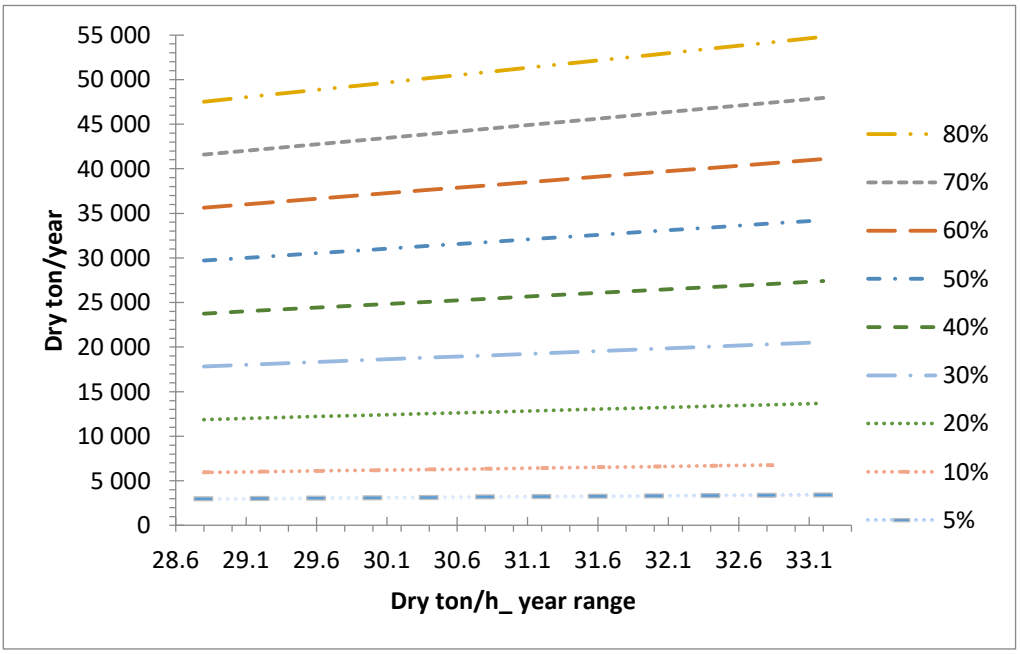

Figure D.1.2: Dry ton/year available from the Hartbeespoort dam per year

Assuming the harvested is at 15°C and a initial hyacinth moisture content of 80%, the total energy required, to heat the moisture to 100°C and remove the moisture, will vary depending the final moisture wanted and design specifics. Heat energy from the reject stream can be redirected to dry the material and the % of the total heat energy required vs the final moisture content. It can be seen that the amount of energy exponentially increases directly with the amount of moisture to be removed. However a thorough investigation is needed to get a realistic estimation of the total heat requirements, efficiencies (heat transfer) and error margins (thermal losses, variability of moisture in feed and the quality of hthe heat source). Drying material thermally to a 30% moisture content can be considered and replace step (B) in Figure .

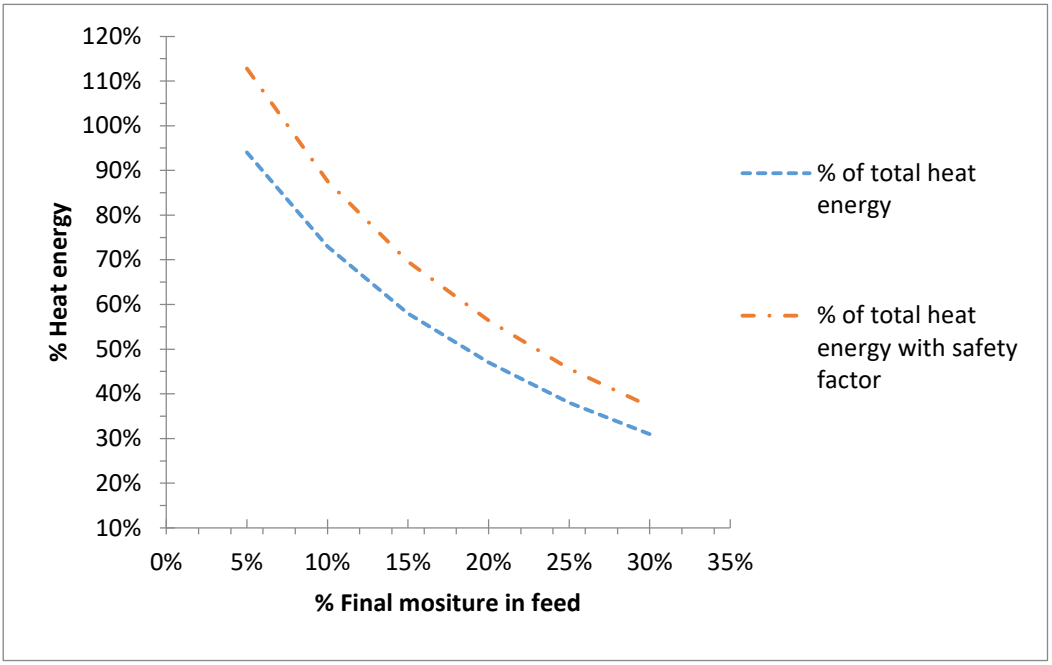

Figure D.1.3: The % of the heat energy stream required to achieve a final moisture content

D.2 Costing

Table D.2.1: Variable cost factors per plant size

Scaling factor	0.75	0.59	1.00	1.68	2.28	3.34	5.62
PlasWEn Plant Size (tpd)		5	10	20	30	50	100
	Qty/MWh						
Process Water		0.059	0.100	0.168	0.228	0.334	0.562
Cooling Water		0.059	0.100	0.168	0.228	0.334	0.562
Argon		0.001	0.001	0.002	0.002	0.003	0.006

Table D.2.2: Cost calculation fractions per plant size

Labour Fractions						
PlasWEn Plant Size (tpd)	5	10	20	30	50	100
Plant Manager	0.0					
Plant Supervisor	0.1	0.2			0.3	
Shift Foreman	0.00					
Process Controller	1.0		2.0			
Process Controller	0.0	1.0	2.0			
Fitter	0.25					
Helper	3.0	5.0	10.0	15.0		
Factory costs fractions						
Electricity Max Demand	0.00					
Protective Clothing	1.00		2.00	3.00	4.00	5.00
Operating Supplies	0.30			0.50	1.00	
Gas Cylinders	1.00					
Other Operating Cost	0.50			0.75	1.00	1.50
Production overheads fractions						
Building Rental	0.0					
SHEQ	0.10					
Plant Overheads	1.00					
Indirect Labour Cost	0.15			0.30	0.50	

D.3 Energy production and sales revenue

.

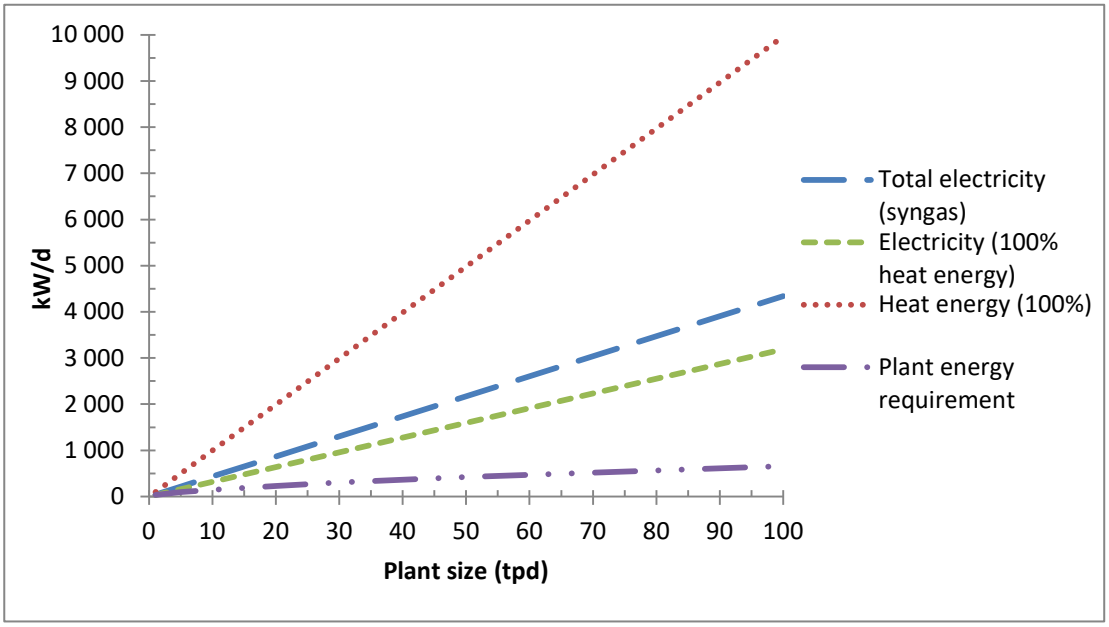

Figure D.3.1: Total energy produces, redirected and required for production

D.4 Financial factors

Indexation from escalation weights is used to calculate an inflated revenue in order to account for the impact of inflation over time. By applying indexation from escalation weights, the inflated revenue estimates provide a more accurate representation of the revenue expected during the plant life time. The annual inflated revenue are shown in Figure D.4.1.

Table D.4.1: Indexation escalation factors for the cot and revenue estimation

Factor	Escalation Weighting	
	Cost	Revenue
Materials	30%	25%
Power	15%	40%
Labour	15%	5%
CPI	20%	15%
PPI	20%	15%

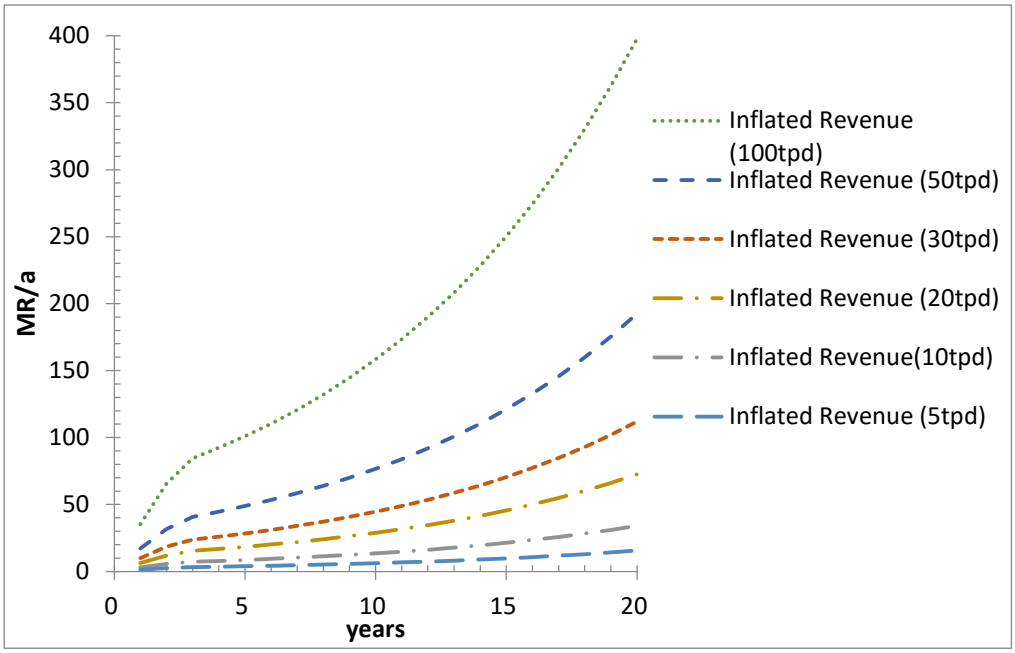

Figure D.4.1 The inflated revenue sales for Scn2

D.5 Sensitivity analysis

The different sales prices are shown in Table D.5.1 for both Scn1 and Scn2. For Scn the electricity sales price is held constant at R1.45/kWh.

Table D.5.1: Different retail prices for electricity and heat energy

Scn1: Electricity		Scn2: Heat	
Case	**R/kWh**	**Case**	**R/kWh**
A.1	0.90	**A.2**	0.15
B.1	1.45	**B.2**	0.29
C.1	1.90	**C.2**	0.44
		D.2	0.58
		E.2	0.73

.

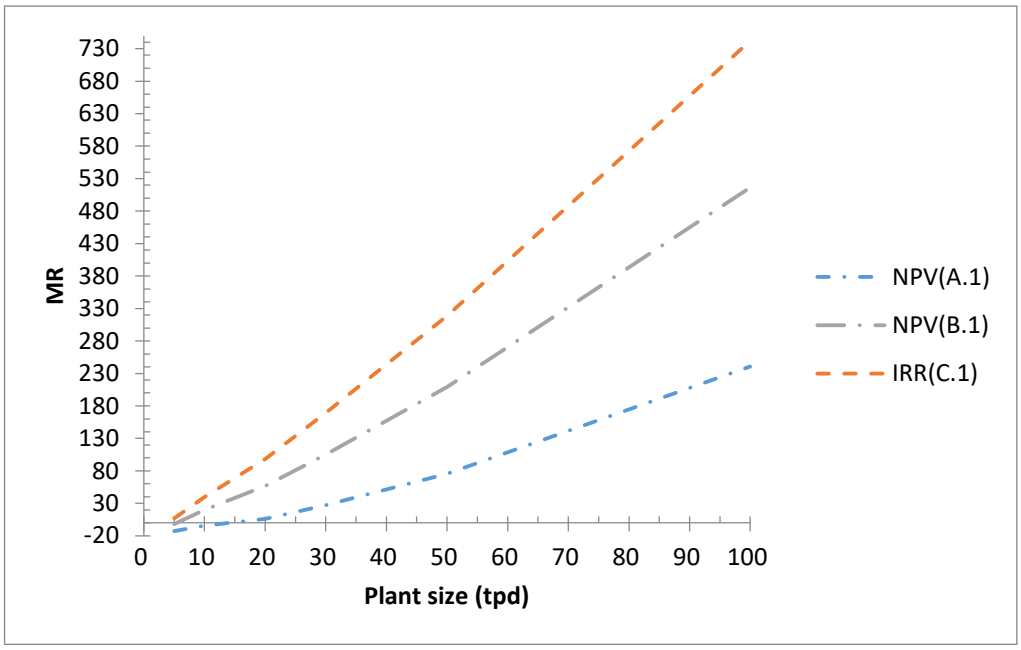

Figure D.5.1: The predicted NPV for plants sized 5 – 100 based on Scn1

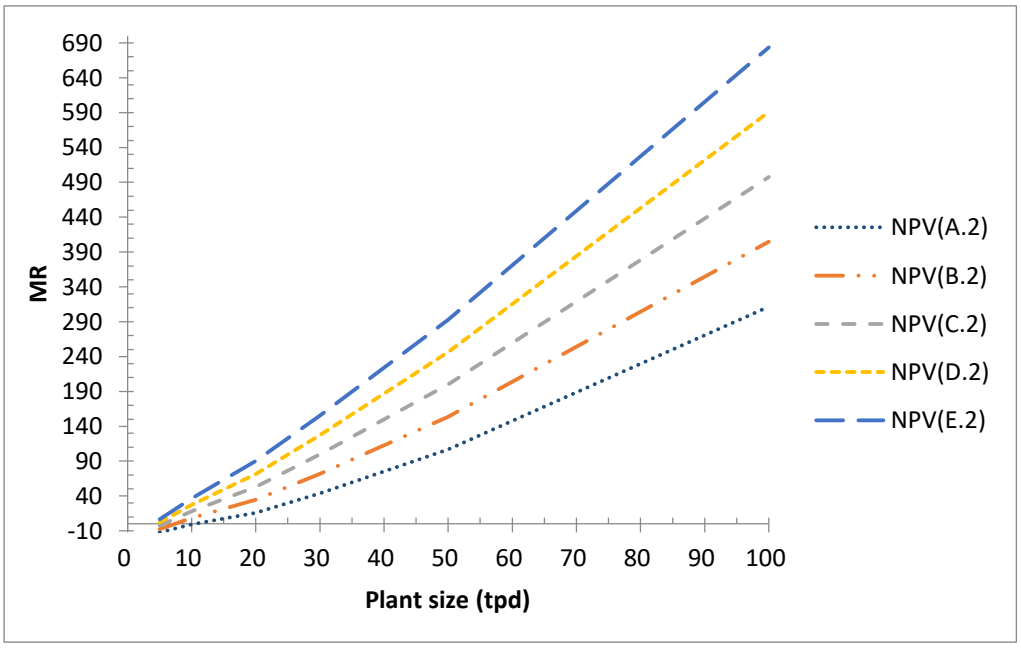

Figure D.5.2 : The predicted NPV for plants sized 5 – 100 based on Scn2

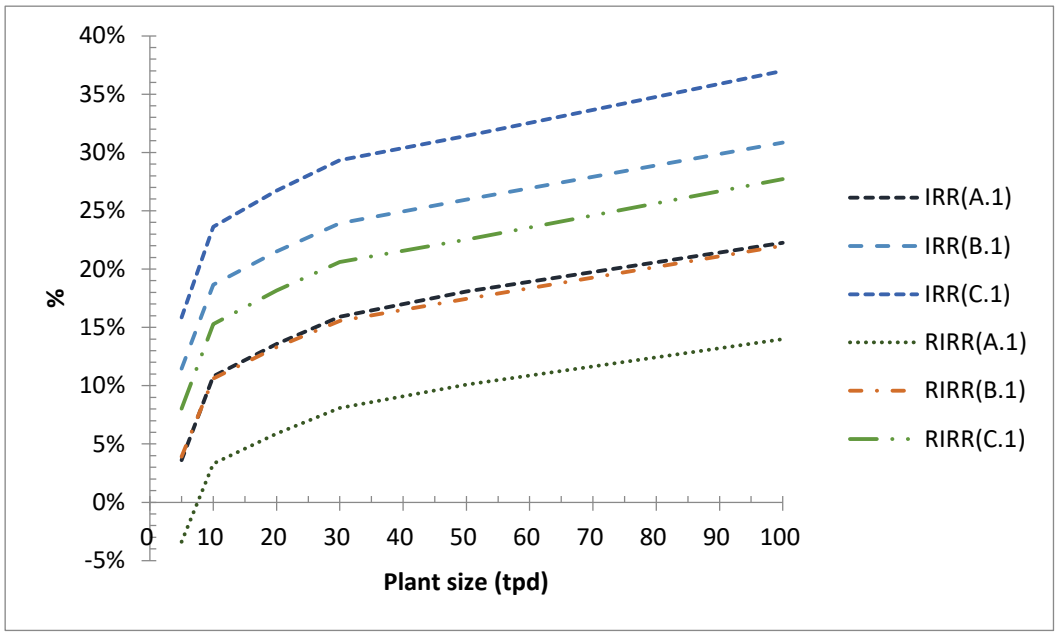

Figure D.5.3: The predicted IRR and RIRR % for 5 – 100 tpd plants following Scn1

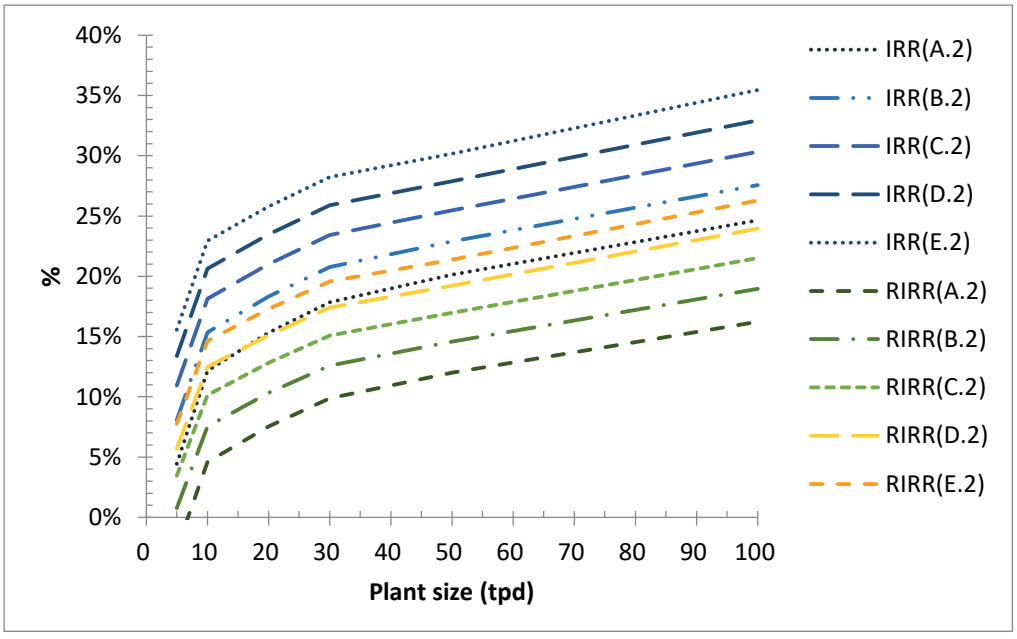

Figure D.5.4: The predicted IRR and RIRR % for 5 – 100 tpd plants following Scn2

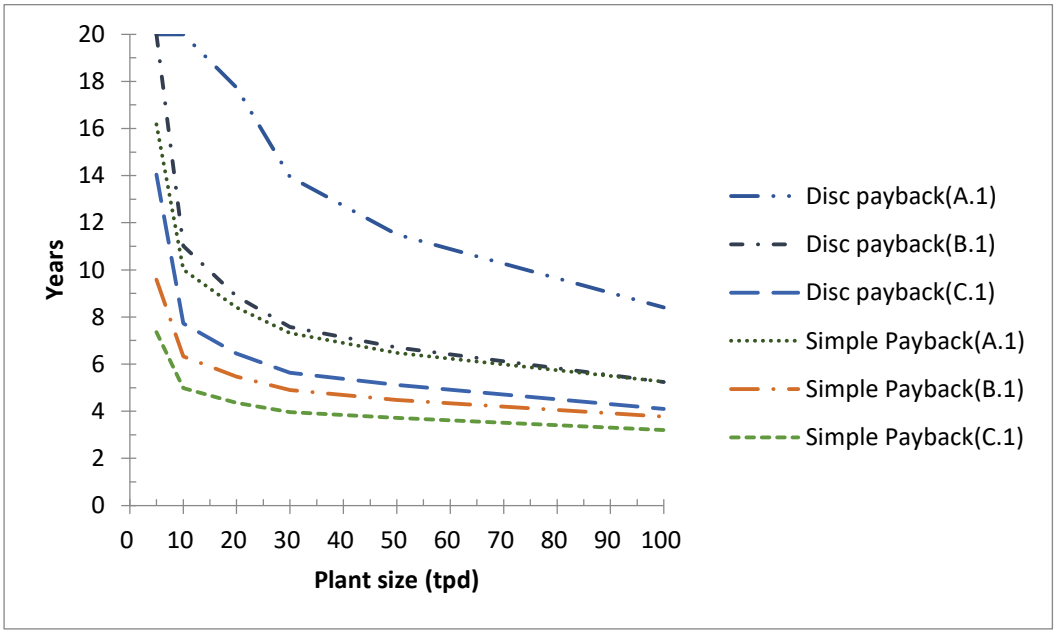

Figure D.5.5: The predicted payback periods for 5 – 100 tpd plants following Scn1

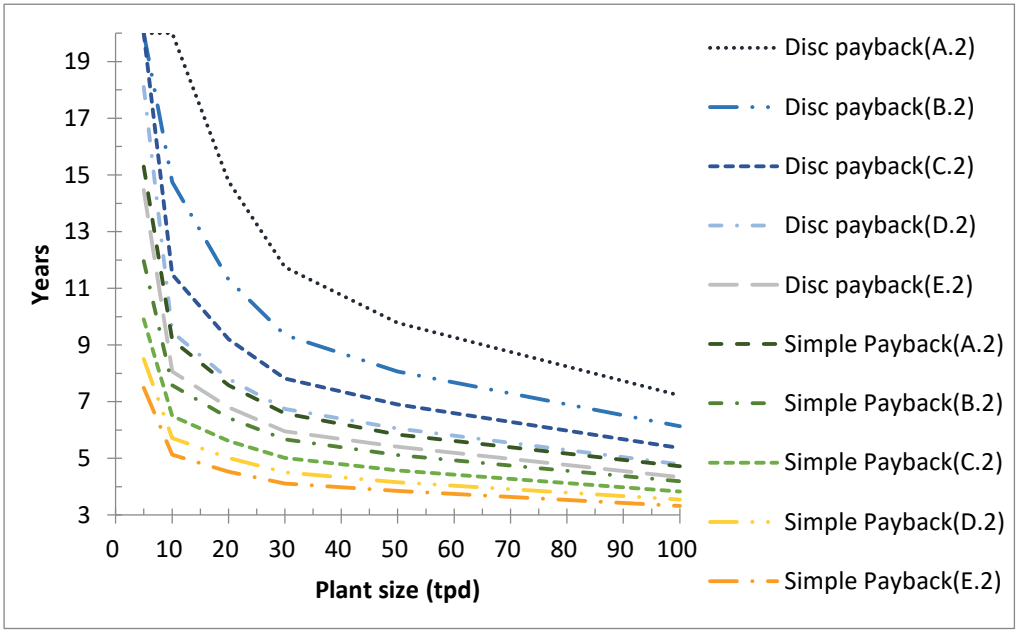

Appendix E: Experimental Results from Literature

E.1 Characterization different waste types

Table E.1.1: Chemical and elemental characterization of different waste types

Parameter	RDF	RCT Coal	Tire	MSW	Low Ash Algae	Treated Wood	Untreated Wood	Pine Needles	Plywoood
Proximate (dry wt %)									
H_2O	20	1.7	1	27.3	31.9	14.6	18.7	9	9.7
VN	76	31	68	71.5	79.9	76	80.2	49	62.5
FC	10.2	57.1	23.2	7.7	14	18.4	17.6	46.5	34.8
Ash	13.8	11.9	8.8	20.8	6.1	5.6	2.2	4.5	2.7
Ultimate (dry wt %)									
C	48.2	73.6	73.8	45.6	50.4	48.6	49.6	46.4	53.6
H	6.4	4.9	6.8	6	6.9	5.7	5.9	6	5.6
N	1.2	2.2	0.3	0.8	7.1	1.1	0.3	1.4	0.4
S	1.1	1	1.3	0.3	0.5	0.1	0.1	0	0
O	28.5	6.4	9	26.5	29	38.9	41.9	41.7	37.7
Molar Ratios (mol/mol)									
H:C	1.6	0.8	1.1	1.6	1.6	1.4	1.4	1.5	1.2
O:C	7	1	1.5	6.9	6.9	9.5	10.1	10.7	8.4
Heating Value (MJ/kg)									
HHV	-	30.4	36	25.1	24.8	20.2	20.1	18.6	17.9
LHV	**-**	29.3	35.4	24	23	18	18.5	17	16.3
Reference	(Janajreh, Raza, & Valmundsson, 2013)								

Table E.1.2: Chemical and elemental characterization of raw and torrified biowaste

Parameter	Pine Wood		Rice Straw		Grape Marc		Forest Residue		Macroalgae	
	Raw	Torrified	Raw	Torrified	Raw	Torrified	Raw	Torrified	Raw	Torrified
Proximate (dry wt %)										
H_2O	6.7	2.5	4.4	1.8	2.9	2.6	6.3	4.2	7.6	3.4
VM	80.2	74.5	74.9	71.3	64.7	51.4	70	61.6	67	48.9
FC	12.9	22.7	11.6	16.1	26.9	38.3	21.6	31.5	17.6	34.3
Ash	0.3	0.4	9.3	10.8	5.6	7.7	2.2	2.7	7.8	13.4
Ultimate (dry wt %)										
C	47.3	55.2	42.6	49	53.7	64.9	52.1	59.5	49.1	63.9
H	6.7	6.2	5.8	5.2	6.8	6.6	6.1	5.6	7.2	6.2
N	0.2	0.2	2.1	5.2	2.3	2.9	0.5	0.6	4.6	6.8
S	-	-	0.1	0.2	0.1	0.1	-	-	0.2	0.1
O	45.9	38.4	49.3	40.5	37.1	25.6	41.3	34.3	38.9	23
Molar Ratios (mol/mol)										
H:C	1.7	1.3	1.6	1.3	1.5	1.2	1.4	1.1	1.8	1.2
O:C	0.7	0.5	0.9	0.6	0.5	0.3	0.6	0.4	0.6	0.3
N:C	0.004	0.003	0.042	0.091	0.037	0.038	0.008	0.009	0.08	0.091
Heating Value (MJ/kg)										
HHV	18.46	21.82	16.6	18.82	21.51	25.47	20.86	23.67	19.59	22.93
LHV	16.83	20.39	15.21	17.64	20.02	24.07	19.36	22.33	17.95	21.67
Reference	Kuo, Illathukandy, Wu, & Chang, 2020									

Table E.1.3: Chemical and elemental characterization of different biomass

Parameter	Hardwood Shavings	* PB & MDFB	Peach Pits	Almond Hulls	Grape Pomace	Coffee Ground
Proximate (dry wt %)						
H_2O	5.72	6.32	36.73	8.01	8.97	54.69
VM	75.3	78.1	50.7	64.4	67.2	37.1
FC	14.95	14.7	11.9	18.9	18.5	7.07
Ash	4.03	0.87	0.72	8.86	5.29	1.14
Ultimate (dry wt %)						
C	48.41	4.98	52.52	44.31	52.74	56.13
H	6.28	6.16	6.18	5.64	6.23	7.16
N	0.13	3.53	0.38	1.06	2.14	2.53
S	< 0.01	0.027	0.46	<0.01	0.12	0.08
O	41.1	41.41	39.74	40.13	33.48	27.03
Molar Ratios (mol/mol)						
H:C	0.13	1.24	0.12	0.13	0.12	0.13
O:C	0.85	8.32	0.76	0.91	0.63	0.48
N:C	0.00	0.71	0.01	0.02	0.04	0.05
Heating Value (MJ/kg)						
LHV	18.5	19.3	20.7	18	21.9	23.8
*PB&MDFB	Particle Board and Medium Density Fiber Board					
Reference	(Diaz, et al., 2015),					

E.2 Plasma gasification system parameters and results

Table E.2.1: Plasma gasification conditions and results for Case study 1

Plasma Gasification									
Parameter	**RDF**	**RCT Coal**	**Tire**	**MSW**	**Low Ash Algae**	**Treated Wood**	**Untreated Wood**	**Pine Needles**	**Plywoood**
Syngas Mol Faction (%)									
H_2	21.04	50.28	54.69	43.5	31.78	29.64	26.69	28.63	22.68
CO	33.79	40.89	34.42	34.5	30.47	38.39	36.18	37.34	36.45
CO_2	0	0.05	0.01	0.03	0.04	0.05	0.6	0.81	0.65
H_2O	11.68	0.72	0.39	16.22	16.18	7.76	10.87	6.28	5.31
CH	-	0.01	0.05	0.01	0	0	0	0	0
H_2S	0.22	0.2	0.28	0.09	0.1	0.03	0.02	0	0
N_2	26.97	7.83	0.07	5.63	21.42	24.12	25.64	26.93	34.9
HCN	-	0	0	0	0	0.01	0	0	0
S		0	0	0	0	0	0	0	0
SO_2		0	0	0	0	0	0	0	0
COS	0	0.01	0.01	0	0	0	0	0	0
NH_3		0	0	0	0	0	0	0	0
C_2H_2		0	0	0	0	0	0	0	0
C (solid)		0	10.09	0	0	0	0	0	0
Heating Value (MJ/kg)									
HHV	10.5	17.43	23.22	14.71	9.76	9.89	8.89	9.34	7.74
LHV	9.55	15.94	21.01	13.44	8.99	9.23	8.31	8.71	7.28
Operating Conditions									
$\dot{m}_{waste}$ (kg/s)		1	1	1	1	1	1	1	1
$\dot{m}_{plasma\ gas}$ (kg/s)		1.31	0.74	0.36	0.78	0.78	0.85	0.89	1.38
Steam Ratio		0.7	1	0.56	0.03	0.03	0	0	0
P_{plasma} (MW)		16.65	11.71	4.06	4.84	4.84	4.84	5.07	7.84
T_{outlet} (°C)		1264	1270	1267	1258	1258	1260	1257	1256
Efficiency (%)		42.1	43	43.3	46.2	46.2	43.5	47	40.51
Oxidant	pure air	steam							
$\dot{m}_{plasma\ gas}$: $\dot{m}_{waste}$	0.782								
*** steam ratio is defined as $\dot{m}_{H2O,plasma}$ / $\dot{m}_{plasma\ gas}$**									
References	Valmundsson & Janajreh, 2011; Janajreh, Raza, & Valmundsson, 2013								

Table E.2.2: Conventional or air gasification for Case study 1

Conventional Gasification								
Parameter	**RCT Coal**	**Tire**	**MSW**	**Low Ash Algae**	**Treated Wood**	**Untreated Wood**	**Pine Needles**	**Plywoood**
Syngas mol fraction (%)								
H_2	8.16	47.4	17.04	19.4	15.3	16.2	14.73	8.82
CO	21.58	25.21	22.7	24.43	23.1	24.08	19.88	15.02
CO_2	4.91	2.28	4.92	3.64	6.9	6.76	8.48	10.72
H_2O	2.83	2.24	0	4.71	6.57	6.64	8.17	7.75
CH	0	0	0	0	0	0	0	0
H_2S	0	0	0	0	0	0	0	0
N_2	61.35	55.3	48.49	46.44	46.85	45.12	47.59	57
HCN	0	0	0	0	0	0	0	0
S	0.11	0.14	0.06	0.08	0.02	0.02	0	0
SO_2	0	0	0	0	0	0	0	0
COS	0.01	0.01	0.01	0.01	0	0	0	0
NH_3	0	0	0	0	0	0	0	0
C (solid)	1.04	1.19	1.12	1.28	1.18	1.17	1.16	0.69
Heating value (MJ/kg)								
HHV_{syngas}	13.75	18.89	22.78	29.98	24.13	25.41	22.89	14.02
LHV_{syngas}	11.99	21.83	26.45	25.79	20.81	21.91	19.71	12.12
Operating conditions								
$\dot{m}_{waste}$ (kg/s)	1	1	1	1	1	1	1	1
$\dot{m}_{air}$ (kg/s)	1.19	1	0.62	0.52	0.49	0.46	0.5	0.76
T_{outlet} (°C)	968	1044	969	994	988	951	908	889
Efficiency (%)	70.25	74.27	75.15	76.57	74.5	75.24	72.59	66.23
Oxidant	air							
References	Valmundsson & Janajreh, 2011; Janajreh, Raza, & Valmundsson, 2013)							

Plasma Gasification						
Parameter	**Hard Wood Shavings**	*** PB & MDFB**	**Peach Pits**	**Almond Hulls**	**Grape Pomace**	**Coffee Ground**
Syngas Mol Fraction (%)						
H_2	55.2	56.4	57	52.4	59.1	77
CO	14.5	14.1	18.8	11.7	14.1	4.1
CO_2	21.5	20.4	15.7	28.3	21.2	14.9
CH_4	3.9	3.9	4.6	1.8	2.8	2.5
N2	3.7	4.1	2.4	4.4	2	1.3
O_2	1	0.7	0.8	1.2	0.5	0.2
Heating Value (MJ/kg)						
LHV	9.3	9.2	10.7	7.9	9.5	9.8
Operating Conditions						
$\dot{m}_{waste}$ (kg/h)	**1.5**	2.5	3.1	3.7	4.8	5.6
P_{plasma} (kW)	**33.3**	22.4	26.3	39	27.2	31.3
Torch (kW)	**13 -15**					
CCE	**60.1**	66.1	62	61.9	56.4	45.8
Efficiency (%)	**24**	44	46	35.4	48.9	51
Oxidant		steam				
$\dot{m}_{Steam}$ (kg/h)	12-Oct					
*** steam ratio is defined as $\dot{m}_{H2O,plasma}$ / $\dot{m}_{plasma\ gas}$**						
References	(Diaz, et al., 2015)					